Pharmacology & Therapeutics 211 (2020) 107550

Contents lists available at ScienceDirect

Pharmacology & Therapeutics

journal homepage: www.elsevier.com/locate/pharmthera

Molecular imaging of inflammation - Current and emerging technologies for diagnosis and treatment

Neil MacRitchie [a,*], Marina Frleta-Gilchrist [a], Atsuko Sugiyama [b], Tristan Lawton [c], Iain B. McInnes [a], Pasquale Maffia [a,d,e,*]

[a] Institute of Infection, Immunity and Inflammation, College of Medical, Veterinary and Life Sciences, University of Glasgow, Glasgow, UK
[b] Canon Medical Systems Corporation, Ōtawara, Japan
[c] Canon Medical Research Europe Ltd, Edinburgh, UK
[d] Institute of Cardiovascular and Medical Sciences, College of Medical, Veterinary and Life Sciences, University of Glasgow, Glasgow, UK
[e] Department of Pharmacy, University of Naples Federico II, Naples, Italy

ARTICLE INFO

Available online 20 April 2020

Keywords:
Inflammation
Magnetic resonance imaging (MRI)
Molecular imaging
Photoacoustic imaging (PAI)
Positron emission tomography (PET)
Surface-enhanced Raman spectroscopy (SERS)

ABSTRACT

Inflammation is a key factor in multiple diseases including primary immune-mediated inflammatory diseases e.g. rheumatoid arthritis but also, less obviously, in many other common conditions, e.g. cardiovascular disease and diabetes. Together, chronic inflammatory diseases contribute to the majority of global morbidity and mortality. However, our understanding of the underlying processes by which the immune response is activated and sustained is limited by a lack of cellular and molecular information obtained in situ. Molecular imaging is the visualization, detection and quantification of molecules in the body. The ability to reveal information on inflammatory biomarkers, pathways and cells can improve disease diagnosis, guide and monitor therapeutic intervention and identify new targets for research. The optimum molecular imaging modality will possess high sensitivity and high resolution and be capable of non-invasive quantitative imaging of multiple disease biomarkers while maintaining an acceptable safety profile. The mainstays of current clinical imaging are computed tomography (CT), magnetic resonance imaging (MRI), ultrasound (US) and nuclear imaging such as positron emission tomography (PET). However, none of these have yet progressed to routine clinical use in the molecular imaging of inflammation, therefore new approaches are required to meet this goal. This review sets out the respective merits and limitations of both established and emerging imaging modalities as clinically useful molecular imaging tools in addition to potential theranostic applications.

Contents

1. Introduction . . . 2
2. Molecular imaging modalities . . . 2
3. Summary and conclusions . . . 23

Abbreviations: AAA, Abdominal aortic aneurysm; ARF, Acoustic radiation force; bFGF, basic fibroblast growth factor; CVD, cardiovascular disease; CEST, chemical exchange saturation transfer; CARS, coherent anti-Stokes Raman scattering; CT, computed tomography; CEUS, contrast-enhanced ultrasound; EPR, enhanced permeability and retention; EAE, experimental autoimmune encephalomyelitis; FMT, fluorescence molecular tomography; FDG, fluorodeoxyglucose; FDA, Food and Drug Administration; FRS, Framingham risk score; gd, gadolinium; GI, gastrointestinal; IMIDs, green immune mediated inflammatory diseases; ICG, indocyanine green; IBD, inflammatory bowel disease; ICAM-1, intercellular adhesion molecule-1; IVUS, intravascular ultrasound; IVM, intravital microscopy; LOX-1, lectin-like oxidized LDL receptor-1; LPS, lipopolysaccharides; MPI, magnetic particle imaging; MPIOs, micron-sized iron oxide particles; MRI, magnetic resonance imaging; MRS, magnetic resonance spectroscopy; MRSI, magnetic resonance spectroscopic imaging; MS, multiple sclerosis; MSOT, multispectral optoacoustic tomography; NAA, *N*-acetyl aspartate; NPs, nanoparticles; NIRF, near-infrared fluorescence; NIRAF, NIR autofluorescence; OCT, optical coherence tomography; Ox-LDL, oxidized low density lipoprotein; PFCs, perfluorocarbons; PAI, photoacoustic imaging; PEG, polyethylene glycol; PET, positron emission tomography; QDs, quantum dots; ROS, reactive oxidant species; RA, rheumatoid arthritis; SPECT, single photon emission tomography; SVS, single voxel spectroscopy; SWNTs, single-walled carbon nanotubes; SSTR, somastatin receptor; SORS, spatially offset Raman spectroscopy; SPIOs, super-paramagnetic iron oxide particles; SERS, surface-enhanced Raman spectroscopy; SLE, systemic lupus erythematosus; ^{99m}TC, technetium-99 m; USPIOs, ultrasmall superparamagnetic iron oxides; US, ultrasound; UCAs, US contrast agents; VAP-1, vascular adhesion protein 1; VCAM-1, vascular cell adhesion molecule-1; VWF, von Willebrand factor.

* Corresponding authors at: Centre for Immunobiology, Institute of Infection, Immunity and Inflammation, College of Medical, Veterinary and Life Sciences, 120 University Place, University of Glasgow, Glasgow G12 8TA, UK.
E-mail addresses: Neil.MacRitchie@glasgow.ac.uk (N. MacRitchie), Pasquale.Maffia@glasgow.ac.uk (P. Maffia).

https://doi.org/10.1016/j.pharmthera.2020.107550

Funding sources . . . 24
References . . . 24

1. Introduction

1.1. Definition of molecular imaging

Molecular imaging concerns the visualization, detection and quantification of physiological and pathologic/disease processes in the body at the cellular or molecular level. To reach such a level of detailed imaging requires specialized instruments (modalities) that either alone or in combination with imaging agents (either targeted or passive) can uncover the status of a tissue via detection of biochemical or other molecular markers, particularly in the context of a disease state.

One of the major aims of molecular imaging is to answer questions of disease processes that are beyond current diagnostic methods. The need is to image biochemical processes in intact living organisms over time in a minimally- or non-invasive manner. As such, molecular imaging has the potential to transform each aspect of medical care including improved and earlier diagnosis, more accurate monitoring of therapy, identifying novel drug targets/drug validation and helping to understand the complex biochemical pathways that interact to create disease states.

1.2. The requirement for molecular imaging of inflammation in modern medicine

We now know that inflammation is a key or major contributing factor in many chronic diseases including cardiovascular disease (CVD), rheumatoid arthritis (RA), inflammatory bowel disease (IBD), colitis, systemic lupus erythematosus (SLE), diabetes, multiple sclerosis (MS) and Alzheimer's disease and is closely related to many aspects of tumor progression. These conditions contribute a significant proportion of worldwide morbidity and mortality and cause substantial socioeconomic burdens on society (Jacobs, Bissonnette, & Guenther, 2011; Mathers & Loncar, 2006).

Although new therapies have brought significant improvements to patient care, a considerable portion of patients still lack sufficient therapeutic effect and incidence of complications remains high, which is often a by-product of the non-specific nature of the treatments provided. There is also a lack of tailoring of drugs to individual patient needs, which is especially important in chronic pathologies that may present with different underlying causes or have distinct clinical stages, each defined by a specific inflammatory environment. We briefly take RA as an example of where a more sophisticated understanding at the molecular level could improve patient care. RA is a disease that affects 0.5–1% of the global population - treatment options are significantly greater than for many other chronic inflammatory conditions. Approved biological therapies for RA, principally anti-TNF antibodies, were a revolutionary breakthrough in advancing RA treatment, adding to the established broad ranging anti-inflammatory treatments such as methotrexate, yet much is still unknown about the drug-disease interactions such as why some patients respond to anti-TNF more than others or why there is frequently a dissociation between clinical scoring and destructive joint progression (Smolen, Aletaha, & McInnes, 2016). It is also recognized that early diagnosis followed by rapid administration of appropriate therapy is the ideal strategy for treating inflammatory RA and improving patient outlook, yet early diagnosis is challenging due to early symptoms going undiagnosed or not being present at all. Studies of pre-clinical RA include individuals with positive autoantibodies and marginally raised inflammatory markers with no visible clinical features (Firestein & McInnes, 2017). This prodromal period can precede the disease for a decade and poses a significant clinical and therapeutic challenge, which could be transformed by better molecular imaging to guide early clinical decision. Currently, clinicians determine disease presence/severity based on several factors: symptoms, detectable disease biomarkers and medical imaging results. The advent of biological therapies targeting inflammatory molecules such as cytokines can, in turn, also lead to new diagnostic approaches with the addition of imaging agents to the targeted antibody allowing visualization of the cytokine concentration in the disease site and to assess whether the unlabeled antibody could be of benefit therapeutically. Information gained from such an approach may also help answer why certain patients are non-responders to a cytokine-targeted therapy. In comparison with cancer, inflammatory diseases such as RA involve multiple tissues and it is yet unexplored if there is considerable mismatch between disease and treatment distribution in the body. Studies exploring lymph node, bone marrow and synovial tissue biopsies would further support the systemic distribution of the disease (van Baarsen et al., 2013). Hence, the ability to visualize disease potentiating molecules can inform clinicians in diagnosis, treatment monitoring and in deciding whether or not a potential therapy may be beneficial (Malviya et al., 2013).

A final point worth noting is that each disease typically has a specific treatment regime which traditionally has ignored potentially common underlying inflammatory components between different diseases that have a strong immune component. This includes the role of inflammation in cancer (Grivennikov, Greten, & Karin, 2010), and the interrelationships between RA and CVD (Mason & Libby, 2015) or chronic obstructive pulmonary disease (COPD) and stroke (Austin, Crack, Bozinovski, Miller, & Vlahos, 2016). Indeed, adverse cardiovascular events are increased in RA patients and are subsequently reduced following introduction of anti-inflammatory therapies although the inflammatory mediators linking these two diseases are unclear (Tocci et al., 2016). These unanswered questions are a result of a lack of understanding of the precise cellular and molecular inflammatory mechanisms that drive each particular pathology (Tabas & Glass, 2013). Ultimately, inflammatory processes are finely tuned systems, with many molecular signals that orchestrate the immune response. For most conditions, it is probable that only limited diagnostic information will be obtained by one or two blood-derived inflammatory markers. The potential strength of molecular imaging is to 'see' into the core of the inflammatory site, targeting multiple biomarkers (multiplexing) to provide a deeper insight into the triggers, cellular interplay, pro- versus anti-inflammatory mediators and the ability to evaluate current and the next generation of therapies for chronic immune diseases with a level of precision and detail not seen before. Implementing molecular imaging, therefore, can uncover new information on disease processes which can in turn offer new targets for disease diagnosis and stratification. In this sense, molecular imaging could confer a discipline defining transition in the next decade with profound potential to revolutionize the management of patients with chronic diseases.

2. Molecular imaging modalities

2.1. Overview

The mainstays of current clinical imaging are computed tomography (CT), magnetic resonance imaging (MRI), ultrasound (US) and the nuclear imaging modalities: positron emission tomography (PET)/single photon emission tomography (SPECT). These imaging techniques have transformed medical imaging in improving disease detection, progression and therapeutic assessment across a wide spectrum of diseases

from oncology and CVD to rheumatic musculoskeletal diseases and neurodegenerative conditions. In patients, these modalities are primarily used for anatomic and functional imaging at the tissue level, although at least for PET, molecular imaging is being realized, despite significant shortcomings as will be detailed throughout this report. However, they retain inherent weaknesses that preclude the combined high sensitivity, high resolution, and simultaneous detection of multiple biomarkers in a non-invasive manner that is the ultimate goal of molecular imaging research.

Other techniques that potentially offer greater promise as molecular imaging tools include mostly pre-clinical stage technologies such as optical imaging including photoacoustics as well as techniques classified as vibrational spectroscopy which includes Raman spectroscopy and surface-enhanced-Raman spectroscopy (SERS). While pre-clinical technologies such as near-infrared fluorescence (NIRF) with quantum dots and spectral imaging using SERS can allow a high level of multiplexing, these are not yet clinic ready. There exists, therefore, a broad range of established and emerging technologies with molecular imaging potential and these will be described and compared, with examples of use relating to inflammation imaging highlighted. Additionally, for each imaging modality, we offer a section dedicated to potential therapeutic use of the technology in modifying disease processes, for example through using imaging agents loaded with anti-inflammatory drugs. Finally, there will be an assessment of the relative strengths and weaknesses of each technique as a tool for molecular imaging and their prospective use within the clinic.

2.2. Imaging agents

Molecular imaging can rely on either direct detection of endogenous molecules or employ exogenous tracers (passive or ligand targeted) that are tailored to a particular modality of choice e.g. fluorescent probes for near-infrared (NIR) optical imaging or radiolabeled tracers for PET/SPECT imaging. Traditionally, exogenous tracers have been small molecules <2 kDa (<4 nm) in size (e.g. iodinated compounds for CT, chelated gadolinium for MRI and ^{18}F-FDG for PET). Despite providing significant advances in diagnosing disease, particularly in the field of oncology, small molecule tracers have important limitations with regard to molecular imaging owing to their rapid clearance, lack of adaptation to allow detection via imaging, potential toxicity and relatively poor signal strength. These limitations have led to development of novel materials to overcome the limitations of current diagnostic molecular imaging and to cater for the new technologies that are emerging, particularly within the optical and vibrational imaging fields. Indeed, for several imaging modalities such as magnetic particle imaging (MPI) and SERS, nanocarriers (or nanoparticles (NPs) as they will be referred to throughtout the remainder of this review) are an essential component for signal induction. In comparison to small molecules, NPs offer a high level of control over design (e.g. contrast agent class/dose, body residence times, targeting ligands, drug delivery). NPs are small nanomaterials, less than 1 μM, that can be composed of a diverse range of materials depending on the requirements of the modality and desired residence times. NPs offer the following advantages over small molecules: 1) They can carry a high quantity of tracer to the site of interest (such as bismuth or gold for CT) in a protective shell, creating a concentrated signal to improve sensitivity coupled with reduced toxicity, assuming the elimination kinetics of the NPs are carefully understood; 2) They can be engineered to various specifications to increase circulation/residence times allowing stable longitudinal imaging; 3) Can be used for passive uptake into tissues via the enhanced permeability and retention (EPR) effect or can be functionalized with biomolecules such as antibodies, peptides or aptamers targeted to a disease related biomarker of interest; 4) The large surface area allows many targeting ligands to be attached to a single NP which increases the binding capacity compared with single molecules. Indeed, this increased binding can be quite substantial, ranging from 1 to 2 orders of magnitude to as high as 5–6 orders of magnitude (Benezra et al., 2011; Hong et al., 2007); 5) The adaptability of NPs to a particular modality coupled with an ability to create multiple 'flavors' of NPs (NPs targeted to different in vivo targets) allows high multiplexing potential. The ability to simultaneously measure multiple biomarkers (Table 1) within the same acquisition window is the key to diagnostic molecular imaging, particularly within the context of inflammation imaging when a single inflammatory marker is insufficient to provide a clinician with the information to diagnose/stratify a disease, particularly when pathological changes may be minimal; 6) Can be engineered to be multi-modal (the detection of one NP by two or more imaging modalities); 7) Can offer novel theranostic strategies e.g. by providing a high sensitivity imaging signal coupled with delivering a drug payload.

2.3. Hybrid imaging platforms

As observed in the last 2 decades, it is unlikely that one single imaging modality will possess all the required attributes (high spatial resolution, high sensitivity, low toxicity, fast scan times, consistent quantification, deep tissue imaging, strong multiplexing etc.) for clinical molecular imaging. Indeed, with common imaging modalities, there is currently an inverse correlation between sensitivity and spatial resolution. These limitations have led to the engineering of hybrid technologies, many of which are now commonplace such as PET/CT, SPECT/CT and the re-emergence of PET/MRI, all of which are being investigated for molecular imaging potential. Pre-clinically, there is also a push towards multi-modal imaging, such as combining two or more optical imaging technologies onto a single probe, or NIRF combined with intravascular ultrasound (IVUS) or even single multi-modal NPs that are amenable to multiple imaging systems, for example a NP with an iron oxide core functionalized via a dextran coating to fluorophores for optical imaging (Wolfbeis, 2015). This report will describe recent developments in hybrid imaging systems using established imaging modalities in the molecular imaging space and the potential of more early stage pre-clinical multi-modal imaging systems and their route to clinical translation.

2.4. Computed tomography (CT)

CT has been a mainstay medical imaging technique since its inception in the 1970s, superseding older X-ray technologies, owing to its greater power in creating 3D anatomical imaging through computational algorithms as opposed to classical 2D X-ray imaging. CT operates with relatively good spatial resolution, at least for anatomical imaging needs (Brenner, 2010). CT can readily distinguish electron-dense structures such as bone and teeth from electron-poor structures such as soft tissues making it an excellent modality for anatomical imaging of skeletal structures. Inherent advantages include fast scan times and body wide imaging. In the absence of a contrast agent, discrimination of anatomical tissues can be challenging (Cormode, Naha, & Fayad, 2014). The most common contrast agents are iodine-based compounds which have found particular use in coronary artery imaging including Coronary Computed Tomography Angiography (CCTA).

2.4.1. Clinical use

CT is primarily an anatomical imaging technique, limited by its low sensitivity, an inability to accurately discriminate soft tissue structures and to accurately quantify contrast agents (Anderson & Butler, 2014). While the advent of dual energy CT (DECT) has greatly improved the technology, clinical advancement has mainly been realized via enhanced detection of lesions, such as in the fields of oncology and CVD. Indeed, CT's main use in CVD has been calcium scoring of plaques to assess atherosclerotic plaque burden and CT calcium scoring is widely practiced for risk stratification within the clinic, although calcification is a product of late-stage pathology limiting its potential in diagnosis of early stage lesions (Sandfort, Lima, & Bluemke, 2015). CT has not

Table 1
Key examples of inflammatory biomarkers targeted by MRI.

Target	Tracer(s)	FDA/CE approved (commercially available)	Disease(s) and study type	Comments	Reference(s)
VCAM-1	VINP-28 (VCAM-1 targeted NP)	No (No)	Atherosclerosis (pre-clinical)	9.4-T imaging in apoE$^{-/-}$ mice	Nahrendorf et al., 2006
	P03011 (VCAM-1 targeted USPIO)	No (No)	Atherosclerosis (pre-clinical)	Imaging of both early and late stage pathology in apoE$^{-/-}$ mice using 17.6-T MRI	Michalska et al., 2012
VCAM-1/P-selectin	Dual-targeted MPIOs	No (No)	Atherosclerosis (pre-clinical)	Dual-targeted MPIOs showed superior binding and MRI signal in apoE$^{-/-}$ mice compared with single targeted particles	McAteer et al., 2008
E-/P-selectin	Targeted glyconanoparticles	No (No)	EAE (MS model) (pre-clinical)	Early inflammation (pre- clinical symptoms) was detectable without loss of blood-brain barrier integrity	van Kasteren et al., 2009
ICAM-1	Targeted MPIOs	No (No)	Mouse stroke model (pre-clinical)	Early inflammation post-stroke was readily visualized in vivo with ICAM-1 targeted MPIOs but not ICAM-1 targeted Gd liposomes. This data supports other studies that MPIOs are superior contrast agents in vivo	Deddens et al., 2013
	Targeted MPIOs	No (No)	EAE (pre-clinical)	Blood vessel inflammation in the brain was detected by MRI in EAE mice without loss of blood-brain barrier integrity	Blezer et al., 2015
Complement receptor type 2 (CR2)	SPIO NP	No (No)	Renal inflammation in mice (nephritis) (pre-clinical)	Targeted but not passive SPIOs were able to visualize inflammation in different kidney compartments in mice with nephritis	Serkova et al., 2010
Fibrin	EP-2104R (Gd based targeted contrast agent)	No (No)	Coronary thrombosis in swine (pre-clinical)	MRI imaging could assess location and size of thrombus within the coronary arteries of pigs using a clot targeted Gd based agent	Botnar et al., 2004
glycoprotein $\alpha_{IIb}\beta_3$	P975 (Gd based targeted contrast agent)	No (No)	Carotid thrombosis in a mouse model (pre-clinical)	MRI signal in thrombotic vessels but not in healthy contralateral carotid. Administration of an $\alpha_{IIb}\beta_3$ antagonist resulted in signal loss indicating target specific imaging	Klink et al., 2010
MMPs	P947 (Gd based targeted contrast agent)	No (No)	Atherosclerosis (pre-clinical)	MRI imaging revealed contrast signal was 3× higher in atherosclerotic vessels than control. Contrast agent was also rapidly cleared from the circulation (~95% within 1 h) allowing minimal background noise	Lancelot et al., 2008
Fibrin	^{19}F-PFC Gd containing NPs	No (No)	Atherosclerosis (pre-clinical)	A ^{19}F combined with Gd T1 based NP targeted to fibrin was tested on isolated human arterial plaques at 4.7-T and revealed specific binding to clot surface at a minimum NP concentration of 1 nM at the clot.	Morawski et al., 2004
	^{19}F-PFC-paraCEST contrast NPs	No (No)	Thrombosis (in vitro blood clots)	Dual paraCEST and ^{19}F imaging of a clot using fibrin targeted NPs allowed MRI imaging by either ^{19}F or paraCEST at NP concentrations below 5 nM	Cai et al., 2012
VCAM-1	^{19}F-PFC NPs	No (No)	Atherosclerosis (pre-clinical)	MRI revealed inflammation in plaque burdened renal arteries via ^{19}F signal via VCAM-1 bound NPs	Southworth et al., 2009
	^{19}F-PFC NPs	No (No)	Atherosclerosis (pre-clinical)	ApoE$^{-/-}$ mice were injected with VCAM-1 targeted ^{19}F-PFC NPs and aortas removed for ex vivo MRI analysis revealing specific binding to arterial areas with lesion formation	Pan et al., 2013
Thrombin	^{19}F-PFC NPs	No (No)	Arterial thrombotic injury (pre-clinical)	Following surgical induction of arterial injury, mice were administered thrombin targeted ^{19}F-PFC NPs and vessels excised and assessed at 11.4-T MRI revealing highly localized accumulation of NPs at clot locations	Myerson et al., 2011
$\alpha_v\beta_3$	lipoCEST targeted NP	No (No)	Angiogenesis	$\alpha_v\beta_3$ targeted NPs were in vivo imaged in new blood vessels within brain tumors of mice using 7-T MRI. Histology revealed NPs were bound to $\alpha_v\beta_3$ expressing cells	Flament et al., 2013
Caspase-1	^{19}F-nanoprobe	No (No)	Induced local inflammation	Caspase-1 is involved in the release of pro-inflammatory cytokines and in this study was targeted using an activatable ^{19}F-nanoprobe, yielding a ^{19}F signal which correlates with Caspase-1 activity.	Akazawa, Sugihara, Minoshima, Mizukami, & Kikuchi, 2018
Elastin	Gd based elastin probe + USPIO	No (Yes)	Abdominal aortic aneurysm (AAA)	The combined assessment of extracellular matrix degradation and inflammatory cell activity was used in a mouse model of AAA to predict the risk of aneurysmal rupture	Brangsch et al., 2019
$\alpha_4\beta_1$	THI0567-targeted liposomal-Gd	No (No)	Atherosclerosis (pre-clinical)	Using a 1-T small animal scanner, atherosclerotic lesions in apoE$^{-/-}$ mice were detected via binding of the tracer to sub-endothelial macrophages within the plaque. Signal was specific to targeted particles and may offer a non-invasive meaure of plaque inflammatory activity with higher signal to noise compared with PET.	Woodside et al., 2018

progressed clinically to the level of true molecular imaging either in oncology, CVD (the two major drivers of CT technology) or other conditions and the inherent low sensitivity, lack of approved tracers and concerns over toxicity means clinical molecular inflammation imaging is lacking.

2.4.2. Pre-clinical use and in-human trials

Micro-computed tomography or "micro-CT" is similar in principle to standard CT but on a smaller scale and with superior resolution and is frequently employed in pre-clinical research. Micro-CT produces high resolution (typically 15–50 μM in pre-clinical studies) (MI Bioresearch Inc.; Biolaurus Inc.) although some in vivo systems offer better performance still. Micro-CT scanners are employed, both in vivo and ex vivo, typically to measure hard tissue structures. Modifications of micro-CT utilizing ionic iodine contrast have been used to measure glycosaminoglycans (GAGs), a major component of healthy joint cartilage with an inverse relationship existing for joint iodine concentration and cartilage density (Palmer, Guldberg, & Levenston, 2006) and such an approach

has been used to measure cartilage growth in rats (Xie, Lin, Levenston, & Guldberg, 2009). Multicolor or spectral CT can differentiate several compounds based on each compound's specific energy-dependent X-ray absorption profile. One such spectral-CT imaging system (MARS small bore scanner; MARS Bioimaging Ltd) has been used to image an excised human tibial plateau (break of tibia bone at knee joint) with discrimination of different joint components possible in a proof of concept study (Rajendran et al., 2017). Spectral CT potentially overcomes some of the obstacles of clinical level CT and MRI in combining fast, high resolution scanning with more accurate tissue resolution and quantification of contrast enhanced areas but requires further refinements to be a viable clinical tool (Rajendran et al., 2017). Translating this to clinical osteoarthritis use would require utilizing the ionic iodine spectral CT to measure disease progression and/or response to therapy. It is worth noting; however, that radiation dose was not measured in this study and remains a key concern with high resolution CT imaging. Attempts using the MARS spectral-CT system have also been employed with a view to advancing spectral-CT imaging of the atherosclerotic plaque. Using this technology on excised human plaques, spectral-CT was able to differentiate multiple plaque components in human tissue sections within the same voxel including lipid, calcium/iron and water containing components with the caveats that high radiation doses were used and calcium and iron could not be distinguished within the same voxel (Zainon et al., 2012). Cormode et al., 2010 employed gold NPs targeted to macrophages (Au-HDL) together with an iodinated contrast emulsion agent for imaging small vessels in addition to endogenous calcium for spectral-CT in apolipoprotein-E (apoE)$^{-/-}$ mice, the gold-standard model for the study of experimental atherosclerosis. Specific uptake by macrophages in plaque regions was evident and the gold signal could be discriminated from iodine and calcium allowing simultaneous imaging of multiple plaque components (Cormode et al., 2010). Pre-clinical development of NPs as CT imaging agents has also progressed - albeit at a much slower and limited rate compared with other modalities such as MRI and PET - with the aim of targeting inflammation in atherosclerosis. An iodinated NP contrast agent, N1177, was developed with the intention of specifically targeting macrophages and imaging plaque inflammation (Hyafil et al., 2007). Using a rabbit model of atherosclerosis involving double balloon injury combined with a high fat diet, N1177 was used for in vivo detection of macrophage containing lesions using a clinical CT scanner 2 h following intravenous administration. CT images of macrophage density showed good correlation with histological staining (Hyafil et al., 2007). N1177 showed superior imaging of plaque density compared with a conventional CT tracer but the dose of iodinated N1177 employed was high and patient tolerability to a functional dose may well be a limiting factor.

2.4.3. Theranostics

The high atomic number of gold coupled with its low toxicity profile make it a more desirable CT imaging agent than iodine and more likely to gain regulatory approval than some of the more exotic metals beings trialed due to its long history of use in humans. A new avenue emerging in the nanoscience field is the design and synthesis of nanomaterials that offer a therapeutic and diagnostic option with photothermal therapy. The combination of NP design and laser excitation wavelength can induce absorption of light and subsequent conversion to heat. Following NP binding to or uptake by cells, the thermal energy from the NP is transferred via convection to the surrounding cellular medium resulting in thermal cell death. Gold NPs can be shaped to allow absorption of heat from an external light source, creating an excellent inducer of the photothermal effect. CT can be utilized with NIR light sources to measure uptake of gold into cells and subsequent response to thermal destruction of tumor cells (von Maltzahn et al., 2009) and in macrophages within arterial lesions (Qin et al., 2015). As will be outlined in subsequent sections, photothermal therapy utilizing gold NPs is a strategy also being developed for other imaging/theranostic modalities.

2.4.4. Advantages and barriers to translation

The key advantages of CT include speed of imaging, the body-wide view and its established use within the clinic for anatomical and limited functional imaging. As one of the main imaging modalities, CT scans have quick clinical turnover and are well tolerated by a majority of patients. In fact, CT is widely used in the field of inflammation imaging as recently reported by the Antoniades group who demonstrated that changes in the lipid and water content of perivascular fat tissue surrounding human coronary arteries was a marker of the underlying vascular inflammation associated with atherosclerotic plaques and could be detected by CT in human patients (Antonopoulos et al., 2017; Oikonomou et al., 2018). This offers the potential of CT as an early diagnostic tool for indirectly measuring inflammation in the early stages of atherosclerosis. However, the low sensitivity (10^{-2}–10^{-3} mol/L), radiation burden and a spatial resolution insufficient to discriminate inflammation 'hot-spots' within the relatively large voxel areas (Sandfort et al., 2015) are likely to be insurmountable obstacles for clinical translation of CT as a true molecular imaging modality.

2.5. Magnetic resonance imaging (MRI)/magnetic particle imaging (MPI)

MRI is one of the most studied modalities for functional, anatomic and cellular imaging at a clinical level. Non-contrast MRI is readily used for acquiring anatomic information but if molecular imaging is needed, it requires the use of contrast agents owing to poor sensitivity, the main limitation of MRI. While sensitivity of MRI is superior to CT with ranges from ~10 μM to ~10 mM (Sinharay & Pagel, 2016), it is orders of magnitude lower than that obtained by nuclear or optical imaging systems (James & Gambhir, 2012) and this limits MRI to situations where contrast agents are highly accumulating through passive means or through binding to highly expressed biomarkers in targeted MRI (Table 1).

There are four principal classes of contrast agents used for MRI and each differs in the mechanism of signal generation:

1) T1 and T2/T2* contrast agents

T1–weighted MRI consists of positive contrast agents, typically chelates of paramagnetic metal ions, usually gadolinium (Gd^{3+}), with detection limits in the micromolar range. These are generally small molecule chelates with many approved for clinical use. Attempts to overcome the low sensitivity have involved encapsulation of Gd^{3+} into various NPs such as dendrimers, micelles or high-density lipoprotein (HDL) type NPs (Kircher & Willmann, 2012). These NPs can allow delivery of larger payloads of imaging agent, improving sensitivity while reducing the likelihood of release of the toxic free Gd^{3+} element.

T2-weighted MRI occurs when negative contrast imaging agents are employed. The mainstay imaging agent for T2 MRI has been the superparamagnetic iron oxide particles (SPIOs) owing to their high magnetization properties. These particles are usually dextran coated and have evolved since their inception in the 1980s to smaller more refined coated particles (USPIOs), with a diameter 10–50 nm and these have been the primary focus to date in moving MRI towards a tool more amenable for molecular imaging. There also exists larger iron oxide-based contrast agents called micron-sized iron oxide particles (MPIOs) that are typically greater than 1 μM in diameter. As will be outlined below, however, even those agents to gain regulatory approval have struggled to maintain a foothold in the imaging market.

2) Fluorinated contrast agents

The ^{19}F nucleus has properties that offer MRI signal intensities approaching that of hydrogen protons (Ruiz-Cabello, Barnett, Bottomley, & Bulte, 2011) yet is present in only trace amounts in the soft tissues of the human body, thus is a suitable choice for an exogenous contrast agent when high signal to noise ratio is required. ^{19}F contrast agents have centered on perfluorocarbons (PFCs) where the hydrogen atoms

are replaced by ^{19}F atoms and which can subsequently be concentrated/encapsulated by a lipid bilayer at near nanoscale size delivery vehicles, allowing targeting to molecular markers or drug conjugation for therapeutic delivery. The key advantage of ^{19}F MRI is that the signal directly correlates to the binding/uptake of ^{19}F at the site of interest, allowing quantification of the target. Being detectable by classical MRI (if a ^{19}F-tuned RF coil is equipped), ^{19}F MRI still requires $>10^{-5}$ M of ^{19}F in the tissue for detection at 1.5-T (Ruiz-Cabello et al., 2011; Terreno & Aime, 2015).

3) Chemical exchange saturation transfer (CEST)/paraCEST

CEST and paraCEST compounds utilize a different form of magnetic imaging, namely reducing the magnetization of the water signal with limited effects on the relaxation rate. The process involves part of the CEST agent undergoing magnetic resonance by application of a radiofrequency pulse which promotes saturation of the proton and chemical exchange with water molecules in which the saturated proton is transferred to the water, resulting in saturation of a proton within the water molecule. The remaining unsaturated water molecules can be used to provide an MRI signal (Sinharay & Pagel, 2016). The limitation of this technique is the slow exchange between molecules resulting in poor sensitivity and the requirement for large concentrations (mM range) of target molecules. ParaCEST exclusively employs exogenous paramagnetic agents capable of exchanging protons or water molecules with endogenous tissues. These may include NPs conjugated to paramagnetic ions, thus exposing them to water protons. By tuning the magnetic resonance frequency to the exchangeable saturated protons, contrast signals can be differentiated from the surrounding bulk water. ParaCEST agents offer faster proton exchange and therefore are a more sensitive adaptation of traditional CEST (Viswanathan, Kovacs, Green, Ratnakar, & Sherry, 2010).

4) Hyperpolarized MRI

Hyperpolarized MRI was/is being developed to overcome the poor sensitivity of traditional MRI. Developed in the early part of this century, with first human trials in 2010, it is fast gaining momentum, owing to its potential exponential gains in imaging resolution. The abundance of water in human tissues means only a small fraction of protons in water molecules require magnetic alignment for a signal to be obtained. Thus, MRI has been developed around detection of hydrogen protons. The detection of other nuclei that may be incorporated into an imaging agent such as ^{13}C or ^{19}F would be present at concentrations orders of magnitude lower than ^{1}H and would not be resolved via traditional MRI but can be resolved by hyperpolarized MRI by increasing the % of atomic nuclei in alignment (Golman, Ardenkjaer-Larsen, Petersson, Mansson, & Leunbach, 2003). Several methods exist for creating hyperpolarized MRI agents but dynamic nuclear polarization (DNP) is the most common and can boost signal intensity by 10,000 times (Ardenkjaer-Larsen et al., 2003) compared with traditional MRI methods.

Magnetic Resonance Spectroscopy (MRS) is a complimentary tool to MRI, used for detecting primarily ^{1}H atoms within certain metabolites present within a single voxel of interest. To detect a ^{1}H signal within molecules present at such a low abundance with respect to water and fat, it is necessary to separate (orsuppress) the water signal during MRS acquisition. The acquisition of molecular spectra by MRS can be used to determine metabolic changes that may reflect pathological processes. Since the signals from the molecules of interest in MRS are present at relatively low concentrations, suitable field strengths are required for clinical MRS, with 3-T scanners offering higher sensitivity and the ability to obtain spectra from smaller voxels (van der Graaf, 2010). The particular method of MRS employed depends on what information is required. Typically, MRS uses single voxel spectroscopy (SVS) for a particular localized region of interest. Imaging of several voxels can be used for mapping spatial distribution of a metabolite of interest (e.g across a tumor) and utilizes magnetic resonance spectroscopic imaging (MRSI) but at the expense of quantification accuracy (Faghihi et al., 2017). MRS can identify various molecules within tissue, dependent on concentration and magnetic field strength. These include creatine, choline, *N*-acetyl aspartate (NAA), alanine, lactate, taurine, glycine, myo-inositol, intracellular lipids and glucose (Verma, Kumar, Verma, Aggarwal, & Ojha, 2016). Of these, NAA, creatine and choline are the most widely utilized and historically, MRS has been a tool applied for studying disorders of the brain.

MPI is a recent technological development (Gleich & Weizenecker, 2005) that directly detects magnetic NPs (almost exclusively iron oxide NPs thus far) and produces positive contrast from the tracer directly (a list of MPI tracers can be found in Panagiotopoulos et al., 2015). MPI offers superior sensitivity and potential gains in spatial resolution over conventional MRI as well as fast imaging times (Gleich & Weizenecker, 2005; Saritas et al., 2013). The basis for these improvements is that the signal (i.e. NP derived) is not present in the body naturally thus offering superior contrast and sensitivity over traditional MRI.

2.5.1. Clinical use

As stated above, MRI is an excellent tool for imaging the soft tissue components within the human body, offering a safer form of imaging, free of ionizing radiation. MRI can form part of the diagnostic work up for investigating abnormalities within the cardiovascular, musculoskeletal, gastrointestinal and other tissues, providing both anatomic and in some circumstances, functional imaging, such as perfusion imaging. The majority of contrast enhanced MRI utilizes T1 based approaches. However, over the history of MRI, a number of iron oxide-based imaging agents have been approved for clinical use, particularly dextran coated NPs, due to low toxicity and straightforward manufacturing (Mulder, Jaffer, Fayad, & Nahrendorf, 2014). Despite a relatively good safety profile (side effects are likely a result of coating material rather than iron oxide per se), use of SPIONs has failed to meet initial expectations and only a select number of agents are still on the market due to poor clinical uptake and low sensitivity/specificity for intended purpose (Smith & Gambhir, 2017).

MRS is a clinically useful tool for studying a range of diseases including brain tumors, Alzheimer's disease and seizures. MRS has also been applied to neuroinflammatory diseases, most notably MS. While inflammatory molecules are not directlty detected, metabolite levels can inform on the severity and clinical stage of the disease, as reviewed in detail by Chang, Munsaka, Kraft-Terry, and Ernst (2013).

2.5.2. Pre-clinical use and in-human trials

Human studies using contrast MRI in the context of measuring inflammation are limited and all have utilized passive uptake of USPIOs/SPIOs by macrophages. Since these studies depend on T2* contrast changes of iron concentrations within the tissue, either as a result of the EPR effect and/or macrophage uptake, they don't meet the criteria of true molecular imaging. Despite this, the use of SPIONs appears an attractive option for imaging inflammation, particularly in disease states such as atherosclerosis, RA and IBD, where macrophages are a key component of the involved pathologic lesion, allowing either passive uptake via phagocytosis or active targeting to macrophage surface receptors. Readers are referred to reviews by Jin, Lin, Li, and Ai (2014) and Neuwelt et al. (2015) which cover the use of SPIO passive imaging by MRI. To our knowledge, there are no in-human trials currently taking place in the context of inflammation that utilse the other forms of MRI described above. Although several trials involving ^{19}F-MRI are underway, particularly in relation of cystic fibrosis, the focus of these trials is not on the inflammatory components of the disease. CEST agents based around glucose detection are in early clinical trials for oncology but as of yet, are not designed for measuring inflammation.

There are, of course, a multitude of studies in animal models, utilizing passive SPIOs/USPIOs and ^{19}F-PFCs to quantify inflammation via macrophage uptake, particularly in the context of atherosclerosis but what follows will only be a review of key pre-clinical work that employ active molecular targeting of MRI compatible imaging agents to keep within the remit of our discussion. Direct targeting of SPIOs via modifications with ligands such as antibodies, aptamers and peptides allows MRI to be used to monitor SPIO binding/uptake at the site of disease, improving signal to noise and diagnostic capability. Key molecules of interest in this area of research have been adhesion molecules including the selectins (P- and E-selectin), vascular cell adhesion molecule-1 (VCAM-1) and intercellular adhesion molecule-1 (ICAM-1), all of which are upregulated on endothelial cells in inflammatory conditions such as atherosclerosis, MS and stroke and are some of the earliest biomarkers signifying cellular inflammation/activation, even before other pathological signs are evident. A summary of targeted MRI studies can be found in Table 1. ^{19}F-PFCs containing chelated gadolinium targeted to fibrin were first validated by Morawski et al. (2004) in human carotid endarterectomy samples (areas of atherosclerotic plaque) at 4.7-T allowing detection of the thrombus via the targeted localized ^{19}F signal and associated anatomical details via the T1 signal from gadolinium. Furthermore, the ^{19}F signal was intense enough to allow spectroscopic quantification of the bound ^{19}F, a proof of concept that demonstrated that multiple configurations of ^{19}F-PFCs, each with distinct spectroscopic profiles, could be used to target multiple biomarkers (Morawski et al., 2004). CEST has found research use in detecting enzyme activity, metabolic function (e.g. glucose utilization), hypoxia, neurotransmitter (glutamate) levels, ion concentration and pH (Sinharay & Pagel, 2016). The large concentrations required of either endogenous or exogenous CEST compatible agents would seemingly limit its usefulness in imaging inflammation. Despite this limitation, glutamate, which is amenable to CEST MRI is elevated in inflammatory brain disorders such as MS and amyotrophic lateral sclerosis (ALD). Results have shown that CEST MRI brain images of glutamate (Glu-CEST) distribution align with PET images (Cai et al., 2012) at 7-T, showing the potential for CEST to indirectly measure inflammation in neurological disease. Moreover, in animal models of Alzheimer's disease, Glu-CEST can differentiate diseased areas from non-diseased areas (Haris et al., 2013). GAGs in cartilage are also detectable by CEST imaging allowing the tracking of joint cartilage changes in human subjects (Ling, Regatte, Navon, & Jerschow, 2008; Schmitt et al., 2011). ParaCEST imaging agents have been combined with ^{19}F-PFCs to offer improved sensitivity and quantifiable targeting of NPs. The use of NP sized formulations has greatly increased the potential of paraCEST, specifically the development of lanthanide containing liposomes (lipoCEST) designed to improve the sensitivity of the system down to the nM level (Flament et al., 2013). A key advantage of CEST based MRI is the ability to image two or more imaging tracers in one scan (duplexing), provided the CEST agents display good sensitivity and have sufficiently different resonance frequencies of their mobile protons (Castelli, Terreno, Longo, & Aime, 2013). This has been demonstrated to be feasible for lipoCEST agents in a proof of concept study using local injection of non-targeted contrast agents into the thigh muscle of a mouse with clear discrimination of the two contrast agents visible on the scans (Terreno et al., 2008). LipoCEST agents have also been functionalized with targeting ligands. This was first attempted by Flament et al. (2013) using $\alpha_v\beta_3$ (integrin present on new forming blood vessels) targeted lipoCEST NPs in a mouse tumor model and although some non-specific binding was observed, it is a starting point towards developing more refined lipoCEST agents which would be desirable given their higher level sensitivity along with the inherent multiplexing capacity of CEST.

The major use of hyperpolarized MRI has been to use ^{13}C- containing compounds such as pyruvate for imaging metabolic pathways as the ^{13}C is passed down through metabolites allowing fast imaging of the metabolic state of the target tissue. Recently, the use of [1-^{13}C] pyruvate imaging in the heart has shown promise for the detection of cardiac inflammation. Lewis et al. (2018) discovered that the metabolism of [1-^{13}C] pyruvate to [1-^{13}C] lactate in infarcted murine and porcine hearts was the result of an increased rate of glycolysis in activated monocytes/macrophages, which was linked to IL-1β release. Thus, hyperpolarized MRI may offer a novel method for imaging inflammation following myocardial infarction (Lewis et al., 2018). ^{13}C-pyruvate has also been researched to detect inflammation through increased metabolism in animal models of arthritis (MacKenzie et al., 2011) and MS (Guglielmetti et al., 2017).

In addition to MS, significant data exists in human studies to demonstrate that MRS can detect metabolic changes indicative of Alzheimer's disease and precursor conditions such as mild cognitive impairment. As the major detectable metabolite in neurons, low NAA can be associated with loss of neuron viability/density while conversely, elevated myo-inositol is a biomarker of glial cell activation/proliferation and these two changes have repeatedly been demonstrated in the brains of Alzheimer's patients (Rami et al., 2007; Zhu et al., 2006). Reduced choline concentration, as an adjunct to NAA and myo-inositol analysis, may also increase sensitivity to brain changes associated with cognitive decline (Tumati, Martens, & Aleman, 2013).

2.5.3. Theranostics

MRI has many features that make it a useful theranostic tool such as good spatial resolution, body wide imaging and a diverse group of combinable carriers and contrast agents that can be adapted to each theranostic application. A recent promising example of iron oxide targeted theranostic NPs was in the context of acute graft rejection. Guo and colleagues utilized CD3 (T cell specific receptor) targeted iron oxide NPs that also contained a therapeutic gene. Both in vitro and in vivo, using a rat heart transplant approach, the authors successfully delivered the gene to T cells, thus reducing the T cell mediated destruction of the transplanted heart with MRI being utilized to monitor the T cell accumulation via the uptaken iron oxide NPs. The effect was shown to be specific to CD3 targeted gene carrying NPs, results confirmed by NIRF imaging (Guo et al., 2012). In the work by Myerson, He, Lanza, Tollefsen, & Wickline, 2011, PFCs targeted to thrombin via an anti-thrombin agent was a novel development whereby the thrombin inhibitor, PPACK, irreversibly binds to thrombin on the clot surface, thus inhibiting thrombin activity (Myerson et al., 2011). Given the low toxicity of PFCs in humans (Palekar, Jallouk, Lanza, Pan, & Wickline, 2015), it is conceivable that targeted PFCs containing ^{19}F substituted atoms and/or Gd^{3+} chelates could be a viable non-invasive tool for delivering and monitoring efficacy of anti-inflammatory drugs targeted to disease specific molecules that show relatively high abundance such as fibrin. CEST and paraCEST agents are being developed and tested preclinically using drug loaded liposomes, to track and monitor drug delivery, mostly in the field of oncology (Castelli, Boffa, Giustetto, Terreno, & Aime, 2014). Proof of concept for monitoring the delivery of anti-inflammatories or modulating inflammatory conditions is lacking.

2.5.4. Advantages and barriers to clinical translation

Iron oxide-based agents, having already been approved for human use, have one less barrier to novel uses for in-human imaging. Rather disappointingly, however, several previous iron oxide-based imaging agents have been discontinued due to poor performance or safety issues, with only Ferucarbotran (Resovist®) retaining use as an MRI contrast agent in a few countries. This leads to a requirement for new agents to be developed if T2 MRI molecular imaging is to be adopted more broadly in a clinical setting. Technical issues associated with USPIO molecular imaging that require to be overcome include low signal to noise ratio, poor specificity associated with ability to clearly discriminate signal between tissue locations, long imaging times and the challenge of standardizing conditions between scans due to patient position and magnetic field discrepancies (Ruehm, Corot, Vogt, Kolb, & Debatin, 2001; Sadat et al., 2014; Schmitz et al., 2000). PFCs, which

dominate the pre-clinical and early phase ^{19}F human trials are strong candidates for regulatory approval due to relatively good biocompatibility, biodistribution and favorable toxicity compared with other contrast agents in clinical use. Indeed, PFCs may be safer for human use than metal-based contrast agents (Palekar et al., 2015). Future studies will need to determine if localized ^{19}F is detectable in human patients at a tolerable administered dose of ^{19}F-PFC NPs. These prospects will be improved by wider clinical adoption of 7-T MRI which allows higher sensitivity detection of ^{19}F (Schmieder, Caruthers, Keupp, Wickline, & Lanza, 2015). CEST agents can be utilized in NP formulations to boost sensitivity although most of these studies have only been at the in vitro level. In vivo comparisons of lipoCEST agents with T1 and T2 based liposomes have shown that the CEST signal is more transient due to accumulation in subcellular compartments of macrophages which suppresses the CEST signal. Hyperpolarized MRI was designed to overcome the limitations of ^{1}H or ^{19}F based MRI with profound increases in sensitivity possible. At present, only a few molecules incorporating hyperpolarized nuclei such as ^{13}C have been tested in vivo and have focused on metabolic molecules as markers of tumor progression or inflammation (not dissimilar to the use of ^{18}F-FDG in PET imaging). The main limitation of hyperpolarized MRI to date has been the transient nature of the hyperpolarized state, making practical use of the technology problematic. Despite this, proof of concept studies have shown that NPs composed of a hyperpolarized ^{29}Si nuclei can be imaged for over 40 min following injection in mice and with low toxicity (Cassidy, Chan, Ross, Bhattacharya, & Marcus, 2013), indicating the potential for future advances towards wider imaging applications.

MPI is a new technology only developed in 2005, thus current deployments center around limited numbers of small pre-clinical scanners designed for rodent sized imaging (Panagiotopoulos et al., 2015; Saritas et al., 2013). The current state of MPI remains as 'a promising technology' that can take the best aspects of MRI and improve on this with better sensitivity, higher temporal resolution and easier interpretation of scans due to the signal intensity correlating with the iron oxide loaded NPs, without any background signal. Since MPI produces no anatomical detail, it will likely be combined with other modalities with combined MPI/MRI imaging already tested for imaging the heart and vasculature (Kaul et al., 2015). Clinical concentrations of Resovist have shown to be suitable for in vivo MPI imaging (Weizenecker, Gleich, Rahmer, Dahnke, & Borgert, 2009) and the development of new SPIONs tailored to MPI use should greatly increase performance and facilitate the clinical testing of MPI as a highly sensitive, fast, quantitative vascular, cellular and potentially molecular imaging tool (Vaalma et al., 2017).

2.6. Nuclear imaging (PET/SPECT)

Like CT and MRI, nuclear imaging offers the ability to image the entire dimensions of the human body. Together, PET and SPECT form the cornerstone of nuclear imaging. PET/SPECT are attractive options for molecular imaging owing to their non-invasive nature and high sensitivity (10^{-10}–10^{-11} M for SPECT and (10^{-11}–10^{-12} M for PET) (Stendahl & Sinusas, 2015). High levels of sensitivity allow reductions in the dosage of contrast agents, which is critical when the contrast agent is radioactive or otherwise toxic. At the center of clinical PET imaging is ^{18}F-FDG, a glucose analogue that is metabolized by metabolically active cells. Tumor cells are highly metabolically active. They undergo rapid rates of division which increases demand for glucose in addition to actively inducing angiogenesis. Increased glycolysis is also a feature of the immune system following activation. This is most evident for those immune cells that can participate in phagocytosis such as macrophages and neutrophils. Therefore, ^{18}F-FDG can be used to identify areas of macrophage activation/accumulation. ^{18}F-FDG sits at the boundary of molecular and metabolic imaging, offering high sensitivity detection (although this is frequently associated with poor signal to noise due to non-specific uptake by healthy cells, particularly cardiomyocytes). PET has also seen numerous radiolabeled small molecules being developed that can be targeted to various inflammatory molecules (Fig. 1) to provide more information on the tissue state than simple energy use. Since PET/SPECT lack anatomical details, to enhance localization and improve diagnostic sensitivity, nuclear medicine modalities are commonly combined with CT in hybrid imaging systems which can provide high resolution anatomic details to be superimposed on the PET/SPECT image. PET/SPECT can also be combined with MRI for similar purposes due to the high soft tissue contrast obtained by MRI.

2.6.1. Clinical use

^{18}F-FDG is routinely used in the clinic within the field of oncology, both to locate the presence of tumors, disease staging and to assess shrinkage of tumors in response to treatment; however, ^{18}F-FDG-PET is also increasingly being used for non-oncological purposes in fields covering CVD (Pelletier-Galarneau & Ruddy, 2019), neurology, infection and inflammatory disorders (Zhuang & Codreanu, 2015). Here, we will only summarize clinical use pertaining to inflammatory diseases. ^{18}F-FDG PET is used for monitoring disease in cardiac sarcoidosis patients (Glaudemans et al., 2013). ^{18}F-FDG PET is useful where MRI may be contraindicated due to implanted cardiac devices. A further advantage of PET in this context is more accurate diagnosis and the identification of disease in extra-cardiac sites such as the liver, bone and spleen (Patel, Gunasekaran, Goettl, Sweiss, & Lu, 2017) which may be missed by MRI due to a narrow view window. Identifying the disease in other organs other than the heart will allow more accurate staging and to initiate treatment accordingly. Other inflammatory conditions including vasculitis are also imaged in the clinic; this is an increasingly common use of PET but requires the operator to be trained in the specific protocols related to this particular pathology (Hautzel, Sander, Heinzel, Schneider, & Muller, 2008). Due to the poor spatial resolution of PET, imaging of vasculitis is restricted to large caliber arteries such as the aorta but imaging of smaller arteries (usually 1 st order aortic branches) is possible if the camera has sufficient resolution (≤ 2.5 mm) allowing differentiation of inflammatory vascular conditions such as giant cell arteritis (GCA), Takayasu's arteritis (TA), and polyarteritis nodosa (PAN) (Glaudemans et al., 2013). Although some encouraging results have emerged from studies using a small number of patients, there is currently insufficient evidence to justify the routine clinical use of ^{18}F-FDG in RA, pancreatitis, IBD, tuberculosis and osteomyelitis. In 2013, combined guidelines from the European Association of Nuclear Medicine (EANM) and the Society of Nuclear Medicine and Molecular Imaging (SNMMI) were published for the use of FDG-PET in inflammation and infection, outlining the clinical evidence (or lack off) for the justification of ^{18}F-FDG in imaging inflammation (Jamar et al., 2013). Readers can refer to this document for a more detailed account of the many issues and criteria that must be addressed/overcome for ^{18}F-FDG to be recommended as a tool to improve clinical diagnosis. It is also worth noting how few the inflammatory disease states are that the EANM and SNMMI consider having sufficient evidence to warrant clinical ^{18}F-FDG imaging. For now, at least, ^{18}F-FDG-PET in the clinic is still primarily a tool for oncologists.

2.6.2. Pre-clinical use and in-human trials

Although ^{18}F-FDG is employed as a diagnostic tool in inflammatory vasculitis conditions, it is not employed clinically to diagnose atherosclerosis, heart attack or stroke. This is despite atherosclerotic plaques being inadvertently detected in patients undergoing scans for cancer and a number of studies indicating potential clinical value as will now be outlined. A widespread assessment of the likelihood of a person developing CVD is called the Framingham risk score (FRS), originally introduced in 1998 and updated in 2008. Interestingly, an assessment of 1181 asymptomatic subjects administered ^{18}F-FDG to measure carotid plaque uptake via PET indicated that persons with elevated plaque uptake of ^{18}F-FDG had an increased chance of an elevated FRS of 10% or more (Odds ratio: 1.9) (Noh et al., 2013). Retrospective studies using ^{18}F-FDG have also demonstrated that this method independently

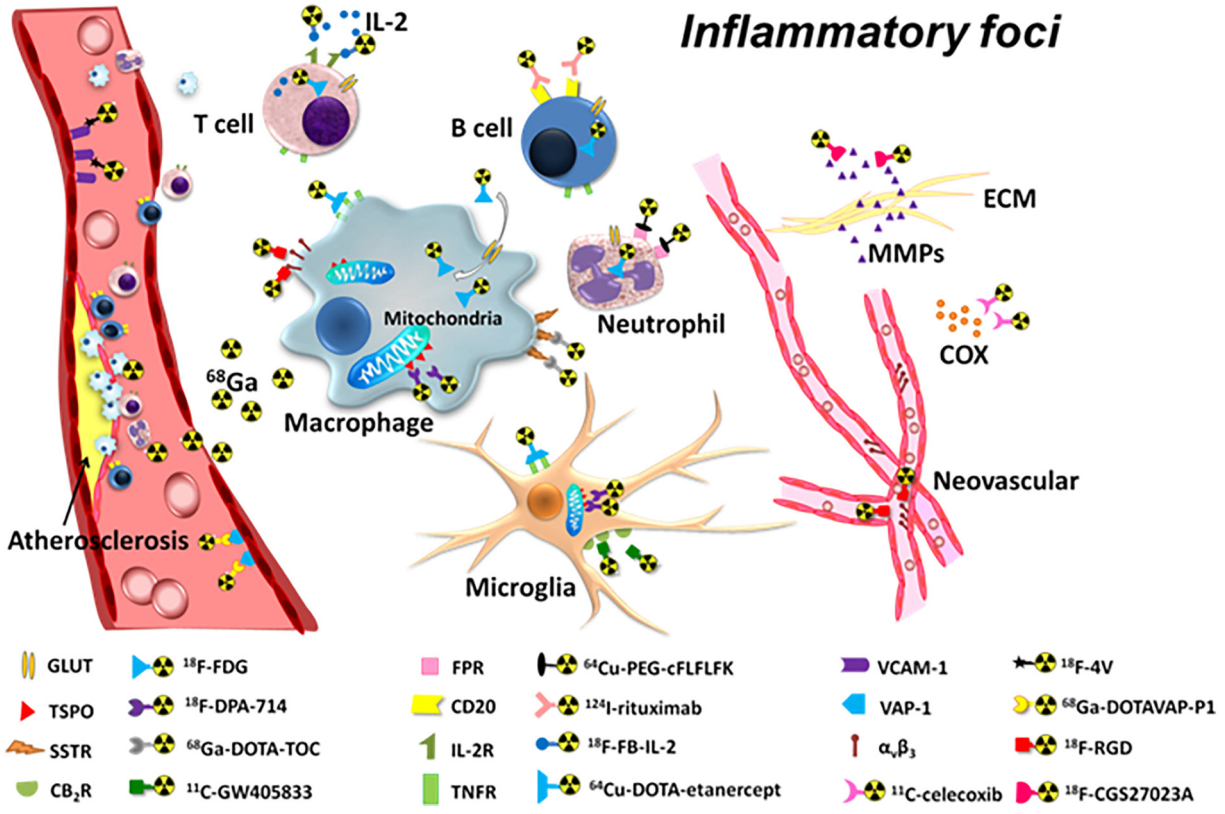

Fig. 1. Selected examples of PET imaging biomarkers related to inflammation. Reprinted from Wu et al. PET imaging of inflammation biomarkers. Theranostics. 2013;3:448–66 (Wu, Li, Niu, & Chen, 2013). Distributed under a Creative Commons Attribution (CC BY-NC) license.

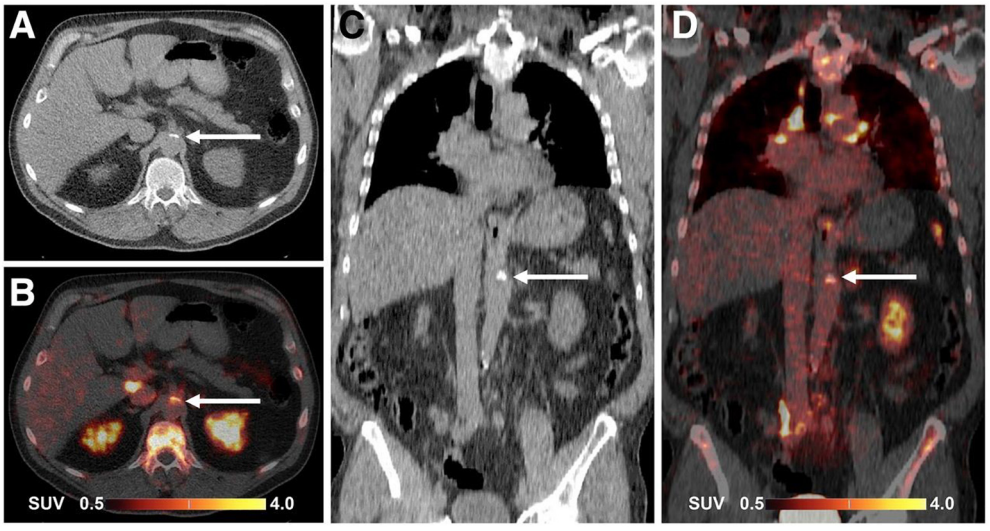

Fig. 2. ^{68}Ga-pentixafor PET/CT images of abdominal aorta in 64-y-old man. CT (A and C) and PET/CT (B and D) images in transaxial (A and B) and coronal (C and D) views show ^{68}Gapentixafor uptake in calcified atherosclerotic lesion (arrows) coincident with calcification. Figure and figure legend reprinted from Weiberg et al. Clinical Molecular Imaging of Chemokine Receptor CXCR4 Expression in Atherosclerotic Plaque Using (68)Ga-Pentixafor PET: Correlation with Cardiovascular Risk Factors and Calcified Plaque Burden. J Nucl Med. 2018;59:266–272. Copyright of the Society of Nuclear Medicine and Molecular Imaging (SNMMI).

predicts CVD risk, even beyond that predicted by FRS (Figueroa et al., 2013). Furthermore, ^{18}F-FDG PET/CT has been employed in human patients to detect symptomatic carotid atherosclerosis (Rudd et al., 2002). One final example where ^{18}F-FDG-PET can have predictive power in CVD is in predicting recurrent stroke. ^{18}F-FDG-PET imaging of carotid artery inflammation in prior stroke patients predicts the recurrence of cerebrovascular stroke, independent of other factors (Marnane et al., 2012). These studies and others highlight the potential of ^{18}F-FDG-PET as a stand-alone tool for assessing atherosclerosis associated inflammation and plaque severity and can yield good signal to noise ratios with little background from healthy arterial walls. This raises hope that by targeting glucose metabolism as an indirect measure of inflammation, PET could also act in co-ordination with classical arterial angiograph methods to guide surgical and pharmacological

intervention. There are several co-morbidities that act to increase the risk of developing CVD. One such disease is psoriasis (Brauchli, Jick, Miret, & Meier, 2009; Prodanovich et al., 2009). Using ^{18}F-FDG-PET, Naik et al., 2015 demonstrated that psoriasis patients with no history of CVD had increased aortic ^{18}F-FDG uptake which increased proportionally with the severity of psoriasis. Therefore, ^{18}F-FDG-PET could be an early diagnostic tool in psoriasis patients for detecting the vascular inflammatory changes that may signify the onset/progression of atherosclerosis. A similar increase in vascular inflammation has also been observed in RA patients, a disease associated with ~50% enhanced CVD risk (Rose et al., 2013).

Several studies have employed ^{18}F-FDG-PET to measure response to anti-inflammatory therapies. To date, there are five classes of drugs used to treat CVD where both clinical endpoint and PET imaging are available. Clinical trial endpoints have shown positive for two classes of treatments (statins and thiazolidinediones) which correlated with ^{18}F-FDG-PET findings of vascular inflammation (Osborn, Kessinger, Tawakol, & Jaffer, 2017). The ability to measure specific pathogenetically related outcomes rather than awaiting clinically significant CVD events improves time and cost of trials, as well as patient safety in case of ineffective treatments. Therefore, ^{18}F-FDG-PET can be used to not only detect inflammation in the primary disease but to assess cross-disease risk, monitor disease progression and even monitor response to therapy.

The use of radiolabeled metabolic precursors is not limited to ^{18}F-FDG. Choline, a molecule involved in the synthesis of cell membranes is taken up by rapidly proliferating cells (such as macrophages during inflammation) and has been utilized for PET as either ^{18}F-choline or ^{11}C-choline. A feasibility study in humans showed the potential of imaging vascular changes associated with CVD using ^{18}F-choline (Bucerius et al., 2008) and this molecule is currently undergoing further evaluation in human trials (ClinicalTrials.gov identifiers: NCT01899014 and NCT02640313).

While Technetium-99 m (^{99m}TC) and ^{18}F-FDG remain central to current nuclear imaging, pre-clinically, a multitude of novel targeted radiolabeled tracers have been developed, many of which target inflammatory molecules (Fig. 1). Table 2 provides a summary of the most important pre-clinical studies utilizing PET and SPECT imaging agents targeted to inflammatory biomolecules. Although, both the clinical and pre-clinical nuclear imaging landscape is dominated by small molecule tracers, NPs conjugated to or containing a core of radiolabeled tracers have been developed. ^{99m}Tc radiolabeled NPs are commonly used in SPECT imaging and usually consist of sulphur colloids ranging from 10 to 1000 nm in diameter. Indeed, with the exception of iron oxide-based NPs used in MRI, ^{99m}Tc labeled colloid NPs remain the only clinically approved NPs for diagnostic imaging (Thakor et al., 2016). Gold NPs conjugated with ICAM-1 targeted antibodies show enhanced gamma ray production in the joints of arthritic rats (Shao et al., 2011). Since ICAM-1 is an early indicator of inflammation in arthritis, this is a key target of interest that could aid early diagnosis in RA in addition to other chronic inflammatory conditions. The first in human testing of a targeted radiolabeled NP has taken place in melanoma patients (Phillips et al., 2014; ClinicalTrials.gov: Identifier: NCT01266096). A more relevant development has been the first receptor-targeted NP agent for cardiovascular imaging approved for clinical trials. The imaging agent (^{64}Cu-25%-CANF-Comb), a 16 nm copolymer based NP that targets natriuretic peptide receptor C (NPRC)- which is upregulated on atherosclerotic plaques- and has completed an early phase 0 biodistribution and safety trial (ClinicalTrials.gov: Identifier: NCT02498379) with a phase 1 trial now ongoing to demonstrate the use of this NP PET agent for identifying atherosclerotic plaques in the carotid arteries via PET/MR (ClinicalTrials.gov: Identifier: NCT02417688). Alternatively, targeted NP based approaches in atherosclerosis are being developed in animal models with CCR5 (chemokine receptor upregulated on atherosclerotic plaques that facilitates immune cell entry into the vessel wall) targeted NPs showing promise in imaging disease in apoE$^{-/-}$ mice (Luehmann et al., 2014).

2.6.3. Theranostics

Direct use of radiolabeled tracers as therapeutic agents in themselves has focused on harnessing the radiolabel to induce cell death in the context of cancer. This involves exchanging the diagnostic gamma or positron emitting radiolabel with a beta emitter. To date, this process has mainly focused on targeting somatostatin receptors (SSTRs) on neuroendocrine tumors where peptide binding to the tumor cells induces internalization of the ligand/radiolabel and accumulation of the beta-emitting isotope, leading to destruction of the tumor cells (van Essen et al., 2009). Alpha emitting isotopes incorporated into tumor-targeted antibodies have also been tested clinically for a variety of cancers due to their highly destructive localized effects (Dekempeneer et al., 2016). Such approaches are unlikely to achieve such a disease specific cell/inflammatory target that would cause a beneficial therapeutic outcome without negative systemic effects on the immune system as a whole, since disease-specific cells/molecules would not be sufficiently localized for a targeted killing.

2.6.4. Advantages and barriers to clinical translation

PET has revolutionized the ability to non-invasively detect malignancies in the body. Great strides have been taken in terms of hardware and data processing to lower radiation dose, improve resolution and combine the major strength of PET (high sensitivity) with the anatomic resolution available from MRI and in particular CT. Despite these advancements, the development pace of PET in terms of expanding beyond ^{18}F-FDG and oncology has been slow. Over 95% of all clinical PET scans are ^{18}F-FDG scans (Goel, England, Chen, & Cai, 2017) and the vast majority are for oncology. Chemistry is not the bottleneck in PET tracer development with a variety of small ligands being radiolabeled and tested to varying degrees in the pre-clinical setting. Indeed, an inspection of the clinical trials database reveals that between 2005 and 2015, there were actually more oncology trials using non ^{18}F-FDG tracers ($n = 288$) than using ^{18}F-FDG ($n = 231$). The non ^{18}F-FDG trials tended to be registered later (2010–2015), be phase 0–2 and involve a smaller number of participants (Chen et al., 2017). This indicates the rapidly expanding area of targeted PET imaging. As outlined above, ^{18}F-FDG-PET imaging has proof of concept in detecting inflammation in CVD patients, to aid prognostic decision making and even to evaluate novel therapies. An important limitation of ^{18}F-FDG-PET, however, is its poor performance in reliably detecting ^{18}F-FDG in coronary arteries, blockages of which are the principal cause of heart attacks. Creation of accurate cardiac images also suffers from motion artifacts and partial-volume effects (Petibon et al., 2017). Moreover, ^{18}F-FDG-PET is only a gross readout of inflammation, focused on a single parameter, namely energy use, providing no information on the phenotype of the cells from which the increased FDG use is derived from.

For targeted PET beyond FDG, several considerations need attention. The first is the suitability of the tracer. It should possess high potency and specificity for the biomarker of interest to provide good signal to noise and minimize radiation exposure. The use of new radiolabeled tracers also requires on-site facilities with automation of manufacturing, a process which may well be challenging and costly due to complex synthesis protocols. The high costs associated with PET tracer synthesis as well as the installation and maintenance of PET scanners frequently results in PET research being confined to specialized well-funded institutions with a historical focus on a particular area of research, most usually in oncology. These high startup costs and lack of access to novel PET tracers can severely restrict research in novel areas and the progress towards clinical translation. Table 3 summarizes many of the key obstacles that may hamper the translation of PET ligands into the clinic.

Table 2
Key examples of inflammatory biomarkers targeted by radiolabeled small molecules.

Target	Tracer(s)	FDA/CE approved (commercially available)	Disease(s) and study type	Comments	Reference(s)
Somastatin receptor (SSTR)	^{68}Ga- DOTATATE (PET)	Approved for detection of SSTR containing neuroendorine tumors (Yes)	Atherosclerosis (clinical)	^{68}Ga-DOTATATE offers superior coronary imaging, excellent macrophage specificity and better power to discriminate high-risk versus low-risk coronary lesions than ^{18}F-FDG	Tarkin et al., 2017
Translocator protein (TSPO)	^{11}C- and ^{18}F- labeled PK11195 or structurally similar molecules (PET)	No (Yes)	Vasculitis (clinical)	Visualized macrophages in inflamed artery walls	Lamare et al., 2011
			Stroke (clinical)	Detected microglial activation in the brains of stroke patients	Gulyas et al., 2012
	^{125}Iiodo-DPA-713 (SPECT)	No (No)	Alzheimer's (pre-clinical)	Constant increase in uptake in brain regions displaying progression of Alzheimer's disease in a mouse model	Maeda et al., 2011
VCAM-1	^{18}F-4V (PET) ^{99m}Tc-cAbVCAM1–5 peptide	No (No)	Atherosclerosis and myocardial infarction model (pre-clinical)	Used in apoE$^{-/-}$ mouse models of atherosclerosis to target plaque with increased uptake at plaque sites.	Nahrendorf et al., 2009
	^{99m}Tc-B2702p1 nanobody (SPECT)	No (No)		^{99m}Tc-peptide and nanobody targeted molecules show higher affinity than ^{18}F-4V	Broisat et al., 2012 Dimastromatteo et al., 2013
Vascular adhesion protein 1 (VAP-1)	^{68}Ga-DOTAVAP-1 and structurally similar molecules	No (No)	Tumor bearing animal model in association with inflammation (pre-clinical)	^{68}Ga-DOTAVAP-1 can show better discrimination of inflammation versus, for example, tumor cell uptake, while ^{18}F-FDG fails to separate the signal source	Autio et al., 2010
	^{68}G-DOTA-Siglec-9 (PET)	No (No)	Atherosclerosis (pre-clinical)	PET signal was specifically increased in atherosclerotic aorta and could be attenuated by blocking VAP-1	Silvola et al., 2016
$\alpha_v\beta_3$ integrin	^{18}F-RGD	No (No)	Atherosclerosis (clinical)	^{18}F-RGD showed specific uptake in human carotid vessels that displayed narrowing (stenosis) but not in contralateral healthy vessels. Results correlated with macrophage density and blood vessel formation	Beer et al., 2014
	^{18}F-flotegatide	No (No)	Atherosclerosis (pre-clinical)	^{18}F-flotegatide, a more easily manufactured tracer than ^{18}F-RGD, is readily imaged in the plaques of atherosclerotic mice with signal intensity correlating with macrophage infiltration and integrin expression	Su et al., 2014
	^{18}F-fluciclatide (PET)		Myocardial infarction (clinical)	^{18}F-Fluciclatide uptake is increased at sitesof recent MI acting as a biomarker of cardiac repair andpredicting regions of recovery	Jenkins et al., 2017
Cathepsin A	^{64}Cu-BMV101	No (No)	Atherosclerosis (pre-clinical)	Could non-invasively image activated macrophages directly releasing plaque-destabilizing compounds. Also developed optical fluorescent cathepsin probes for optical imaging	Withana et al., 2016
Matrix Metalloproteinases	^{123}I or ^{125}I-CGS 27023A	No (No)	Atherosclerosis (pre-clinical)	Allows visualization of plaque formation in mouse models	Fujimoto et al., 2008
	^{99m}Tc-RP-805 (SPECT)				Ohshima et al., 2009
Lectin-like oxidized LDL receptor-1 (LOX-1)	^{99m}Tc-LOX-1-mAb	No (No)	Atherosclerosis (pre-clinical)	^{99m}Tc-LOX-1-mAb antibody was found to effectively target macrophage dense atherosclerotic lesions in hyperlipidemic rabbits	Ishino et al., 2008
	^{111}In-liposome–LOX-1 antibody-DiI (SPECT)	No (No)		^{111}In-liposome–LOX-1 antibody-DiI (a liposome encapsulated LOX-1 antibody) Shown to selectively bind to plaque shoulder – an area frequently associated with plaque rupture in humans – in two murine models of atherosclerosis	Li et al., 2010
CD20	^{124}I-rituximab (PET)	No (No)	RA (clinical)	5 RA patients were treated with B cell specific ^{124}I-rituximab imaging agent. B cells were detected within the joint, but the clinical significance based on such a small cohort is unclear	Tran et al., 2011
IL-2 receptor	^{18}F-FB-IL-2(PET)	No (Yes)	Mouse tumor model (pre-clinical)	Proved useful in monitoring T cell infiltration into tumors as a response to chemotherapy. Potential to guide therapeutics	Hartimath et al., 2017
GPIIb/IIIa	^{18}F-GP1 (PET)	No (Yes)	Model of arterial injury (pre-clinical)	Strong signal observed specifically in areas of arterial injury associated with thrombus formation in primates.	Lohrke et al., 2017
			Thrombosis (clinical)	Completed phase 1 clinical trial for imaging thrombosis (ClinicalTrials.gov Identifier: NCT02864810)	
P2X purinoceptor 7	^{18}F-EFB (PET)	No (No)	Systemic rat model of	^{18}F-EFB is the first P2X7 receptor ligand to cross	Fantoni et al.,

(continued on next page)

Table 2 (*continued*)

Target	Tracer(s)	FDA/CE approved (commercially available)	Disease(s) and study type	Comments	Reference(s)
(P2X7 receptor)			inflammation (LPS injection) (pre-clinical)	the blood-brain barrier and was detected in the brains of rats injected systemically with LPS. This opens new avenues for exploring an important marker of neuroinflammation in the brain	2017
CXCR4	^{68}Ga-pentixafor (PET)	No (No)	Atherosclerosis (clinical)	Patients with higher arterial binding of ^{68}Ga-pentixafor displayed more co-morbidities and history of CVD events	Li et al., 2018
			Atherosclerosis (clinical)	^{68}Ga-pentixafor arterial uptake was correlated with plaque severity, CVD risk factors and prior adverse CVD events (Fig. 2)	Weiberg et al., 2018
Mannose receptor	^{111}In-tilmanocept (SPECT)	Yes (for lymph node mapping) (Yes)	Atherosclerosis (pre-clinical)	Specific uptake of ^{111}In-tilmanocept was observed in the plaques of apoE$^{-/-}$ mice. Blocking mannose receptors attenuated signal intensity.	Varasteh et al., 2017
Receptor for advanced glycation end-products (RAGE)	^{64}Cu-Rho-G4-CML NP (PET/Optical)	No (No)	Hindlimb ischaemia (pre-clinical)	The use of a multi-modal NP (PET/optical) allowed whole body imaging in mice with the greatest concentrations found in the ischaemic hindlimb. The larger size of the NP may also allow a drug payload for therapeutic utility.	Konopka et al., 2018
IL-1β and CD11b	^{89}Zr-α-IL-1β and ^{89}Zr-α-CD11b (PET)	No (No)	IBD (pre-clinical)	Il-1β and CD11b (macrophage marker) were found to increase in a murine model of IBD with IL-1β levels correlating with disease severity. PET was able to out perform MRI and translation to humans may offer a non-invasive diagnostic tool in comparison with endoscopy.	Dmochowska et al., 2018
LFA-1	^{111}In-DOTA-butylamino-NorBIRT (DANBIRT) (SPECT)	No (No)	Atherosclerosis (pre-clinical)	SPECT/CT imaging of apoE$^{-/-}$ mice revealed the tracers were bound to CD68 macrophages and other LFA-1 expressing immune cells within the growing atheromas.	Meester et al., 2018

2.7. Acoustic imaging (contrast-enhanced ultrasound (CEUS))

US is an established medical imaging technology and one of the most used diagnostic modalities in the clinic. US is commonly used for abdominal, testicular, breast, neck and musculoskeletal examinations in its non-invasive form. US can also be applied to assess the status of blood vessels and determine the presence and gross morphology of atherosclerotic plaques and thrombus. Although this can be assessed non-invasively, improved invasive forms of US (IVUS) are being developed. IVUS uses a catheter-based approach for imaging the wall of blood vessels. It's high spatial resolution and ability to discriminate plaque components in a superior manner to invasive angiography has helped transform our understanding of atherosclerosis. IVUS can be thought of as a moderately high resolution (150–250 μm) morphological imaging tool, rather than a true molecular imaging tool. Therefore, a discussion of standard (non-contrast enhanced) IVUS here is not warranted. For true molecular imaging, as per all the techniques described so far, all forms of US require the use of contrast agents (contrast-enhanced ultrasound; CEUS). US contrast agents (UCAs) generate resonance reflection signals, which provide high signal to noise based on increased acoustic scattering properties. The most common contrast agents in US are gas filled microbubbles. Microbubbles have a size of 1–8 μM which confines their location to the circulation, making them excellent UCAs for imaging the vasculature, allowing visualization of micro-vessels normally hidden on standard Doppler US. In brief, microbubbles all share 3 properties: 1) a core containing a compressible and acoustically reflective gas; 2) a protective biocompatible coating (shell) and 3) a diameter of 1–8 μM allowing body wide vasculature perfusion. While microbubbles dominate the CEUS landscape, other nanoscale UCAs have been developed and are currently being investigated in pre-clinical research. These include echogenic liposomes (ELIPs), nanobubbles, nanodroplets and nanoparticles. The use of nanoscale UCAs opens up avenues to target molecules beyond the vessel wall, owing to their smaller size and ability to enter tumors or inflammatory sites through the EPR effect. Although less well tested, they can also be used as vehicles for drug delivery.

2.7.1. Clinical use

A number of microbubble UCAs have been developed and several are commercially available for clinical use and there now exists a long safety record of use in humans (Schinkel, Kaspar, & Staub, 2016). This high safety threshold is due to microbubbles being able to pass into the pulmonary circulation. After injection of microbubbles, imaging can begin after a few minutes. Following acoustic shattering of the microbubbles, the shell is safely removed via the reticuloendothelial system and the gases are released via the lungs (Schinkel et al., 2016). The clinically approved UCAs are all untargeted microbubbles that have found clinical use in improving US resolution of organ abnormalities (Guvener et al., 2017). US has also made dramatic advances in areas of inflammation medicine e.g. in the field of rheumatology – herein US together with power doppler is now used routinely to detect synovial inflammation, tendon damage/inflammation and even to provide preliminary evidence of bone erosion. Furthermore, the use of both non-contrast and CEUS for assessing gastrointestinal (GI) disorders including IBD is increasing within the clinic. US can detect structural changes in the bowel and surrounding mesentery indicative of inflammatory processes while the use of contrast agents enhances diagnostic sensitivity and the distinguishing features of focal inflammation in Crohn's disease (Kucharzik, Kannengiesser, & Petersen, 2017). Although US imaging of the GI tract can be more challenging than other organs due to the presence of gas artifacts, it can be a valuable, safer and more cost-effective method of GI imaging than other clinical modalities (Kucharzik et al., 2017; Muradali & Goldberg, 2015). No clinically approved use currently exists for molecular CEUS imaging.

2.7.2. Pre-clinical use and in-human trials

Although the clinical use of CEUS is yet to reach the level of molecular imaging, the first in-human clinical trial of targeted molecular ultrasound has now been completed (Willmann et al., 2017) and involved microbubbles (1.5 μM diameter, a perfluorobutane/nitrogen core, surrounded by a phospholipid shell) targeted to kinase insert domain receptor (KDR) (Abou-Elkacem, Bachawal, & Willmann, 2015), a key regulator of neoangiogenesis which is expressed on several cancers including ovarian and breast. The imaging agent was well tolerated by

Table 3
PET: Barriers from tracer design to clinical practice.

Cost	Expertise	Collaboration	Funding
• Tracer synthesis • Infrastructure • Scans • Maintenance	• Radiochemistry • GMP • Radiologists • Lack of PET uptake beyond core areas[a]	• Tracer development • Scanning protocols & data collection • Clinical-trial co-ordination • Lack of multi-discipline approaches (playing to strengths)[a]	• Challenging to secure for novel PET tracers[a] • Not considered a priority area by funding bodies[a] • Lack of clarity on which body has remit for funding[a]

[a] MRC Review of 'Positron Emission Tomography (PET) within the Medical Imaging Research Landscape', 2017.

40 patients and US molecular imaging showed good correlation with histological analysis of biopsy samples. Importantly, the safety profile of the trial (in which no patients withdrew due to side effects) was similar to that reported for a non-targeted UCA (BR38) (Schneider et al., 2011) indicating that the addition of targeting ligands may not substantially change the in vivo profile of the UCA. Pre-clinical imaging of CEUS in inflammatory conditions has produced some fruitful results with advances in detection, image processing and quantification using protocols based on the destruction-replenishment method and acoustic radiation force (ARF) imaging (Abou-Elkacem et al., 2015).

Adhesion molecules have been a keen area of exploration for targeted UCAs in inflammatory disease including IBD and atherosclerosis. We will now briefly consider each of these diseases in turn:

US could be employed alongside CT, MRI and endoscopy to offer earlier diagnosis and identify treatment responders from non-responders in the case of IBD where endoscopy is supplemented with medical imaging (particularly CT but also MRI). As an example, microbubbles targeted to adhesion molecules have been used in animal models of colitis, including the use of dual-targeted (P- and E-selectin) UCAs (Wang et al., 2013). This approach of dual-targeting adhesion molecules shows very close correlation with ex vivo histology in terms of grading the extent and stage of inflammation that could justify the clinical non-invasive use of CEUS for staging IBD and quantifying the inflammation present using a molecular imaging modality that offers greater speed and more tolerable contrast agents than CT and MRI. Moving this prospect closer to reality was the study by Wang et al., 2015 using the same clinical grade dual-targeted microbubble as used previously. In a porcine model of ileitis, the authors demonstrated the feasibility of using CEUS to detect intestinal inflammation (Fig. 3). The novelty of this approach was the use of a clinical US scanner on a large animal, an important step towards translating a quantitative molecular imaging approach for inflammatory bowel conditions into the clinic.

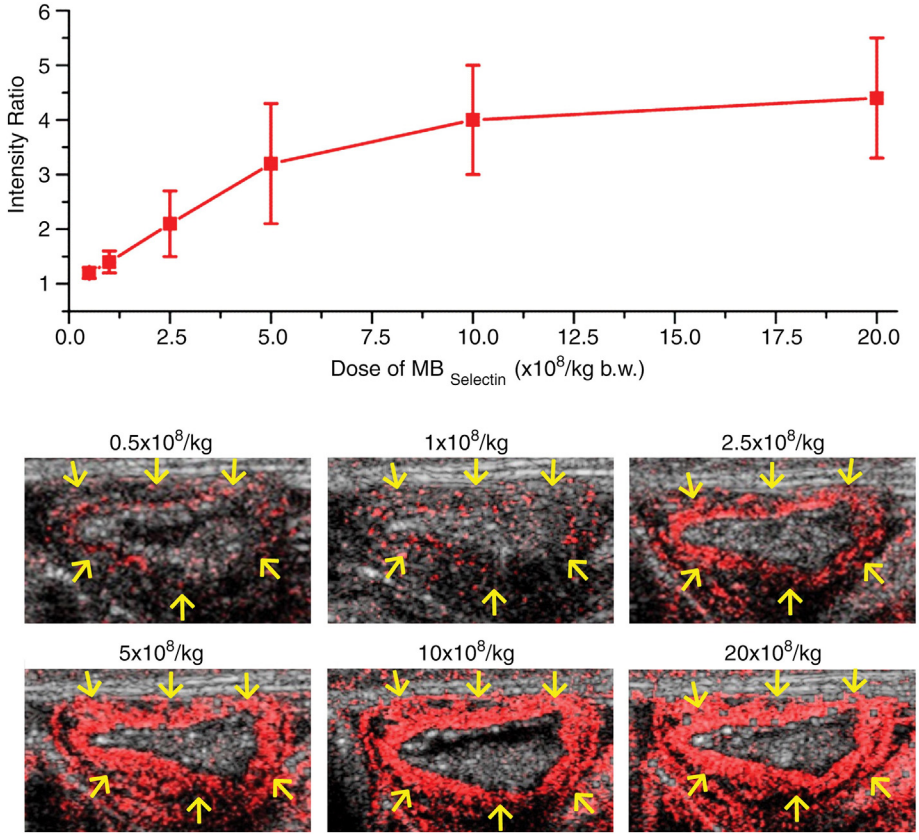

Fig. 3. Dose dependent increase in quantitative US signal in five pigs with ileitis. (a) Graph summarizes quantitative US signal intensities (represented as signal intensity ratios) observed in five pigs with acute terminal ileitis with increasing doses (0.5, 1.0, 2.5, 5.0, 10, and 20 × 10^8/kg) of dual-selectin–targeted contrast MBs (MBSelectin). b.w = body weight. (b) Representative transverse US images obtained six times in approximately the same location of an inflamed ileum segment (arrows) in one pig show increasing imaging signal (overlaid in red onto the anatomic B-mode images) with increasing MBSelectin doses. The different US scans were each separated by a 30-minute pause to allow contrast agent clearance. Figure and figure legend reprinted from Wang et al. Quantitative assessment of inflammation in a porcine acute terminal ileitis model: US with a molecularly targeted contrast agent. Radiology 2015;276:809–817. Permission granted by the Radiological Society of North America (RSNA®).

VCAM-1 presents early in atherosclerosis, being present on endothelial cells even before the first signs of plaque formation. VCAM-1 targeted microbubbles were able to evaluate the different stages of atherosclerosis in mice. Furthermore, reductions in VCAM-1 intensity could also be used as a marker of efficacy of statin therapy (Kaufmann, Lewis, Xie, Mirza-Mohd, & Lindner, 2007; Khanicheh et al., 2013). Other molecules to have been successfully targeted using microbubbles include ICAM-1 on inflamed endothelium (Wu et al., 2013) and platelet-endothelial cell interactions using microbubbles targeted against glycoprotein-Ibα (GPIbα) on platelets and von Williebrand factor (VWF) on endothelial cells (Shim et al., 2015), which may help in dissecting the role of platelets in the initiation of atherosclerosis and in the detection of thrombotic events in late stage pathology. In addition to detecting thrombotic events, CEUS may be used to monitor response to treatments that induce reduction in thrombus size/formation (thrombolysis) (Wang et al., 2012). Further information on the comparison of US with other modalities for imaging atherothrombosis has been described elsewhere (Wang & Peter, 2017). A recent advance in CEUS signaling employed the ARF technique mentioned above in mice. Not only is this method quantitative, it reduces imaging times substantially. Indeed, the use of VCAM-1 or P-selectin targeted microbubbles in a murine vascular inflammatory model resulted in significant detection of adhesion molecules in the abdominal aorta and an ability to discriminate mice with inflammation from control animals in just 180 s scanning time (Wang et al., 2017).

A final example of targeted microbubble US in inflammatory disease comes from myocarditis, an inflammatory heart condition not associated with ischemia. Endomyocardial biopsy is employed for diagnosis yet is an invasive procedure and has relatively poor diagnostic prediction. Microbubbles targeted to CD4+ T cells and inflamed endothelium (two hallmark inflammatory changes in myocarditis) have been used in a mouse model of the disease. In addition, a third microbubble targeted to a generic marker on all immune cells was also employed (Steinl et al., 2016). Using CEUS, the authors could detect increased signal from the targeted microbubbles in animals with moderate disease with signal increasing with disease severity. Furthermore, it was the first demonstration that targeted microbubbles could be used to detect CD4+ T cell infiltration into an inflammatory site (Steinl et al., 2016).

While the transcutaneous non-invasive CEUS studies above used targeted microbubbles as UCAs, most studies utilizing contrast enhanced IVUS have employed targeted perfluocarbon nanoemulsions or liposomes, rather than microbubbles. Studies have included the detection of ICAM-1 (Demos et al., 1999) and tissue factor (Lanza et al., 2000) in porcine atherosclerotic arteries. A more comprehensive study involved the use of liposomes conjugated to 5 markers of inflammation and thrombosis in an atherosclerotic swine model. IVUS imaging was performed at 20 MHz and results correlated well with post-mortem histological analysis. It should be pointed out that this was not a multiplexing experiment. Each liposome preparation had only one targeting ligand and each animal only received one liposome preparation (Hamilton et al., 2004). Nevertheless, these studies suggest that IVUS with targeted UCAs could be used to better detect and characterize vascular injury and atherosclerosis over standard non-contrast enhanced IVUS.

2.7.3. Theranostics

Therapeutic delivery of drugs via UCAs is an attractive option. Theoretically, a 3 μM wide microbubble could carry millions of proteins or small molecules and these carriers display favorable safety profiles, confirmed by their long history of clinical use. The next issues to address after safety are technical, such as ensuring delivery of the UCA to the intended site (such as via molecular targeting or EPR effect) and finally, release of the payload in a manner that is not destructive to the target tissue. The process most investigated for microbubble-based drug delivery is sonoporation. A detailed explanation of this process can be found in Castle et al., 2013. In brief, microbubbles undergo oscillation upon exposure to acoustic energy. At high amplitude exposure, these oscillations expand in intensity and the shell of the microbubble can rupture causing release of the core materials. This process can serve as the release mechanism for the drug. When an oscillating microbubble is in close proximity to a cell (such as bound via molecular targeting or forced near to the vessel wall by the ARF process), transient, reversible increases in the permeability of the cell membrane can occur due to the interaction of acoustic energy and the oscillating microbubble. When the pulse sequence is controlled, cells can undergo reversible permeability without loss of viability (Juffermans, Dijkmans, Musters, Visser, & Kamp, 2006). The use of US and microbubbles for therapeutic drug delivery has already progressed to human case studies and even clinical trials in the fields of cancer (Dimcevski et al., 2016) and for promoting drug delivery through the blood brain barrier (ClinicalTrials.gov Identifier: NCT02343991).

UCAs have also been employed as theranostic agents with a view to utilize them as carriers of thrombolytic drugs to thrombotic areas of the vasculature. In a swine thrombosis model, Culp et al., 2004 demonstrated that microbubbles tagged with the GP IIb/IIIa receptor inhibitor eptifibatide (a thrombolytic drug) caused clot dissolution in 6 of 8 pigs following transcutaneous US while 0 of 7 pigs treated with eptifibatide alone showed clot dissolution. It has been demonstrated that microbubbles passing over an intravascular thrombosis can induce dissolution of the clot when a high mechanical index US pulse is employed (Xie, Lof, Matsunaga, Zutshi, & Porter, 2009). An important development by Wang et al., 2016 involved the use of theranostic microbubbles for simultaneous detection, thrombolysis and monitoring of response via a single dual-conjugated microbubble. The microbubbles were conjugated firstly with the same novel single chain antibody directed against GP IIb/IIIa (Wang et al., 2012) along with urokinase plasminogen activator (a thrombolytic agent). These theranostic particles were utilized for US imaging in the carotid arteries of a mouse thrombosis model where they performed a multi-functional role in detecting thrombi, reducing thrombus size and acting as readout of the efficacy of the conjugated urokinase plasminogen activator. When compared with commercial urokinase alone, the microbubbles were just as effective but with a better safety profile owing to greatly reduced bleeding times compared with urokinase alone. This is significant as the increased risk of bleeding is often a contraindication against the use of urokinase and similar thrombolytic agents in many patients with myocardial infarction and stroke. US targeted microbubbles have also been employed in conjunction with liposome carrying drugs to improve local delivery via ultrasound induced cavitation. Sheng et al., 2018 demonstrated that liposomes loaded with basic fibroblast growth factor (bFGF) could be used to increase the delivery of bFGF to the kidney of diabetic rats and that tissue delivery of bFGF was enhanced in the presence of focal microbubble destruction within the kidney (causing greater drug permeability). This resulted in a reduction in inflammation and improvement of renal function. Such a dual approach can not only improve residence times of reagents such as bFGF, which otherwise have short circulating half-lives, but can also increase the uptake of drugs specifically in the target organ (Sheng et al., 2018).

Microbubbles can also be used for the delivery of genes to target tissues (gene therapy). With regard to inflammatory diseases, diabetes has been the main focus of this approach to date with microbubble based approaches being applied to successfully deliver proinsulin genes to the pancreas in rat models (Chen et al., 2006; Chen et al., 2010) with optimized gene delivery inducing almost complete recovery of the β-cell population that persisted for at least 6 months (Chen, Shimoda, Chen, Matsumoto, & Grayburn, 2012), a promising result that offers a safer delivery vehicle of genes to tissue compared with viral based methods. Successful use of US targeted microbubbles has also been demonstrated to reduce clinical scores in a rat model of arthritis with microbubbles providing local delivery of plasmids encoding the tumor necrosis factor (TNF)-α receptor (TNFR) gene (Wang, Tang, Xiang, Tang, & Qiu, 2019).

IVUS has also been deployed for therapeutic purposes both ex vivo and in vivo. ARF uses the energy/momentum of acoustic waves to propagate particles in the directional flow of the energy (Dayton, Allen, & Ferrara, 2002) and can therefore be used to direct drug delivery to specific areas of pathology. When combined with microbubbles, an IVUS catheter with a diameter compatible with human coronary arteries was found to function in a model system involving delivery of a fluorescent small molecule to swine arteries ex vivo (Kilroy, Patil, Rychak, & Hossack, 2014) and in vivo (Kilroy, Klibanov, Wamhoff, Bowles, & Hossack, 2014). Importantly, fluorophore delivery was localized to the area where the ARF pulse was employed (Kilroy, Klibanov, et al., 2014) thereby demonstrating the feasibility of guided delivery of drugs to focal areas of the artery wall. A similar device was used in vivo in a swine following vascular injury induced by balloon angioplasty. Arteries treated with rapamycin (immunosuppressant drug) loaded microbubbles and subjected to 5.1 MHz IVUS displayed a 50% reduction in neointimal formation when compared with arteries treated with rapamycin loaded microbubbles alone (Kilroy et al., 2015).

2.7.4. Advantages and barriers to clinical translation

US has a number of advantages that may allow expedited advance into the clinic as a molecular imaging tool. It is a relatively simple, well-tolerated and safe method of imaging that is well accepted in routine clinical practice by both patients and clinicians. In comparison with other routinely used imaging modalities such as CT or MRI requiring radiologist review, specialized US imaging is typically performed at the bedside by specialists requesting the investigation (thus minimizing delays, interspecialty variability and chance of miscommunication). The benefits of US use, therefore are many and can be summarized as follows: 1) high spatial and temporal resolution; 2) no ionizing radiation; 3) real-time data analysis and processing; 4) ease of operation; 5) portable; 6) relatively low cost; 7) long established use in clinic; 8) few side effects; 9) ability to acquire anatomic and molecular information in a single scan; 10) good potential for quantitative data; 11) attractive to the clinician who is a non expert and in private practice. The short interval between contrast agent injection and commencement of imaging is a distinguishing feature of US from other modalities. Microbubbles have a very short half-life in vivo (3.5 mins; Willmann et al., 2008). The key advantage to this is that imaging of the bound targeted UCA can begin shortly after injection (several minutes), unlike PET or SPECT which usually require at least 1 h between administration of the tracer and commencement of imaging (Kircher & Willmann, 2012). This feature of CEUS also allows repeated scans or additional scans of other anatomical areas during the same imaging session.

Promising pre-clinical work on large animals is driving quantitative guided CEUS forward at pace; however, more advanced algorithms will be required for human patients to account for variations in US frequency and imaging depths in addition to more advanced motion-correction methods to account for motion artifacts (Abou-Elkacem et al., 2015; Wang et al., 2017). A limitation of quantitative CEUS is that it may preclude the real-time imaging that is such a strong advantage of current clinical US; however, this area is constantly evolving with ever more refined systems being developed. If US is to be considered a viable alternative to nuclear imaging in clinical practice, these techniques will require clinical grade systems with improved quantitative volumetric analysis including three- and four- dimensional imaging in the presence of UCAs (Castle et al., 2013). A recent technical review on the state of three-dimensional real-time US imaging may be of interest to some readers (Huang & Zeng, 2017). The examples presented above in relation to guiding and localized release of a drug is a major asset for any theranostic modality in achieving therapeutic levels of a drug at a target site without potential systemic complications. Therefore, utilizing UCAs with site directed US to induce microbubble release only at the desired location is of clinical value.

One significant disadvantage of CEUS compared with optical and vibrational modalities is a lack of multiplexing potential within a single scan. This could severely restrict the ability of UCAs to be used to stratify inflammatory diseases and make diagnostic decisions. The sequential use of microbubbles targeted to more than one inflammatory molecule can provide some extra value in terms of enhanced specificity and information but the inability to separate the signal of multiple targeted UCAs in a single imaging session is a clear limitation. Another disadvantage already touched upon is that the current CEUS imaging landscape is dominated by microbubbles, which restricts the disease biomarkers to the endothelium thus reducing the spectrum of inflammatory targets available, such as those present on sub-endothelial inflammatory cell infiltrates.

With the first clinical trial for molecular targeted CEUS completed successfully (Willmann et al., 2017), this should lead to further and more expansive trials in oncology, which will hopefully increase the pace of more sophisticated and accurate quantitative software and more robust standardization of treatment regimens that could readily transfer to clinical studies looking at inflammatory markers. With fewer safety barriers to regulatory authorities, coupled with cost effectiveness compared with nuclear imaging, CEUS is well placed as both a diagnostic and theranostic molecular imaging tool. Indeed, the studies outlined in this chapter that demonstrate UCAs can be efficient carriers of immune-modulating drugs and genes paves the way for an exciting future for US as both a site-specific delivery modality combined with real-time monitoring of therapeutic outcomes.

2.8. Optical imaging

2.8.1. Fluorescence imaging

Fluorescence imaging involves the detection of emission spectrum from a fluorescent molecular probe that has been excited by a laser at an appropriate wavelength. Probes can be targeted or not and can act as 'smart probes' which are molecules that are conditioned to be activated at a particular site within the body, for example via enzymatic conversion from a non-fluorescent substrate to a fluorescent product. In addition to a 'yes' or 'no' response as to whether a molecule is present, the intensity of the fluorescence produced can be used to measure the activity of the catalytic enzyme, thus potentially signifying a shift in disease state (Scales et al., 2016; Wildgruber, Swirski, & Zernecke, 2013). Fluorescent imaging typically utilizes the near-infrared spectrum (wavelengths between 650 and 1000 nm) and is thus referred to as near-infrared fluorescence (NIRF) imaging (MacRitchie et al., 2018). The advantages of imaging at these wavelengths are the lack of photonic absorbance from biological components such as hemoglobin, lipids and water, allowing greater depth of imaging. There is also less tissue autofluorescence at NIR wavelengths, thereby increasing signal to noise ratio and hence specificity (Suter et al., 2011). NIRF imaging has a number of advantages including good spatial resolution (rapidly decreasing with depth) and sensitivity, relative low cost, lack of ionizing radiation and importantly for disease detection, the ability to discriminate multiple fluorescent signals due to discrete emission spectrums. NIRF imaging can be performed ex vivo on tissue sections and in vivo, either non-invasively or more commonly via intravital microscopy (IVM) or through the use of catheter/probe systems. Improvements in NIRF imaging probes are advancing at pace with significant gains in brightness, solubility and stability as well as the range of fluorophores available (Hilderbrand & Weissleder, 2010). Fluorophores are typically either proteins (e.g. green fluorescent protein (GFP)), small molecules or quantum dots (QDs). QDs are small (<10 nm) fluorescent NPs typically consisting of a semiconductor metal core encapsulated in a shell (usually ZnS or ZnSe) amenable to functionalization and fine tuning of particle properties. This ability to modify QDs to improve their properties has made them the most valuable imaging tool in NIRF microscopy, having increased brightness and narrower emission spectrums than other fluorescent based probes (Stevenson, Hueber, Hutton, McInnes, & Graham, 2011).

2.8.2. Photoacoustic imaging (PAI)

PAI, also referred to as optoacoustics, is an imaging modality that uses nonionizing optical radiation and ultrasonic detection. Short laser pulses (typically nanosecond long light pulses) directed at tissue creates US waves due to transient thermoelastic expansion that can be detected non-invasively by a detector outside the patient. Recent advances in both laser technology and detection strategies have seen a significant advance in the capability of PAI. By combining the advantages of both optical and acoustic imaging, PAI can overcome the main limitation of optical technology, namely restricted imaging depths which precludes non-invasive imaging of any sub-dermal human tissue. PAI can image in model systems depths in the 5–6 cm range and superficial structures can be imaged at a spatial resolution of ~5 μM, superior to that obtainable from standalone optical microscopy (Li & Chen, 2015). Like fluorescence imaging, there is a trade off in PAI between resolution and depth with spatial resolution diminishing at deeper depths due to energy dissipation/dispersion of the emitted photons through tissue. Certain endogenous molecules can be detectable by PAI including melanin and hemoglobin, but these are relatively weak absorbers of light and diagnostic use is restricted to a narrow range of physiological functions or pathologies such as vascular perfusion or skin cancer diagnosis. To increase the intensity and scope of PAI requires the use of exogenous contrast agents of which strong light absorbing NPs are the most utilized. NPs absorb light from short applied laser pulses, resulting in heating, thermal expansion and the emission of broadband US waves that can be detected across a range of frequencies by an US transducer. NPs have been utilized in PAI for over 10 years, but recent developments have led to a 100-fold increase in the detection level of contrast agent, bringing photoacoustic sensitivity down to the picomolar range (de la Zerda et al., 2012). A versatile range of nanoscale materials have been tested as PAI contrast agents including both organic (melanin, carbon and semiconducting polymer based) and inorganic (gold, TiS_2) based materials. Detailed descriptions of the current probe designs used for photoacoustic/MSOT imaging can be found in reviews by Jiang & Pu, 2017 and Gujrati, Mishra, & Ntziachristos, 2017.

2.8.3. Multispectral optoacoustic tomography (MSOT)

PAI has a powerful ability to spatially resolve optical energy absorption signatures via excitation at a single wavelength. The next step towards a more powerful molecular imaging tool is the use of multiple excitation wavelengths to identify multiple endogenous or exogenous contrast agents (multiplexing). This method exploits the different absorption properties of the target tracers/molecules. The multiplexing capacity of MSOT creates a potentially powerful imaging tool where endogenous molecules or external tracers can be identified based on their absorption spectra. While MSOT can be used to differentiate endogenous photoacoustic detectable molecules, a potentially more important development is the capacity for targeted molecular imaging. This requires the use of tracers/nanomaterials with steep absorption curves (or spectral bands) that can be resolved within a single imaging session through the separation of narrow spectral bands.

2.8.4. Clinical use

None of the optical techniques just described are used clinically in relation to inflammatory disorders. Indeed, only NIRF imaging is used at all on a clinical basis. To date, the only clinically approved fluorescent contrast agents are fluorescein, methylene blue and indocyanine green (ICG) with ICG being the only compound that is actively used for fluorescence imaging (principally for lymph node mapping and solid tumor detection). Optical coherence tomography (OCT) is a high-resolution morphological imaging tool that is increasingly commonly used clinically for measuring the status of blood vessels. OCT offers superior resolution to IVUS when phenotyping atherosclerotic plaques, being able to measure the thickness of the fibrous cap in addition to providing other more detailed morphological information (Fenning & Wilensky, 2014). Despite OCT being a valuable tool in diagnosing and investigating atherosclerosis, the Providing Regional Observations to Study Predictors of Events in the Coronary Tree (PROSPECT) trial indicated that morphological information alone was not sufficient to predict subsequent coronary plaque ruptures (Stone et al., 2011) thus highlighting the need for molecular imaging modalities to supplement established technologies. Despite OCT not bring a true molecular imaging tool its inclusion here is due to its high spatial resolution to pin point regions of interest that when combined with a molecular imaging technique such as NIRF, can create powerful multi-modal imaging devices with examples listed below.

2.8.5. Pre-clinical use and in-human trials

Out of the modalities listed above, NIRF has the most pre-clinical studies in chronic inflammatory disease (almost exclusively CVD at a molecular level). These studies vary in design and complexity, utilizing a variety of methods, both invasive and non-invasive to harness the strengths of NIRF imaging and overcome the major limitations.

Fluorescence molecular tomography (FMT), a volumetric imaging technique capable of highly sensitive (picomolar level) 3-D detection of fluorescent probes, can improve localization and deeper tissue imaging (Ntziachristos, Tung, Bremer, & Weissleder, 2002). FMT allows simultaneous quantitative molecular imaging of one or more tracers labeled with dyes operating with distinct NIR spectra and has been employed in pre-clinical studies on rodents. Table 4 lists the key studies in the cardiovascular field of NIRF imaging that utilize exogenous tracers with both non-invasive and invasive studies included. In addition to the studies in Table 4 that employ exogenous tracers, some studies have also taken advantage of the naturally occurring NIR fluorescent molecules that exist in the body to perform NIR autofluorescence (NIRAF) imaging without any external tracer. NIRAF has yielded interest in the fields of cancer, ophthalmology and CVD. Combined OCT-NIRAF plaque imaging using an intravascular optical fiber catheter has been used in patients undergoing percutaneous coronary intervention where NIRAF signal intensity correlated with plaque stage and high macrophage density regions as assessed by OCT (Ughi et al., 2016). A later study employing a vulnerable plaque mouse model identified the blood breakdown product bilirubin as the source of the autofluorescence in that model, with bilirubin resulting from intraplaque hemorrhage (Htun et al., 2017). This is an important finding since intraplaque hemorrhage is a key histological feature of human plaque instability (Virmani et al., 2005). Combining these data with the patient data by Ughi et al., 2016 suggests that in humans bilirubin may also be the source of the NIRAF; however, other molecules such as oxidized lipoproteins may also contribute and further work will be required to optimize the detection wavelength and define in more detail which autofluorescent molecules are present and at what stage of pathology in human atherosclerosis. The few studies to date suggest a tantalizing prospect for intravascular NIRAF as a modality to reliably detect the vulnerable plaque.

PAI, while combining strong attributes from both optical and acoustic imaging has shown a slow development, with few imaging agents tailored to molecular PAI (Gargiulo, Gramanzini, & Mancini, 2016). Early studies using gold-based NPs demonstrated that PAI could reliably detect adhesion molecules in cells and isolated atherosclerotic vessels (Wang et al., 2009). Gold nanoshells conjugated to VCAM-1 are also able to bind endothelial VCAM-1 and be detected by PAI while displaying no toxicity in mice (Rouleau et al., 2013). Fluorescence microscopy struggles to provide accurate spatial localization which hinders quantification due to scattering effects of the photons within tissue. To attempt to localize with high precision activated proteases, Razansky et al. (2012) employed MSOT with a protease activatable probe and subsequently measured the absorption changes of the activated probe. The authors were able to measure with high specificity and spatial location the presence of the activated probe in isolated atherosclerotic human arteries. The added benefit of optoacoustics is that it

Table 4
Essential NIRF imaging publications on CVD.

Target	Tracer(s)	FDA/CE approved (commercially available)	Disease(s) and study type	Comments	Reference (s)
Ox-LDL	LO1-750	No (No)	Atherosclerosis (pre-clinical)	Utilized a natural anti-Ox-LDL antibody conjugated to a fluorescence dye for non-invasive in vivo FMT-CT quantitative imaging of atherosclerosis in mouse models and via intravascular NIRF in a rabbit model	Khamis et al., 2016
VCAM-1	VNP (VHSPNKK-modified multi-modal magnetofluorescent NP)	No (No)	Atherosclerosis (pre-clinical)	Use a VCAM-1 peptide targeted magnetofluorescent NP to target activated endothelium in atherosclerotic mice that are detectable by MRI and fluorescent IVM	Kelly et al., 2005
Non-targeted	^{64}Cu-TNP (Triple modality PET/MRI/fluorescence NP)	No (No)	Atherosclerosis (pre-clinical)	First tri-modal NP tested in vivo for detecting macrophages in apoE$^{-/-}$ mice. Each modality showed good inter-mode correlation with doses below those used clinically in PET studies	Nahrendorf et al., 2008
Cysteine-protease	ProSense750 (Cysteine-protease activatable probe)	No (Yes)	Atherosclerosis (pre-clinical)	Employed a NIRF probe on a clinical grade catheter to measure protease activity in the aorta of atherosclerotic rabbits in real-time following injection of protease activatable probe	Jaffer et al., 2008
Cysteine-protease	Prosense VM110 (Cysteine-protease activatable probe)	No (Yes)	Atherosclerosis (pre-clinical)	Similar study type to that performed above by Jaffer et al. (2008). Important advances towards clinical translation include: 1) a NIRF probe capable of imaging 360° with accurate geometry and co-registration with IVUS 2) Able to image larger caliber (human scale coronary) arteries in blood flow 3) Use of clinical monorail catheter	Jaffer et al., 2011
Non-targeted	ICG	Yes (Yes)	Atherosclerosis (pre-clinical)	20 min injection of sub-clinical doses of ICG revealed highly selective uptake in atherosclerotic lesions in a rabbit model, both via ex vivo imaging and intravascular catheter Key finding is that an FDA approved imaging agent can detect plaques in a rabbit CVD model at a dose/kg that is safe for humans	Vinegoni et al., 2011
Passive uptake by atherosclerotic plaque	ICG	Yes (Yes)	Atherosclerosis (pre-clinical)	Tested a dual OCT-NIRF intravascular catheter with ICG contrast agent in swine models of atherosclerosis and arterial injury. While NIRF could assess plaque severity and inflammation, ICG showed lack of specificity in plaque (due to its lack of fine targeting)	Kim et al., 2016
Mannose receptors	MMR-Cy5.5/Cy7 (fluorescent macrophage mannose receptor targeted NP)	No (No)	Atherosclerosis (Pre-clinical)	Authors employed both IVM and intravascular dual OCT-NIRF probes to detect plaque macrophages via a fluorescent NP targeted to mannose receptors. The probe demonstrated high affinity for macrophages and low toxicity	Kim et al., 2016
Not targeted	ICG	Yes (Yes)	Atherosclerosis (Clinical)	First in-human test of ICG for plaque imaging. Patients undergoing carotid endarterectomy surgery were administered ICG prior to removal of arterial plaque for ex vivo analysis. ICG illuminated several plaque components including endothelial disruption, macrophage/lipid accumulation and intraplaque hemorrhage	Verjans et al., 2016
$\alpha_v\beta_3$	IRDye800Cw and AF680 NIR fluorescent probes	No (Yes)	RA (pre-clinical)	Successfully imaged inflamed joints in a mouse model of arthritis and modelled potential clinical imaging depths using simulations.	Bhatnagar et al., 2019

reveals the underlying morphology of the plaque, allowing localization of the protease in 3 dimensions (Razansky et al., 2012).

The fact that the spatial resolution of PAI/MSOT is not affected by scatter is a significant advantage over comparative fluorescent approaches. Perhaps the most interesting animal study to date utilized an ICG conjugated PEGylated polymer in a novel nanoprobe (ICG@PEG-Ag_2S) for imaging in mice using an inVision 256 PAI system (iThera Medical). ICG@PEG-Ag_2S was designed for long residence times and being lipophilic in nature, should show preferential homing to atherosclerotic plaques. Interestingly, following administration of ICG@PEG-Ag_2S, excellent aortic localization was demonstrated with signal lasting for up to 24 h. This was in contrast to mice injected with free ICG where signal was 6-fold lower and had dissipated by 1 h. The authors, therefore, had successfully tested a high contrast real-time PAI system in an atherosclerotic model (Wu, Zhang, Li, Li, & Wang, 2016). MSOT has also been employed to assess adhesion molecule expression in animal models of RA using fluorescently targeted nanocarriers. Using an L-selectin/P-selectin targeted probe in arthritic mice, Beziere et al. (2014) were able to non-invasively image the arthritic joint at a depth of ~5 mm, superior to what could be achieved by fluorescence. An imblanace in redox signaling, resulting in enhanced reactive oxidant species (ROS) production, is a central component of inflammation, including vascular inflammation. Recently, an elegant study employed a dual glutathione (GSH)/hydrogen peroxide (H_2O_2) probe with differential absorbance wavelengths allowing a measure of redox status. Use of this probe provided information on both oxidant and anti-oxidant levels within the plaque of LDLR$^{-/-}$ and apoE$^{-/-}$ mice, a result attributed to changes in macrophage number/activation. Importantly, the information gained from redox status could be used to differentiate stable from unstable plaques (Gao et al., 2018). Finally, MSOT has also been used to detect endogenous signs of inflammation (predominately oxygenated hemoglobin) in the colon in a mouse model of colitis using non-invasive imaging with a resolution of 75 μM. The non-invasive imaging results by MSOT correlated well with the diagnostic data obtained from colonoscopy (Bhutiani et al., 2017). Turning to human studies, since PAI/MSOT can image both oxy and deoxy-hemoglobin (allowing oxygen levels and angiogenesis to be assessed) without external contrast agents, PAI imaging of joints in human RA patients has revealed the potential of PAI for early non-invasive diagnosis of RA. Jo et al. (2017) utilized a novel point-of-care PAI system to measure the oxygenation of hemoglobin in the joint tissue of RA patients and healthy subjects. Hypoxia, which is a signature feature of the inflamed joint in RA, related to inflammatory cell infiltration and oxidative stress, was found to be visualized in the joints of RA patients whereas healthy subjects showed significantly higher oxygenated hemoglobin (normoxia) (Fig. 4). This promising result in 10 patients is currently being expanded upon in a clinical trial of 120 RA patients (ClinicalTrials.gov Identifier: NCT00748254). Following on from promising results in mice utilizing PAI for imaging the inflamed colon, a pilot study is currently underway

to investigate the usefulness of MSOT in diagnosing inflammatory bowel disease (ClinicalTrials.gov Identifier: NCT02622139).

2.8.6. Theranostics

PAI/MSOT is perhaps the only optical imaging technology discussed that has a potential therapeutic use due to its extensive utilization of metallic nanoscale NPs and its inherent reliance on the induction of heat in the photoacoustic target. Under laser irradiation, PAI contrast agents produce heat which can cause thermal ablation and death of targeted cells, a process termed photothermal therapy. Hyperthermic approaches can also be used to induce drug release from a nanocarrier at the intended release site (Fomina, Sankaranarayanan, & Almutairi, 2012), with the avoidance of potential systemic side effects and concentrating the drug locally. In an in vitro thrombus model, the acoustic pulse pressure produced under laser excitation creates a cavitation bubble which could promote local drug release/delivery into the vessel wall (Shangguan, Casperson, Shearin, & Prahl, 1996). A more recent and potentially elegant multi-modal delivery system was created and takes advantage of the fact that the photoacoustic effect is not just generated by thermal expansion but also by vaporization. The system involves a protein shell carrier loaded with PFC nanodroplets and optically absorbent gold nanostructures. Under optical excitation, the heat generated by the gold nanostructures induce a liquid to gas phase transition (vaporization) of the PFCs, resulting in a strong photoacoustic signal. Since the photoacoustic effect is greater through vaporization than thermal expansion, this system offers the potential for more powerful PAI as well as a tracer capable of acting as a targeted drug delivery vehicle (Wilson, Homan, & Emelianov, 2012). In fact, this process has already been validated in an in vivo cancer model using the anti-cancer drug, paclitaxel, in combination with tumor cell targeted photoacoustic NPs, with the result being local drug release and tumor destruction (Zhong, Yang, Wen, & Xing, 2016). Other developments include even more complex multi-modal NPs for drug delivery and release, the most interesting being a fluorescent/PAI/CT compatible NP for photothermal therapy and/or drug/gene delivery and such a NP has recently been successfully tested in a murine cancer model (Duan, Yang, Zhang, Zhao, & Xu, 2017). More recently, PAI has been used in combination with NIR light to both monitor retention of dexamethasome loaded nanocarriers and to induce photothermal release of the drug following injection of the nanocarrier into the joint cavity of mice with osteoarthritis. Such an approach allows a targeted high dose administration of an anti-inflammatory compound into the joint with only minimal systemic effects (Zhao et al., 2019).

2.8.7. Advantages and barriers to clinical translation

Optical imaging, encompassing all its forms from microscopy to endoscopy and specimen/biopsy analysis is the most common clinical imaging tool. Yet, as has been outlined throughout this chapter, their use for in vivo imaging is severely restricted by poor penetration depths accompanied by decreasing spatial resolutions, lack of biocompatible fluorescent probes and challenges in quantification. All these issues severely limit the potential for clinical translation. Several methods are being developed in an attempt to improve NIRF imaging depths while also allowing quantification. FMT-CT has evolved as a tool for quantifying with greater precision the anatomical location of fluorescent imaging agents. While FMT-CT offers a high sensitivity tool for quantitative assessment of a fluorescent signal within a region of interest, it doesn't overcome the poor spatial resolution of fluorescence at deeper imaging depths, hence only large changes in pathology can be discerned and it becomes impossible to localize the signal precisely without doing subsequent ex vivo correlation experiments on isolated vessels or tissue sections thus negating any benefit of non-invasive imaging.

Since depth of imaging is not of such high importance in intravascular NIRF, it is much more feasible that imaging of arteries -with all the added molecular detail that NIRF can bring, especially when combined with OCT- will be the first clinical use of NIRF in assessing an inflammatory disease (atherosclerosis). Before this can happen though, it needs to be established in controlled trials that NIRF can demonstrate better risk stratification than current methods such as coronary artery calcium scoring and FRS.

PAI/MSOT is now a fast-moving technology with significant potential in the field of medical imaging. It can offer higher spatial resolution than NIRF microscopy, can provide anatomic and functional information in the absence of external contrast agents or additional hybrid modalities, which can be extended to molecular imaging by targeted external contrast agents such as metallic NP based tracers. Furthermore, MSOT extends PAI to a multiplexing modality by being able to distinguish different spectral signatures and therefore assessing different molecular pathways or events (Gujrati et al., 2017). It is clear that PAI differentiates itself from other optical modalities by offering high resolution imaging with mm to cm penetration depths. PAI utilizing NIR light can move beyond NIRF imaging (depths ~0.5–1 mm where spatial resolutions can be sub 20 μM) (Zhang, Maslov, Stoica, & Wang, 2006) extending out to several cms while maintaining resolutions in the 100 μM range (Ma, Taruttis, Ntziachristos, & Razansky, 2009). Entire body imaging is possible on small rodents, in particular albino mice, which lack melanocytes whereas the more pigmented skin in, for example, C57BL/6 mice may result in interference from superficial melanin when imaging deeper tissues. In humans, larger organs including human breast (Ermilov et al., 2009) have also been visualized. Since PAI receives acoustic signals, it shares the advantage of real-time imaging with US, allowing dynamic processes to be viewed in living organisms. The advantages of PAI and in particular MSOT, in addition to real-time imaging and improved spatial resolution, are versatile contrast agents, portability, scalability

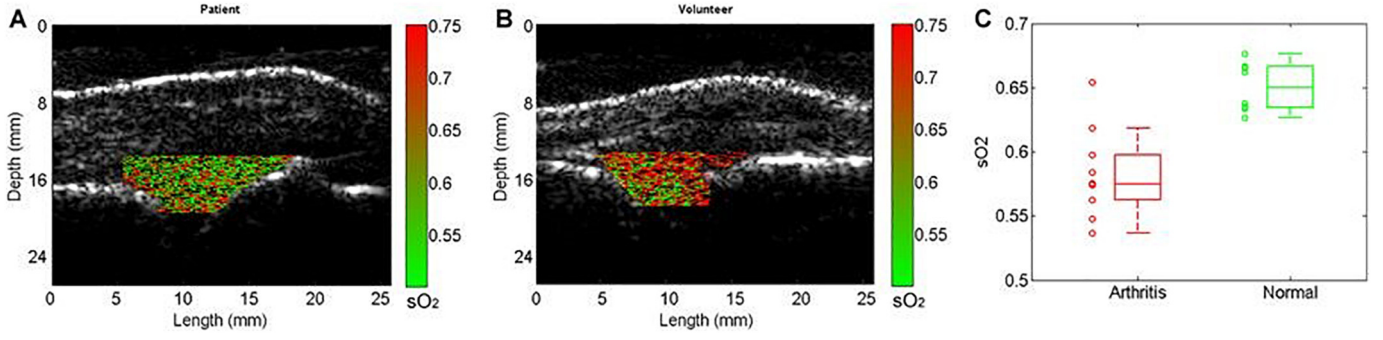

Fig. 4. PA hemoglobin oxygenation (sO2) image superimposed on the gray-scale US image of human MCP joint. (A) Imaging result from an unequivocal inflammatory MCP joint. (B) Imaging result from a healthy MCP joint. (C) Averaged sO2 levels in the joint space: 10 unequivocal inflammatory joints (Arthritis) vs. 10 healthy joints (Normal). Figure and figure legend reprinted from Jo et al. A Functional Study of Human Inflammatory Arthritis Using Photoacoustic Imaging. Sci Rep. 2017;7:15026. Distributed under a Creative Commons CC BY license (https://creativecommons.org/licenses/by/4.0/).

and cost effectiveness coupled with a lack of ionizing radiation (Ntziachristos & Razansky, 2010). Like NIRF imaging, the major limitation regarding human use of PAI is penetration (sensitivity of detection at increasing depth). While the spatial resolution of PAI has been studied in some detail, less studied is the sensitivity of detection of contrast agents. In vivo estimates vary from study to study ranging from sub nM (de la Zerda et al., 2012, 2010) to low nM detection (Haedicke et al., 2017). Variables that effect sensitivity include depth, type of contrast agent, magnitude of light applied, and the US detector employed. Like NIRF, in terms of PAI being used for in human imaging of inflammatory diseases, this may initially involve intravascular (CVD) or endoscopic (IBD) devices where the restricted depth and other tissue penetration limitations are not a limiting factor. In these circumstances, the high resolution, multiplexing capability of MSOT could bring significant clinical value over current techniques such as OCT or IVUS in identifying cell types or inflammatory signatures within the tissue, thus reflecting the stage and severity of the pathology. Additionally, PAI has been demonstrated to be capable of imaging human joints, potentially bringing arthritis into its sphere of clinical utility (Wang, Chamberland, & Jamadar, 2007). One last area that requires extensive research is quantification of the photoacoustic signal. MSOT, in principle can identify multiple biomarkers by their absorption spectra. However, there are challenges associated with multi-wavelength measurements arriving through biological tissue. Tissue attenuation of light is directly related to depth and wavelength and requires sophisticated algorithms to retrieve and quantify the signal, a feature made more complex when multi-spectral analysis is required. However, significant progress is being made in improving the software data processing of PAI and indeed, NIRF imaging. The goal then is the setting of common standards between instruments and institutions that would be required for clinical level use, alongside stable laser setups and ease of use hardware and software.

Clinical trials in PAI are now underway (predominately first in-human or phase I) and these will focus on feasibility, safety and proof of concept effectiveness. While many of these trials are in oncology (as described by Valluru, Wilson, & Willmann, 2016), most interestingly for the reader are the two trials outlined above in respect of RA and IBD. Early results from RA are promising as described by Jo et al. (2017). Optimism too is warranted with the first results to emerge from the clinical trial in IBD where MSOT analysis of hemoglobin in the colon wall could distinguish between active Crohn's disease and patients in remission (Knieling et al., 2017). If the outcome of these trials and other phase 1 trials are successful, then larger phase II trials should follow to demonstrate value and reimbursement pathways for regulatory bodies that will determine clinical translation potential assuming biological effectiveness and safety meet the endpoint criteria.

2.9. Raman spectroscopy/surface-enhanced Raman spectroscopy (SERS)

Raman spectroscopy is a form of vibrational spectroscopy that can provide data through molecularly specific spectra which are based on the vibrational energies of chemical bonds within molecules following excitation with a light (laser) source. This approach can provide detailed information on the molecular composition of cells and tissue. Raman spectroscopy can also identify multiple molecules in solution or within tissue through a high multiplexing capacity, allowing dynamic changes of molecular composition to be followed over time. The spectra produced by biological molecules creates a chemical fingerprint of the sample allowing detailed analysis of the changing molecular phenotype of a sample at a spatial resolution down to 1 μM (Bunaciu, Hoang, & Aboul-Enein, 2017). Classical Raman spectroscopy is limited by low depth (μM range) imaging and therefore its use will be confined to ex vivo analysis of blood/urine and tissue biopsies or for analysis of skin disorders or placement within modified catheters for invasive use; however, advances in Raman technology now allow for deeper imaging, making in vivo non-invasive imaging a realistic prospect as will be described below.

Raman spectroscopy is highly capable at characterizing the biochemical changes within cells and tissue. Raman generates fingerprint spectra within the 2000–400 cm^{-1} wavelength window. Raman obtains spectra from the inelastic scattering of light (visible, NIR or UV) from a laser. This is when incident (or arriving) photons from a laser interact with molecular vibrations, resulting in the emitted photons having a different wavelength and these wavelength shifted photons (inelastically scattered) can be used to create molecularly specific fingerprint spectra. Molecular distribution maps of proteins and lipids can be created by plotting the signal intensity of a peak of interest at each pixel imaged. For imaging beyond superficial tissue, a modified form of Raman called spatially offset Raman spectroscopy (SORS) may be deployed. These attributes make Raman an attractive tool for non-destructively acquiring biological information; however, it does have a major disadvantage, namely the inherent weakness of the Raman effect. Only about 1 photon in a million undergoes inelastic scattering resulting in poor sensitivity which results in long imaging times and an inability to discriminate low-level target analytes from background noise. Finally, many biological molecules are spectrally similar requiring complex chemometric analysis to separate spectra of interest (MacRitchie et al., 2018). To overcome the low sensitivity of Raman, two modifications to Raman spectroscopy, termed stimulated Raman scattering (SRS) and coherent anti-Stokes Raman scattering (CARS) have been developed. Classical Raman is often referred to as spontaneous Raman spectroscopy when used in comparison to these two other modifications. Both SRS and CARS are orders of magnitude more sensitive than spontaneous Raman, utilize more than one light source and depend on specific resonance parameters between the lasers and the molecules being analyzed. A detailed explanation of SRS and CARS can be found in a well-written review by Tipping, Lee, Serrels, Brunton, and Hulme (2016). Both SRS and CARS allow rapid image acquisition, a major advantage over spontaneous Raman, although they probe only one vibrational signature at a time as there are no spectra obtained from the non-resonant background (Laing, Jamieson, Faulds, & Graham, 2017).

The shortcomings associated with Raman spectroscopy outlined above have led not only to advancements in label-free Raman spectroscopy but also to the development of SERS, a highly sensitive advancement of conventional Raman spectroscopy. A variety of different metal surfaces can be used to provide surface-enhanced Raman but typically gold or silver surfaces which are plasmonic in nature are favored. This allows maximum electromagnetic enhancement due to the plasmonic coupling with the frequency of light used to excite the molecules being interrogated. Silver and gold can be used in a variety of different forms including electrodes, roughened metal films, vapor deposited films or very routinely as NPs. Silver or gold NPs are easily prepared through a metal reduction process which is scalable and controllable to give defined shapes and sizes of plasmonic NPs with degrees of enhancement that can be tuned to fit different laser excitations and also different surface chemistries. Most relevant to this review is the fact that they can be generated for use in vivo, functionalized with targeting molecules such as antibodies and tuned to work across a wide range of wavelengths from the visible to the near IR. SERS NPs can be used in a multiplexed manner by incorporation of spectrally distinct reporter molecules into the NP (Raman reporters). These are often dyes that are carefully selected so that when the obtained spectra from multiple Raman reporters (and hence different NP conjugates) are overlaid, each distinct reporter/NP can be distinguished by a spectral peak (or peaks) unique to that particular reporter (Noonan et al., 2018). This also allows quantification of the signal based on the intensity of the peaks obtained following comparison with a reference standard and subtraction of the background signal from the medium/tissue. These unique properties have given rise to a number of potentially promising biological applications of SERS and the current use and future potential of SERS for imaging inflammation will be discussed in the following sections.

2.9.1. Clinical use

Raman spectroscopy/SERS are not yet clinically approved for the diagnosis or treatment of disease. To our knowledge, the only current clinical uses within the biological sciences is for real-time bacterial strain identification using commercially available Raman microscopes (Eberhardt, Stiebing, Matthaus, Schmitt, & Popp, 2015) and an in vitro multiplex SERS-PCR assay for fungi identification (White et al., 2014).

2.9.2. Pre-clinical use and in-human trials

The major use for vibrational spectroscopy as a clinical diagnostic tool in immune disorders can be envisaged either as a tool for screening biological fluids or biopsy samples for disease specific molecular signatures or as a tool for in vivo imaging via molecular probes e.g. catheters introduced into vessels to monitor atherosclerotic plaque status or for monitoring the condition of the colon. Only the latter use will be discussed in this review and while progress is being made in developing vibrational spectroscopy for imaging inflammatory diseases, vibrational techniques are still at the proof of concept stage of pre-clinical development.

An area where vibrational spectroscopy might yield great clinical value is through integration of a Raman probe onto a catheter for intravascular use or for colonic examination of colitis and cancer. In 2005, Motz and colleagues developed an intravascular Raman probe for use on human patients. The first use of this intravascular Raman probe in humans was performed in 2006 on patients undergoing carotid endarterectomy and femoral artery bypass surgery. Quantitative characterization of the plaque stage was performed and compared with histological analysis of excised segments. Sensitivity and specificity of Raman detection was 79% and 85% respectively (Motz et al., 2006). Advancing on this methodology was the creation of a multi-modal imaging catheter developed by Scepanovic et al., 2011. Here, the authors employed a similar approach to Motz and colleagues on patients undergoing carotid endarterectomy and femoral bypass surgery. The fiber optic catheter consisted of a combination of reflectance IR spectroscopy, fluorescence (to measure autofluorescence from plaque components) and Raman detection. Each of these modalities provides complimentary information on the biochemical composition of the lesion including detection of collagen, elastin, lipids, hemoglobin and calcium. This was the first demonstration of a triple multi-modal system acquiring spectra from a vessel wall in human patients. The authors then used the system on ex vivo artery sections and used the combined biochemical data to stratify the stage and complexity of the lesion with the data subsequently correlated with gold standard histology. The data obtained from the multi-modal probe showed a correlated sensitivity of 93% and specificity of 72% compared with histological classification (Scepanovic et al., 2011) which are very promising preliminary results.

SERS has had rather limited use in vivo with earlier studies demonstrating proof of principle that multiple spectrally distinct NPs can be detected in vivo (Qian et al., 2008) and also one study demonstrated simultaneous detection of three distinct NPs targeted to 3 tumor biomarkers following direct injection into a mouse tumor (Dinish, Balasundaram, Chang, & Olivo, 2014), an important stepping stone to the in vivo multiplexed use of SERS. Our laboratory has been working to developing SERS as a multiplexing in vivo imaging tool for detection of vascular inflammation. In our first series of experiments, we were able to demonstrate that Pegylated NPs conjugated to an anti-ICAM-1 antibody could be employed to detect ICAM-1 expression on aortic sinus tissue sections from apoE$^{-/-}$ mice with a signal to noise ratio greater than that produced by immunofluorescence (McQueenie et al., 2012). We also supplemented this data with in vivo experiments using an intradermal inflammatory challenge model (LPS) in the ear pinna. LPS upregulates ICAM-1 expression in the ear vasculature and 24 h following LPS administration, FITC conjugated anti-ICAM-1 antibodies or anti-ICAM-1 functionalized SERS NPs were intravenously injected and non-invasively imaged by either two-photon fluorescence microscopy or SERS 30 min later. Both techniques detected upregulated ICAM-1 expression on blood vessel walls relative to isotype but as per the ex vivo studies, SERS showed superior sensitivity of detection (McQueenie et al., 2012). Recently, Gold Nanorods were deployed as SERS probes for the detection of adhesion molecules on inflamed macrophages (Pissuwan & Hattori, 2016). More recently we have utilized a SERS based system for the multiplex detection of VCAM-1, ICAM-1 and P-selectin on activated human macrophages and endothelial cells, human arterial and venous samples and a novel in-house developed in vivo model (Human adipose engraftment mouse model (^{HA}NSG)) that allows us to maintain viable human vascularized adipose tissue implants in an immunocompromised mouse (NSG mouse) in which we can test our SERS functionalized NPs (targeted to human specific inflammatory molecules) against our 3 inflammatory targets on human vessels in vivo following intravenous injection (Noonan et al., 2018). In this work, we successfully obtained SERS spectroscopy and microscopy data from cultured inflammed endothelial cells, human arterial segments and most importantly from non-invasive SERS spectral analysis of adhesion molecules present within mice containing the transplanted human tissue following inflammatory challenge (Fig. 5). We have therefore demonstrated the feasibility of using the SERS-NP platform for simultaneous targeted multiplex detection of adhesion molecules in vivo. Adhesion molecules have been utilized in previous molecular imaging studies using established techniques such as PET and MRI; however, these studies predominantly explored single target molecule detection (Broisat et al., 2012; Dimastromatteo et al., 2013; McAteer et al., 2008; Nahrendorf et al., 2009). Recent advances have shown that the simultaneous identification and discrimination of 24 parameters is possible in vitro using an SRS approach (Wei et al., 2017) which makes extending the multiplexing potential of SERS in vivo a distinct possibility in the very near future thus allowing a more detailed interrogation of the molecular events that differentiate diseased from healthy tissue.

Endoscopic probes utilizing SERS NPs targeted to known cancer molecules on the luminal surface of the colon have been developed in tandem with fiber-optic Raman endoscopes for SERS detection of cancerous and pre-cancerous lesions. The most significant advance in this field is the creation of a human compatible, flexible Raman fiber optic device that can be used in the GI tract. It is a non-contact device and when applied in the colon has a working distance up to 25 mm from the colon wall. The device is also highly sensitive, being able to detect targeted NPs only sparsely bound to colonic wall cells (~240 NPs per cell) (Garai et al., 2015). It has also been demonstrated in similar studies that superficially introduced NPs into the colon do not pass over into the systemic circulation, even after 3 days and indeed most are naturally excreted within 24 h (Thakor et al., 2011), thus eliminating any potential off-site exposure. Assessing studies that have utilized either fluorescent or SERS NPs for detection of biomarkers using endoscope techniques has demonstrated to date a detection sensitivity of <1 f. for SERS compared with ≥ 10 f. for fluorescence-based methods. Therefore, SERS offers not only superior sensitivity but also the ability to multiplex a greater number of markers using a single monochromatic laser (Laing et al., 2017).

2.9.3. Theranostics

As introduced in Section 2.4, photothermal therapy utilizing NP size agents can offer a viable method for inducing cell death. NP designs including single-walled carbon nanotubes (SWNTs) and gold nanorods are particularly effective in inducing cell death in vivo (Chakravarty et al., 2008; Dickerson et al., 2008; von Maltzahn et al., 2009). While these studies were oncology focused, SWNTs are also readily uptaken by macrophages in carotid arteries in mice following carotid ligation. Following exposure of excised arteries to NIR laser excitation, macrophages engulfing SWNTs undergo photothermal cell death (Kosuge et al., 2012). The induction of apoptosis only following targeted excitation with NIR light provides a high level of specificity in targeting only lesion resident macrophages. Further refinements of photothermal

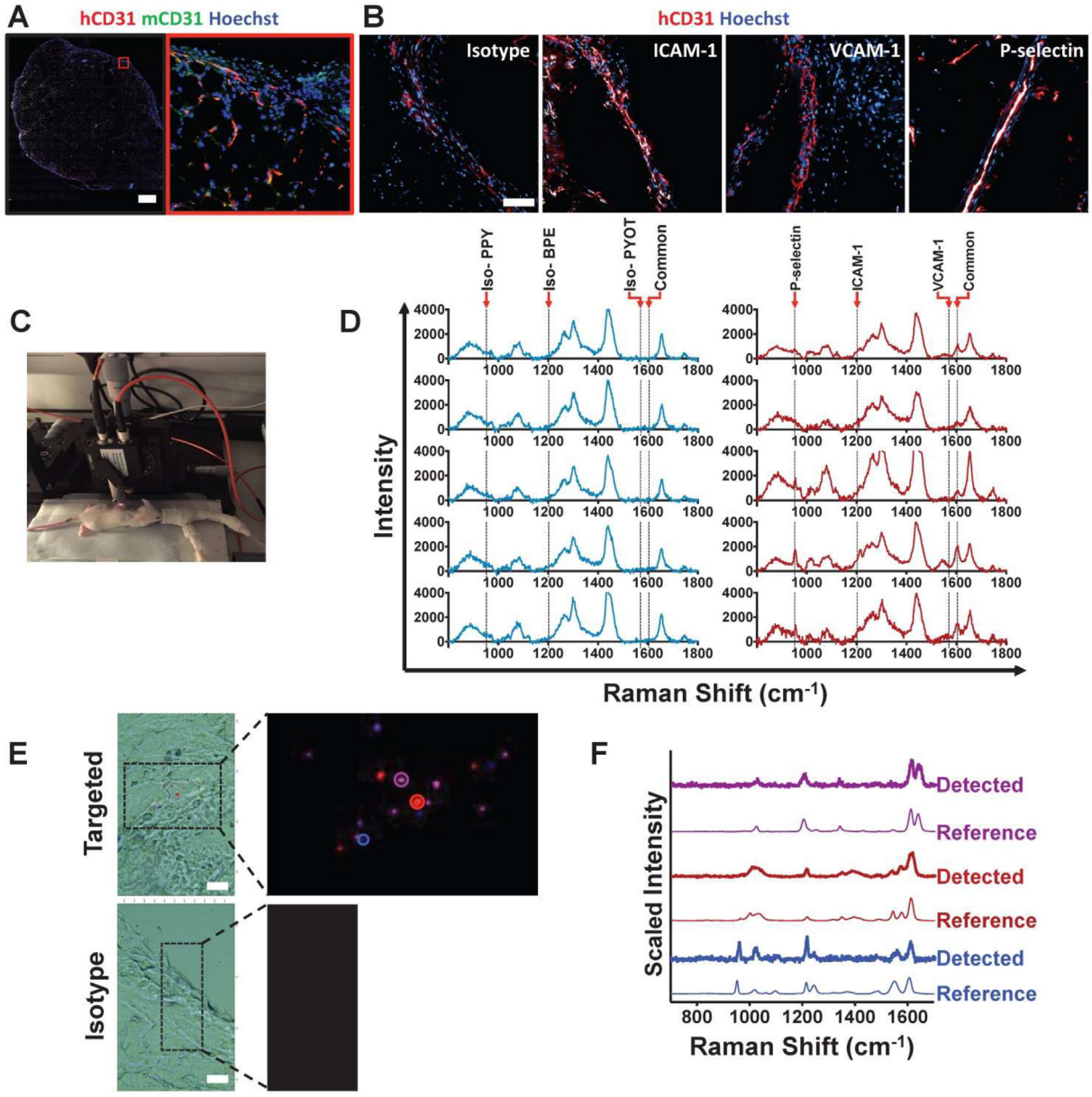

Fig. 5. In vivo SERS-BFNP molecular imaging of adhesion molecules. Following engraftment of human adipose, ^{HA}NSG mice were allowed to recover for 3 weeks. Mice were then injected intravenously with 5 μg of human recombinant TNF-α 4 h prior to receiving an intravenous injection of BFNP. (A) Following SERS-BFNP molecular imaging, adipose grafts were excised and immunofluorescently stained for human (red) and murine (green) CD31. (B) Isotype control, ICAM-1, VCAM-1, and P-selectin staining are also shown in white counterstained with human CD31 (red). Nuclei were counterstained using Hoechst 33342 (blue). (C) To conduct SERS-BFNP molecular imaging, ^{HA}NSG mice were anaesthetized and their adipose grafts non-invasively analyzed in vivo using SERS spectroscopy. (D) SERS spectra were acquired from mice that received a mixture of isotype-PPY, -BPE and -PYOT (blue spectra), or anti-P-selectin-PPY, anti-ICAM-1-BPE, anti-VCAM-1-PYOT BFNP (red spectra). The spectra shown are from 5 isotype vs. 5 targeted mice, with each spectrum acquired from a different mouse. (E) In addition to immunofluorescence microscopy, excised adipose grafts were analyzed using SERS microscopy. Detection of BFNP from sections of adipose tissue isolated from ^{HA}NSG mice that received anti-ICAM-1 (purple), anti-VCAM-1 (red), and anti-P-selectin (blue) (upper panels) or Isotype-BPE (purple), Isotype-PYOT (red), and Isotype-PPY (blue) (lower panels) are shown superimposed on darkfield tissue images alongside a magnified image of Raman maps from the scanned areas (black boxes). The colored circles in the Raman map ((E) upper panel) correlate to the acquired spectra shown in (F) above their respective reference spectra. The optical image in (E) is a darkfield image. Scale bars: (A) = 1000 μm; (B) = 100 μm; (E) = 20 μm. Figure and figure legend reprinted from Noonan et al. In vivo multiplex molecular imaging of vascular inflammation using surface-enhanced Raman spectroscopy. Theranostics. 2018;8:6195–6209. Distributed under the terms of a Creative Commons Attribution (CC BY) license (https://creativecommons.org/licenses/by/4.0/).

therapy may include the use of multi-modal NPs to guide photothermal therapy and monitor outcomes. Gao and colleagues developed a gold NP (nanostar configuration that is highly amenable to heat absorption and with high sensitivity of detection (1 fM) that was surrounded with Gd chelates making the particle amenable to both SERS and MRI and with no observed toxicity out to 30 days following administration in mice (Gao et al., 2015). Remarkably, photothermal NP therapy has already been trialed in human atherosclerotic patients in the Plasmonic Nanophotothermal Therapy of Atherosclerosis trial (NANOM-FIM; ClinicalTrials.Gov identifier: NCT01270139) performed between 2007 and 2012. The combination of intravascular or transcutaneous NIR laser excitation with macrophage targeted NPs resulted in a reduction in total plaque volume, no adverse events throughout the 1 year follow up and increased survival in the treatment group (Kharlamov et al., 2015).

Another therapeutic avenue where SERS could be implemented is for delivery of anti-inflammatory drugs to the site of pathology and subsequent monitoring of drug release. The use of NP-drug conjugates that

emit contrasting optical signatures pre- and post-drug release that can be detected by SERS offers the potential for measuring drug release under acidic pH conditions, such as found in lysosomes where internalized drug-NP conjugates are trafficked to following endothelial cell adhesion molecule targeting (Kelly et al., 2005; Muro et al., 2003; Ricard, Payet, & Dupuis, 1998; Serrano, Bhowmick, Chadha, Garnacho, & Muro, 2012). SERS-functionalized gold NPs carrying pH triggered doxorubicin release have successfully been targeted to cancer cells and drug delivery was confirmed by SERS tracking (Song, Zhou, & Duan, 2012). A similar method employing doxorubicin conjugated to gold NPs via a pH sensitive hydrazine linker was employed to also target doxorubicin to cancer cells (Kang, Afifi, Austin, & El-Sayed, 2013). Such an approach has not yet been applied to vascular endothelial cells or to deliver anti-inflammatory drugs but the utility of SERS sensitive NPs in such a context creates a potent dual-modality tool for both delivering and tracking therapeutic compounds to inflammatory sites.

2.9.4. Advantages and barriers to clinical translation

Raman probes either alone or on multi-modal catheters can map the biochemistry of the plaque with good sensitivity and specificity. The system created by Motz et al., 2005 was the first real-time imaging system for measuring Raman spectra intravascularly. In those studies, the entire duration of spectral acquisition, data processing and diagnostic read out was less than 5 s, although the in vivo acquisition was less than 1 s. One limitation of the Raman probe used by Motz et al. (2006) and the multi-modal system used by Scepanovic et al. (2011) is that they don't provide a real-time image of the vessel wall in the way that IVUS and OCT do. Therefore, the goal would be to combine a fast high resolution real-time imaging technique such as OCT (which can pinpoint areas interest) with Raman or a multi-modal system which can acquire the detailed molecular information. This would yield a highly powerful tool for investigating intravascular or colonic pathologies.

SERS is still at an early stage of development in terms of application to in vivo imaging, yet it has a number of strengths that may address the limitations of current imaging modalities. These can be outlined as follows:

1) Fast acquisition times; 2) high sensitivity, (enhancement over Raman can be as much as 10^{10}–10^{11} and even higher when the laser frequency is in resonance with the SERS molecule (Guerrini & Graham, 2012; McNay, Eustace, Smith, Faulds, & Graham, 2011)); 3) Low toxicity of AuNPs in animal models and early human trials; 4) Not susceptible to photobleaching; 5) Deep tissue imaging possible (up to 5 cm reported by Asiala, Shand, Faulds, & Graham, 2017); 6) Compatible with a broad range of fluorophores in the NIR window; 7) Multiple Raman reporters can be excited at a single wavelength; 8) Narrow emission spectrum allow accurate deconvolution of the data and high multiplexing; 9) Portable systems now available expanding the use beyond specialized research labs; 10) NPs can be configured for theranostic use such as photothermal therapy or as a site specific drug release vehicle.

In terms of barriers to translation, the ability to accurately deconvolute spectral data is a key requirement for all forms of vibrational spectroscopy. As the complexity of the sample matrix increases, more sophisticated mathematical and statistical data analysis routines are required to provide clear and concise data from the spectroscopic signals. The quantification of Raman and SERS data is a rapidly progressing area of research with highly promising results indicating SERS spectra can be quantified accurately using multiple mathematical models including Bayesian modeling (Zhong, Girolami, Faulds, & Graham, 2011) which we have successfully demonstrated shows a linear increase in proportion to increasing NP concentration (Noonan et al., 2018). When aiming for the use of SERS NPs in human patients, the toxicity of the NPs must be accurately known including their residence times and fate within the patient (Cicha et al., 2018). Studies will need to address where SERS NPs accumulate, how this relates to NP size, shape and functionalization and any possible degradation prior to excretion. Gold per se is not a toxic metal and has been used in medicines for many years, for example gold based compounds are used to treat RA (Alkilany & Murphy, 2010); however, the toxic status of nanoscale gold particles remains obscure with differential toxic effects found in cellular and animal models depending on size, shape, charge, shell material and dose of NPs administered (Fratoddi, Venditti, Cametti, & Russo, 2015; Gerber, Bundschuh, Klingelhofer, & Groneberg, 2013). Shell material such as PEG has shown to be biocompatible and displays very low toxicity in human patients (Alexander, Ajazuddin, Khan, Saraf, & Saraf, 2013), being used in many pharmaceutical formulations around the world to improve drug residence times. PEG also reduces the toxicity of the NP by encapsulating the gold thus bare gold is not freely available in the circulation as well as acting as an anchor for conjugating targeting antibodies or peptides. Despite mixed pre-clinical results to date regarding the toxicity of NPs, silica-gold pegylated NPs have progressed to human clinical trials for thermal ablation of cancer (Stern et al., 2016). A safety evaluation trial in 22 prostate cancer patients who were administered an intravenous infusion of 'Aurolase' NPs and monitored for 6 months revealed only 2 minor adverse events related to the therapy. Interestingly and importantly, the FDA classified those NPs as a medical device rather than a drug (Stern et al., 2016) which reduces the time to regulatory approval. Multi-modal SERS NPs are also being developed. In an excellent study by Dinish et al., 2015, the authors created targeted NPs containing a NIR dye detectable by both SERS and photoacoustics in an in vivo mouse tumor model at a depth of several cm and at μM resolution allowing precision location of the tumor. The authors noted an accumulation of NPs in the liver and spleen but were cleared within 72 h, which is encouraging in terms of a lack of organ retention (Dinish et al., 2015). More generally, the creation of multi-modal SERS probes combined with modalities that offer visualization of tissue will greatly facilitate the location and optimum time point to initiate SERS data acquisition. To conclude our discussion on SERS, it is clear that SERS has many intrinsic advantages that may meet clinical needs currently unserved by classical imaging modalities, yet it will require substantial investment of resources across multiple disciplines to determine if these inherent advantages can be translated to a clinically useful imaging modality.

2.10. Summary table of molecular imaging modalities

Modality	Resolution	Sensitivity (mol/L)	Depth	Strengths	Limitations	Stage of development
CT	15–50 μm	10^{-2}–10^{-3}	Body-wide	Non-invasive, fast imaging, good spatial resolution	Low sensitivity, radiation exposure, poor soft tissue contrast, limited multiplexing	Clinical (pre-clinical for sub mm resolutions)
MRI	0.5–1.5 mm (1.5 T) 10–200 μm (>3 T)	10^{-3}–10^{-5}	Body-wide	Good spatial resolution, non-invasive, high soft tissue contrast, no radiation exposure, low toxicity tracers with some already clinically used	Poor sensitivity, long imaging times often required, poor signal to noise ratio, lack of multiplexing outside of specialist CEST MRI.	T1/T2 (clinical) Other forms pre-clinical/clinical trials
MPI	~0.5 mm * (proportional to field strength)	10^{-6} to 10^{-8} *	Body-wide	Fast real-time imaging, Good signal to noise, higher sensitivity than MRI, can utilize established MRI contrast agents, no radiation exposure, quantifiable	Limited in vivo data, sensitivity is unlikely to match PET/SPECT, no anatomic information, no multiplexing	Pre-clinical
PET	4-6 mm (clinical) 1–2 mm (pre-clinical)	10^{-11}–10^{-12}	Body-wide	Non-invasive, high sensitivity, clinical grade scanners well established	Poor spatial resolution, radiation exposure, high cost, short half-life of radionucleotides requires on-site cyclotron, no anatomic detail without hybrid CT/MRI, no multiplexing	Clinical
SPECT	0.5–2 mm	10^{-10}–10^{-11}	Body-wide	Non-invasive, high sensitivity, cheaper than PET and more widely available	Poor spatial resolution, radiation exposure, no anatomic detail without hybrid CT/MRI, very limited multiplexing capacity	Clinical
CEUS	50–500 μm	Not well defined. In vivo estimates are 10^{-6} to 10^{-9}	Body-wide	Low cost, good sensitivity, no radiation exposure, anatomic and molecular information in a single scan, high speed real-time imaging, amenable to bedside testing, microbubble contrast agents are clinically approved, can be used on catheters for invasive imaging, potential to act as a drug delivery theranostic tool	Signal to noise ratio can be poor, lack of vascular penetration confines microbubble approaches to vascular molecules, no multiplexing	Clinical (pre-clinical/clinical trials for targeted CEUS)
NIRF	10 μM-2 mm (depending on depth and tissue type)	10–^{10} to 10–^{11}	<2 cm	High spatial resolution at shallow depths, high sensitivity, no radiation exposure, relatively low cost, multiplexing, can be used on catheters for invasive imaging	Imaging restricted to superficial structures or via surgical exposure, potential toxicity of pre-clinical tracers, multiplexing ability is poor compared with vibrational spectroscopy	Clinical (anatomic using ICG) Pre-clinical (targeted NIRF)
PAI/MSOT	<50 μM to several hundred μM (depth dependent)	$<10^{12}$	<5–6 cms	High sensitivity, no radiation exposure, superior penetration depths compared with other optical modalities, low cost, anatomic and molecular information in a single scan, high speed real-time imaging, can be used on catheters for invasive imaging, multiplexing with MSOT, potential to act as a drug delivery theranostic tool	Poor penetration depths when compared with current clinical imaging modalities, tracers not approved for human use, data acquisition and processing still to be optimized, less multiplexing capacity than vibrational spectroscopy	Pre-clinical (Early clinical trials)
Raman spectroscopy	<1 μM to several hundred μMs	~10^{-5} to 10^{-6} for analytes in solution*	Several mms	Label free analysis, low cost, portable, real-time or near real-time imaging, high spatial resolution, able to discriminate a wide set of molecular structures, can be used on catheters for invasive imaging	Low sensitivity leading to long imaging times, poor imaging depths restricting use to ex vivo or catheter probes, requires complex chemometric analysis to separate analytes from spectra	Pre-clinical
SERS	<100 nm to several μM	10–^{11} to 10–^{14}	Up to 5 cms with SESORS	High sensitivity, utilizes gold NPs that display low toxicity, fast imaging times, no photobleaching, can utilize a broad range of existing dyes for multiplexing, deep tissue imaging possible with SESORS, portable hand held devices now available, SERS NPs can be tuned for photothermal therapy or targeted drug release	Spectra can be sensitive to changes in NP orientation and interference from adjacent structures, tracers not approved for human use, complex statistical algorithms are required for separation and quantification of multiplexed spectra	Pre-clinical

* Based on a very small number of published values.

3. Summary and conclusions

To summarize, an ideal molecular imaging modality (either alone or as a hybrid with another) should possess high sensitivity and spatial resolution, fast imaging times, be able to image structures at depth within the body (unless utilized solely as an invasive catheter), be quantifiable and reproducible, have low economic burden and have the ability to assess multiple targets in a single scan. For successful clinical translation, short imaging times, patient comfort, accuracy, reproducibility, invasiveness of the procedure and necessity for hospitalization should be carefully considered. Highly specialized imaging modalities create an additional barrier by requiring trained reporting staff, thus wider application is easier with more approachable methods, such as US.

In a world where medical authorities and institutions demand greater value for money, systems that can be brought to clinical specifications with less regulatory hurdles are going to be highly prized. Of the current clinical modalities, CEUS and MRI may compete as safe, cost-effective molecular and theranostic imaging tools, with similar capabilities and limitations. CEUS with more extensive use of microbubble contrast agents and targeted microbubbles now in clinical trials is further on this development path than MRI, although as ^{19}F MRI progresses into human use, only then will it be possible to judge the respective merits of these two modalities as potential molecular imaging tools that bring added diagnostic value over current systems. There appears little enthusiasm to move PET to clinical targeted imaging of disease biomarkers beyond oncology, but this may not be a permanent restriction. However, PET/SPECT will always be constrained by radiation exposure

Table 5
Barriers to clinical translation.

Cost	Safety	Technology	Clinical value
• Research • Upscaling from animals to human • Clinical trials • In-clinic cost	• Tracer properties (dose, radiation, heavy metal, tissue accumulation) • Modality (magnetic field, laser, acoustic energy) • Exposure limits may limit exploratory use	• Does not conform to expectations • Pre-clinical devices not compatible/modifiable to clinical specifications • Designed for a single anatomic site • Quantification/standardization	• Minimal advance in biological data • Poor performance in other areas (e.g. oncology) • Insufficient improvement over established methods

and the lack of multiplexing. The potential for clinical molecular imaging of emerging technologies is even harder to judge with any certainty given the scarcity of in-human (and even pre-clinical when it comes to the most recent technologies such as MPI and SERS) testing and the lack of completed clinical trials. We would suspect PAI will accelerate quicker than the other pre-clinical modalities and there is much hope within the pre-clinical academic community that it can translate to a clinical molecular imaging device. The application of SERS in vivo is just beginning to be realized with only a handful of publications in this area hence the technology is very early stage. However, its powerful set of attributes will continue to be tested in animal models and human tissue samples to build the robust, standardized quantification models that are necessary to make datasets consistent and comparable thus allowing progression to more rigorous diagnostic testing trials. We believe that the next decade will be key for all forms of vibrational spectroscopy in demonstrating whether they have a place in the clinic.

Major barriers to clinical translation of a molecular imaging modality include safety, cost, overcoming technological hurdles in signal acquisition and processing and performance versus established technologies/clinical utility (Table 5). As demands on healthcare services increase, then the cost of implementing new technologies has to have a high threshold of clinical value. Although development costs are cheaper for a diagnostic imaging agent, costs are still substantial due to the lengthy development process because regulatory authorities treat molecular imaging agents as they would any other drug. An advantage of PET tracer development in the US - due to their trace amount administered dose - is that an exploratory investigative new drug application (eIND) pathway is available which reduces the time between pre-clinical and first in-human trials due to less stringent requirements for pre-clinical animal testing (Abou-Elkacem et al., 2015). This pathway is not open to other novel contrast agents such as targeted microbubbles or metallic NPs (Cicha et al., 2018). However, it is quite conceivable that as regulatory authorities become more convinced of the general safety of a contrast agent then expedited routes to clinical testing may be available if only the targeting ligand is changed on an otherwise previously tested safe contrast agent. Validation of this is emerging in CEUS with the KDR targeted microbubble used in a clinical trial in breast cancer showing excellent patient tolerability, comparable with a similar non-targeted microbubble. It is also interesting to note that the FDA classified the first pegylated gold NP therapeutic agent (Aurolase) as a medical device rather than a drug, reducing the burden and time towards regulatory approval. Whether this will remain the case for targeted gold NPs, such as those utilized in SERS or PAI is unclear as regulatory approval has not been granted for these imaging agents. At present, photoacoustic studies in humans rely on endogenous contrast agents or approved fluorescent molecules such as ICG (Valluru et al., 2016). Regardless, the lack of observed adverse events in patients treated with Aurolase could be a key milestone in the subsequent translation of metallic NP based agents into further human trials based around diagnostic imaging.

When considering costs, it is also important to keep in mind what the primary goal of molecular imaging is, namely to identify disease at an early stage or better predict its evolution and to monitor response to therapeutics. In this regard, clinicians require more robust integrated patient data that may include patient history, clinical scores, serum biomarkers and real-time, high resolution molecular imaging that can not only add clinical value, but better inform on the underlying cellular and molecular mechanisms in a patient-specific manner. The current inability to quantify individual disease progression in inflammatory conditions impairs our therapeutic choices and prevents personalized medicine. Our current approach to capture inflammatory processes is outdated, cumbersome and poses a substantial clinical limitation to precision medicine. Therefore, molecular imaging has the potential to bring many benefits to the clinic including improved patient outcomes, reduced diagnostic costs, reduced physical and emotional burden on patients and further cost savings to Health Authorities via the reduced demand for surgery and ineffective treatments due to improved decision making arising from the results of molecular imaging.

Funding sources

Our lab is also supported by the British Heart Foundation grants [PG/12/81/29897 and PG/19/84/34771 to P.M., RE/13/5/30177]; the Engineering and Physical Sciences Research Council (EPSRC) grant [EP/L014165/1 to P.M.]; the European Commission Marie Skłodowska-Curie Individual Fellowships [661369 to P.M.]; and a Wellcome Trust grant [204820/Z/16/Z].

Declaration of Competing Interest

Drs McInnes and Maffia received by Canon Medical Systems Corporation a grant to support the completion of this review. Drs Sugiyama and Lawton are employees of Canon Medical Systems Corporation and Canon Medical Research Europe Ltd., respectively.

References

Abou-Elkacem, L., Bachawal, S. V., & Willmann, J. K. (2015). Ultrasound molecular imaging: Moving toward clinical translation. *European Journal of Radiology 84*(9), 1685–1693. https://doi.org/10.1016/j.ejrad.2015.03.016.

Akazawa, K., Sugihara, F., Minoshima, M., Mizukami, S., & Kikuchi, K. (2018). Sensing caspase-1 activity using activatable (19)F MRI nanoprobes with improved turn-on kinetics. *Chemical communications (Cambridge, England) 54*(83), 11785–11788. https://doi.org/10.1039/c8cc05381b.

Alexander, A., Ajazuddin, Khan, J., Saraf, S., & Saraf, S. (2013). Poly(ethylene glycol)-poly (lactic-co-glycolic acid) based thermosensitive injectable hydrogels for biomedical applications. *Journal of Controlled Release 172*(3), 715–729. https://doi.org/10.1016/j.jconrel.2013.10.006.

Alkilany, A. M., & Murphy, C. J. (2010). Toxicity and cellular uptake of gold nanoparticles: What we have learned so far? *Journal of Nanoparticle Research 12*(7), 2313–2333. https://doi.org/10.1007/s11051-010-9911-8.

Anderson, N. G., & Butler, A. P. (2014). Clinical applications of spectral molecular imaging: Potential and challenges. *Contrast Media & Molecular Imaging 9*(1), 3–12. https://doi.org/10.1002/cmmi.1550.

Antonopoulos, A. S., Sanna, F., Sabharwal, N., Thomas, S., Oikonomou, E. K., Herdman, L., et al. (2017). Detecting human coronary inflammation by imaging perivascular fat. *Science Translational Medicine 9*(398). https://doi.org/10.1126/scitranslmed.aal2658.

Ardenkjaer-Larsen, J. H., Fridlund, B., Gram, A., Hansson, G., Hansson, L., Lerche, M. H., et al. (2003). Increase in signal-to-noise ratio of > 10,000 times in liquid-state NMR. *Proceedings of the National Academy of Sciences of the United States of America 100*(18), 10158–10163. https://doi.org/10.1073/pnas.1733835100.

Asiala, S. M., Shand, N. C., Faulds, K., & Graham, D. (2017). Surface-Enhanced, Spatially Offset Raman Spectroscopy (SESORS) in tissue analogues. *ACS Applied Materials & Interfaces 9*(30), 25488–25494. https://doi.org/10.1021/acsami.7b09197.

Austin, V., Crack, P. J., Bozinovski, S., Miller, A. A., & Vlahos, R. (2016). COPD and stroke: Are systemic inflammation and oxidative stress the missing links? *Clinical Science (London, England) 130*(13), 1039–1050. https://doi.org/10.1042/CS20160043.

Autio, A., Ujula, T., Luoto, P., Salomaki, S., Jalkanen, S., & Roivainen, A. (2010). PET imaging of inflammation and adenocarcinoma xenografts using vascular adhesion protein 1 targeting peptide 68Ga-DOTAVAP-P1: Comparison with 18F-FDG. *European Journal of Nuclear Medicine and Molecular Imaging 37*(10), 1918–1925. https://doi.org/10.1007/s00259-010-1497-y.

van Baarsen, L. G., de Hair, M. J., Ramwadhdoebe, T. H., Zijlstra, I. J., Maas, M., Gerlag, D. M., et al. (2013). The cellular composition of lymph nodes in the earliest phase of inflammatory arthritis. *Annals of the Rheumatic Diseases 72*(8), 1420–1424. https://doi.org/10.1136/annrheumdis-2012-202990.

Beer, A. J., Pelisek, J., Heider, P., Saraste, A., Reeps, C., Metz, S., et al. (2014). PET/CT imaging of integrin alphavbeta3 expression in human carotid atherosclerosis. *JACC: Cardiovascular Imaging 7*(2), 178–187. https://doi.org/10.1016/j.jcmg.2013.12.003.

Benezra, M., Penate-Medina, O., Zanzonico, P. B., Schaer, D., Ow, H., Burns, A., et al. (2011). Multimodal silica nanoparticles are effective cancer-targeted probes in a model of human melanoma. *The Journal of Clinical Investigation 121*(7), 2768–2780. https://doi.org/10.1172/JCI45600.

Beziere, N., von Schacky, C., Kosanke, Y., Kimm, M., Nunes, A., Licha, K., et al. (2014). Optoacoustic imaging and staging of inflammation in a murine model of arthritis. *Arthritis & Rhematology 66*(8), 2071–2078. https://doi.org/10.1002/art.38642.

Bhatnagar, S., Khera, E., Liao, J., Eniola, V., Hu, Y., Smith, D. E., et al. (2019). Oral and subcutaneous Administration of a near-infrared fluorescent molecular imaging agent detects inflammation in a mouse model of rheumatoid arthritis. *Scientific Reports 9*(1), 4661. https://doi.org/10.1038/s41598-019-38548-0.

Bhutiani, N., Grizzle, W. E., Galandiuk, S., Otali, D., Dryden, G. W., Egilmez, N. K., et al. (2017). Noninvasive imaging of colitis using multispectral optoacoustic tomography. *Journal of Nuclear Medicine 58*(6), 1009–1012. https://doi.org/10.2967/jnumed.116.184705.

Blezer, E. L., Deddens, L. H., Kooij, G., Drexhage, J., van der Pol, S. M., Reijerkerk, A., et al. (2015). In vivo MR imaging of intercellular adhesion molecule-1 expression in an animal model of multiple sclerosis. *Contrast Media & Molecular Imaging 10*(2), 111–121. https://doi.org/10.1002/cmmi.1602.

Botnar, R. M., Buecker, A., Wiethoff, A. J., Parsons, E. C., Jr., Katoh, M., Katsimaglis, G., et al. (2004). In vivo magnetic resonance imaging of coronary thrombosis using a fibrin-binding molecular magnetic resonance contrast agent. *Circulation 110*(11), 1463–1466. https://doi.org/10.1161/01.CIR.0000134960.31304.87.

Brangsch, J., Reimann, C., Kaufmann, J. O., Adams, L. C., Onthank, D. C., Thone-Reineke, C., et al. (2019). Concurrent molecular magnetic resonance imaging of inflammatory activity and extracellular matrix degradation for the prediction of aneurysm rupture. *Circulation. Cardiovascular Imaging 12*(3), e008707. https://doi.org/10.1161/CIRCIMAGING.118.008707.

Brauchli, Y. B., Jick, S. S., Miret, M., & Meier, C. R. (2009). Psoriasis and risk of incident myocardial infarction, stroke or transient ischaemic attack: An inception cohort study with a nested case-control analysis. *The British Journal of Dermatology 160*(5), 1048–1056. https://doi.org/10.1111/j.1365-2133.2008.09020.x.

Brenner, D. J. (2010). Should we be concerned about the rapid increase in CT usage? *Reviews on Environmental Health 25*(1), 63–68 Retrieved from http://www.ncbi.nlm.nih.gov/pubmed/20429161.

Broisat, A., Hernot, S., Toczek, J., De Vos, J., Riou, L. M., Martin, S., et al. (2012). Nanobodies targeting mouse/human VCAM1 for the nuclear imaging of atherosclerotic lesions. *Circulation Research 110*(7), 927–937. https://doi.org/10.1161/CIRCRESAHA.112.265140.

Bucerius, J., Schmaljohann, J., Bohm, I., Palmedo, H., Guhlke, S., Tiemann, K., et al. (2008). Feasibility of 18F-fluoromethylcholine PET/CT for imaging of vessel wall alterations in humans–first results. *European Journal of Nuclear Medicine and Molecular Imaging 35*(4), 815–820. https://doi.org/10.1007/s00259-007-0685-x.

Bunaciu, A. A., Hoang, V. D., & Aboul-Enein, H. Y. (2017). Vibrational micro-spectroscopy of human tissues analysis: Review. *Critical Reviews in Analytical Chemistry 47*(3), 194–203. https://doi.org/10.1080/10408347.2016.1253454.

Cai, K., Haris, M., Singh, A., Kogan, F., Greenberg, J. H., Hariharan, H., et al. (2012). Magnetic resonance imaging of glutamate. *Nature Medicine 18*(2), 302–306. https://doi.org/10.1038/nm.2615.

Cai, K., Kiefer, G. E., Caruthers, S. D., Wickline, S. A., Lanza, G. M., & Winter, P. M. (2012). Quantification of water exchange kinetics for targeted PARACEST perfluorocarbon nanoparticles. *NMR in Biomedicine 25*(2), 279–285. https://doi.org/10.1002/nbm.1746.

Cassidy, M. C., Chan, H. R., Ross, B. D., Bhattacharya, P. K., & Marcus, C. M. (2013). In vivo magnetic resonance imaging of hyperpolarized silicon particles. *Nature Nanotechnology 8*(5), 363–368. https://doi.org/10.1038/nnano.2013.65.

Castelli, D. D., Boffa, C., Giustetto, P., Terreno, E., & Aime, S. (2014). Design and testing of paramagnetic liposome-based CEST agents for MRI visualization of payload release on pH-induced and ultrasound stimulation. *Journal of Biological Inorganic Chemistry 19*(2), 207–214. https://doi.org/10.1007/s00775-013-1042-0.

Castelli, D. D., Terreno, E., Longo, D., & Aime, S. (2013). Nanoparticle-based chemical exchange saturation transfer (CEST) agents. *NMR in Biomedicine 26*(7), 839–849. https://doi.org/10.1002/nbm.2974.

Castle, J., Butts, M., Healey, A., Kent, K., Marino, M., & Feinstein, S. B. (2013). Ultrasound-mediated targeted drug delivery: Recent success and remaining challenges. *American Journal of Physiology. Heart and Circulatory Physiology 304*(3), H350–H357. https://doi.org/10.1152/ajpheart.00265.2012.

Chakravarty, P., Marches, R., Zimmerman, N. S., Swafford, A. D., Bajaj, P., Musselman, I. H., et al. (2008). Thermal ablation of tumor cells with antibody-functionalized single-walled carbon nanotubes. *Proceedings of the National Academy of Sciences of the United States of America 105*(25), 8697–8702. https://doi.org/10.1073/pnas.0803557105.

Chang, L., Munsaka, S. M., Kraft-Terry, S., & Ernst, T. (2013). Magnetic resonance spectroscopy to assess neuroinflammation and neuropathic pain. *Journal of Neuroimmune Pharmacology 8*(3), 576–593. https://doi.org/10.1007/s11481-013-9460-x.

Chen, S., Ding, J. H., Bekeredjian, R., Yang, B. Z., Shohet, R. V., Johnston, S. A., et al. (2006). Efficient gene delivery to pancreatic islets with ultrasonic microbubble destruction technology. *Proceedings of the National Academy of Sciences of the United States of America 103*(22), 8469–8474. https://doi.org/10.1073/pnas.0602921103.

Chen, S., Shimoda, M., Chen, J., Matsumoto, S., & Grayburn, P. A. (2012). Transient overexpression of cyclin D2/CDK4/GLP1 genes induces proliferation and differentiation of adult pancreatic progenitors and mediates islet regeneration. *Cell Cycle 11*(4), 695–705. https://doi.org/10.4161/cc.11.4.19120.

Chen, S., Shimoda, M., Wang, M. Y., Ding, J., Noguchi, H., Matsumoto, S., et al. (2010). Regeneration of pancreatic islets in vivo by ultrasound-targeted gene therapy. *Gene Therapy 17*(11), 1411–1420. https://doi.org/10.1038/gt.2010.85.

Chen, Y. P., Lv, J. W., Liu, X., Zhang, Y., Guo, Y., Lin, A. H., et al. (2017). The landscape of clinical trials evaluating the theranostic role of PET imaging in oncology: Insights from an analysis of ClinicalTrials.gov database. *Theranostics 7*(2), 390–399. https://doi.org/10.7150/thno.17087.

Cicha, I., Chauvierre, C., Texier, I., Cabella, C., Metselaar, J. M., Szebeni, J., Dézsi, L., Alexiou, C., Rouzet, F., Storm, G., Stroes, E., Bruce, D., MacRitchie, N., Maffia, P., & Letourneur, D. (2018). From design to the clinic: practical guidelines for translating cardiovascular nanomedicine. *Cardiovasc Res 114*, 1714–1727.

Cormode, D. P., Naha, P. C., & Fayad, Z. A. (2014). Nanoparticle contrast agents for computed tomography: A focus on micelles. *Contrast Media & Molecular Imaging 9*(1), 37–52. https://doi.org/10.1002/cmmi.1551.

Cormode, D. P., Roessl, E., Thran, A., Skajaa, T., Gordon, R. E., Schlomka, J. P., et al. (2010). Atherosclerotic plaque composition: Analysis with multicolor CT and targeted gold nanoparticles. *Radiology 256*(3), 774–782. https://doi.org/10.1148/radiol.10092473.

Culp, W. C., Porter, T. R., Lowery, J., Xie, F., Roberson, P. K., & Marky, L. (2004). Intracranial clot lysis with intravenous microbubbles and transcranial ultrasound in swine. *Stroke 35*(10), 2407–2411. https://doi.org/10.1161/01.STR.0000140890.86779.79.

Dayton, P. A., Allen, J. S., & Ferrara, K. W. (2002). The magenitude of radiation force on ultrasound contrast agents. *The Journal of the Acoustical Society of America 112*(5 Pt 1), 2183–2192 Retrieved from http://www.ncbi.nlm.nih.gov/pubmed/12430830.

Deddens, L. H., van Tilborg, G. A., van der Toorn, A., van der Marel, K., Paulis, L. E., van Bloois, L., et al. (2013). MRI of ICAM-1 upregulation after stroke: The importance of choosing the appropriate target-specific particulate contrast agent. *Molecular Imaging and Biology 15*(4), 411–422. https://doi.org/10.1007/s11307-013-0617-z.

Dekempeneer, Y., Keyaerts, M., Krasniqi, A., Puttemans, J., Muyldermans, S., Lahoutte, T., et al. (2016). Targeted alpha therapy using short-lived alpha-particles and the promise of nanobodies as targeting vehicle. *Expert Opinion on Biological Therapy 16*(8), 1035–1047. https://doi.org/10.1080/14712598.2016.1185412.

Demos, S. M., Alkan-Onyuksel, H., Kane, B. J., Ramani, K., Nagaraj, A., Greene, R., et al. (1999). In vivo targeting of acoustically reflective liposomes for intravascular and transvascular ultrasonic enhancement. *Journal of the American College of Cardiology 33*(3), 867–875 Retrieved from http://www.ncbi.nlm.nih.gov/pubmed/10080492.

Dickerson, E. B., Dreaden, E. C., Huang, X., El-Sayed, I. H., Chu, H., Pushpanketh, S., et al. (2008). Gold nanorod assisted near-infrared plasmonic photothermal therapy (PPTT) of squamous cell carcinoma in mice. *Cancer Letters 269*(1), 57–66. https://doi.org/10.1016/j.canlet.2008.04.026.

Dimastromatteo, J., Broisat, A., Perret, P., Ahmadi, M., Boturyn, D., Dumy, P., et al. (2013). In vivo molecular imaging of atherosclerotic lesions in ApoE−/− mice using VCAM-1-specific, 99mTc-labeled peptidic sequences. *Journal of Nuclear Medicine 54*(8), 1442–1449. https://doi.org/10.2967/jnumed.112.115675.

Dimcevski, G., Kotopoulis, S., Bjanes, T., Hoem, D., Schjott, J., Gjertsen, B. T., et al. (2016). A human clinical trial using ultrasound and microbubbles to enhance gemcitabine treatment of inoperable pancreatic cancer. *Journal of Controlled Release 243*, 172–181. https://doi.org/10.1016/j.jconrel.2016.10.007.

Dinish, U. S., Balasundaram, G., Chang, Y. T., & Olivo, M. (2014). Actively targeted in vivo multiplex detection of intrinsic cancer biomarkers using biocompatible SERS nanotags. *Scientific Reports 4*, 4075. https://doi.org/10.1038/srep04075.

Dinish, U. S., Song, Z., Ho, C. J. H., Balasundaram, G., Attia, A. B. E., Lu, X., et al. (2015). Single molecule with dual function on nanogold: biofunctionalized construct for in vivo photoacoustic imaging and SERS biosensing. *Advanced Functional Materials 25*(15), 2316–2325. https://doi.org/10.1002/adfm.201404341.

Dmochowska, N., Tieu, W., Keller, M., Wardill, H., Mavrangelos, C., Campaniello, M., et al. (2018). Immuno-PET of innate immune markers CD11b and IL-1beta detect inflammation in murine colitis. *Journal of Nuclear Medicine*. https://doi.org/10.2967/jnumed.118.219287.

Duan, S., Yang, Y., Zhang, C., Zhao, N., & Xu, F. J. (2017). NIR-responsive polycationic gatekeeper-cloaked hetero-nanoparticles for multimodal imaging-guided triple-combination therapy of Cancer. *Small 13*(9). https://doi.org/10.1002/smll.201603133.

Eberhardt, K., Stiebing, C., Matthaus, C., Schmitt, M., & Popp, J. (2015). Advantages and limitations of Raman spectroscopy for molecular diagnostics: An update. *Expert Review of Molecular Diagnostics 15*(6), 773–787. https://doi.org/10.1586/14737159.2015.1036744.

Ermilov, S. A., Khamapirad, T., Conjusteau, A., Leonard, M. H., Lacewell, R., Mehta, K., et al. (2009). Laser optoacoustic imaging system for detection of breast cancer. *Journal of Biomedical Optics 14*(2), 024007. https://doi.org/10.1117/1.3086616.

van Essen, M., Krenning, E. P., Kam, B. L., de Jong, M., Valkema, R., & Kwekkeboom, D. J. (2009). Peptide-receptor radionuclide therapy for endocrine tumors. *Nature Reviews. Endocrinology 5*(7), 382–393. https://doi.org/10.1038/nrendo.2009.105.

Faghihi, R., Zeinali-Rafsanjani, B., Mosleh-Shirazi, M. A., Saeedi-Moghadam, M., Lotfi, M., Jalli, R., et al. (2017). Magnetic resonance spectroscopy and its clinical applications: A review. *Journal of Medical Imaging and Radiation Sciences 48*(3), 233–253. https://doi.org/10.1016/j.jmir.2017.06.004.

Fantoni, E. R., Dal Ben, D., Falzoni, S., Di Virgilio, F., Lovestone, S., & Gee, A. (2017). Design, synthesis and evaluation in an LPS rodent model of neuroinflammation of a novel (18)F-labelled PET tracer targeting P2X7. *EJNMMI Research 7*(1), 31. https://doi.org/10.1186/s13550-017-0275-2.

Fenning, R. S., & Wilensky, R. L. (2014). New insights into the vulnerable plaque from imaging studies. *Current Atherosclerosis Reports 16*(3), 397. https://doi.org/10.1007/s11883-014-0397-1.

Figueroa, A. L., Abdelbaky, A., Truong, Q. A., Corsini, E., MacNabb, M. H., Lavender, Z. R., et al. (2013). Measurement of arterial activity on routine FDG PET/CT images improves prediction of risk of future CV events. *JACC: Cardiovascular Imaging 6*(12), 1250–1259. https://doi.org/10.1016/j.jcmg.2013.08.006.

Firestein, G. S., & McInnes, I. B. (2017). Immunopathogenesis of rheumatoid arthritis. *Immunity 46*(2), 183–196. https://doi.org/10.1016/j.immuni.2017.02.006.

Flament, J., Geffroy, F., Medina, C., Robic, C., Mayer, J. F., Meriaux, S., et al. (2013). In vivo CEST MR imaging of U87 mice brain tumor angiogenesis using targeted LipoCEST contrast agent at 7 T. *Magnetic Resonance in Medicine 69*(1), 179–187. https://doi.org/10.1002/mrm.24217.

Fomina, N., Sankaranarayanan, J., & Almutairi, A. (2012). Photochemical mechanisms of light-triggered release from nanocarriers. *Advanced Drug Delivery Reviews 64*(11), 1005–1020. https://doi.org/10.1016/j.addr.2012.02.006.

Fratoddi, I., Venditti, I., Cametti, C., & Russo, M. V. (2015). How toxic are gold nanoparticles? The state-of-the-art. *Nano Research 8*(6), 1771–1799. https://doi.org/10.1007/s12274-014-0697-3.

Fujimoto, S., Hartung, D., Ohshima, S., Edwards, D. S., Zhou, J., Yalamanchili, P., et al. (2008). Molecular imaging of matrix metalloproteinase in atherosclerotic lesions: Resolution with dietary modification and statin therapy. *Journal of the American College of Cardiology 52*(23), 1847–1857. https://doi.org/10.1016/j.jacc.2008.08.048.

Gao, W., Li, X., Liu, Z., Fu, W., Sun, Y., Cao, W., et al. (2018). A Redox-responsive self-assembled nanoprobe for photoacoustic inflammation imaging to assess atherosclerotic plaque vulnerability. *Analytical Chemistry*. https://doi.org/10.1021/acs.analchem.8b04912.

Gao, Y., Li, Y., Chen, J., Zhu, S., Liu, X., Zhou, L., et al. (2015). Multifunctional gold nanostar-based nanocomposite: synthesis and application for noninvasive MR-SERS imaging-guided photothermal ablation. *Biomaterials 60*, 31–41. https://doi.org/10.1016/j.biomaterials.2015.05.004.

Garai, E., Sensarn, S., Zavaleta, C. L., Loewke, N. O., Rogalla, S., Mandella, M. J., et al. (2015). A real-time clinical endoscopic system for intraluminal, multiplexed imaging of surface-enhanced Raman scattering nanoparticles. *PLoS One 10*(4), e0123185. https://doi.org/10.1371/journal.pone.0123185.

Gargiulo, S., Gramanzini, M., & Mancini, M. (2016). Molecular imaging of vulnerable atherosclerotic plaques in animal models. *International Journal of Molecular Sciences 17*(9). https://doi.org/10.3390/ijms17091511.

Gerber, A., Bundschuh, M., Klingelhofer, D., & Groneberg, D. A. (2013). Gold nanoparticles: Recent aspects for human toxicology. *Journal of Occupational Medicine and Toxicology 8*(1), 32. https://doi.org/10.1186/1745-6673-8-32.

Glaudemans, A. W., de Vries, E. F., Galli, F., Dierckx, R. A., Slart, R. H., & Signore, A. (2013). The use of (18)F-FDG-PET/CT for diagnosis and treatment monitoring of inflammatory and infectious diseases. *Clinical & Developmental Immunology 2013*, 623036. https://doi.org/10.1155/2013/623036.

Gleich, B., & Weizenecker, J. (2005). Tomographic imaging using the nonlinear response of magnetic particles. *Nature 435*(7046), 1214–1217. https://doi.org/10.1038/nature03808.

Goel, S., England, C. G., Chen, F., & Cai, W. (2017). Positron emission tomography and nanotechnology: A dynamic duo for cancer theranostics. *Advanced Drug Delivery Reviews 113*, 157–176. https://doi.org/10.1016/j.addr.2016.08.001.

Golman, K., Ardenkjaer-Larsen, J. H., Petersson, J. S., Mansson, S., & Leunbach, I. (2003). Molecular imaging with endogenous substances. *Proceedings of the National Academy of Sciences of the United States of America 100*(18), 10435–10439. https://doi.org/10.1073/pnas.1733836100.

van der Graaf, M. (2010). In vivo magnetic resonance spectroscopy: Basic methodology and clinical applications. *European Biophysics Journal 39*(4), 527–540. https://doi.org/10.1007/s00249-009-0517-y.

Grivennikov, S. I., Greten, F. R., & Karin, M. (2010). Immunity, inflammation, and cancer. *Cell 140*(6), 883–899. https://doi.org/10.1016/j.cell.2010.01.025.

Guerrini, L., & Graham, D. (2012). Molecularly-mediated assemblies of plasmonic nanoparticles for surface-enhanced Raman spectroscopy applications. *Chemical Society Reviews 41*(21), 7085–7107. https://doi.org/10.1039/c2cs35118h.

Guglielmetti, C., Najac, C., Didonna, A., Van der Linden, A., Ronen, S. M., & Chaumeil, M. M. (2017). Hyperpolarized 13C MR metabolic imaging can detect neuroinflammation in vivo in a multiple sclerosis murine model. *Proceedings of the National Academy of Sciences of the United States of America 114*(33). https://doi.org/10.1073/pnas.1613345114 E6982–E6991.

Gujrati, V., Mishra, A., & Ntziachristos, V. (2017). Molecular imaging probes for multi-spectral optoacoustic tomography. *Chemical Communications (Cambridge, England) 53*(34), 4653–4672. https://doi.org/10.1039/c6cc09421j.

Gulyas, B., Toth, M., Schain, M., Airaksinen, A., Vas, A., Kostulas, K., et al. (2012). Evolution of microglial activation in ischaemic core and peri-infarct regions after stroke: A PET study with the TSPO molecular imaging biomarker [((11))C]vinpocetine. *Journal of the Neurological Sciences 320*(1–2), 110–117. https://doi.org/10.1016/j.jns.2012.06.026.

Guo, Y., Chen, W., Wang, W., Shen, J., Guo, R., Gong, F., et al. (2012). Simultaneous diagnosis and gene therapy of immuno-rejection in rat allogeneic heart transplantation model using a T-cell-targeted theranostic nanosystem. *ACS Nano 6*(12), 10646–10657. https://doi.org/10.1021/nn3037573.

Guvener, N., Appold, L., de Lorenzi, F., Golombek, S. K., Rizzo, L. Y., Lammers, T., et al. (2017). Recent advances in ultrasound-based diagnosis and therapy with micro- and nanometer-sized formulations. *Methods 130*, 4–13. https://doi.org/10.1016/j.ymeth.2017.05.018.

Haedicke, K., Brand, C., Omar, M., Ntziachristos, V., Reiner, T., & Grimm, J. (2017). Sonophore labeled RGD: A targeted contrast agent for optoacoustic imaging. *Photoacoustics 6*, 1–8. https://doi.org/10.1016/j.pacs.2017.03.001.

Hamilton, A. J., Huang, S. L., Warnick, D., Rabbat, M., Kane, B., Nagaraj, A., et al. (2004). Intravascular ultrasound molecular imaging of atheroma components in vivo. *Journal of the American College of Cardiology 43*(3), 453–460. https://doi.org/10.1016/j.jacc.2003.07.048.

Haris, M., Nath, K., Cai, K., Singh, A., Crescenzi, R., Kogan, F., et al. (2013). Imaging of glutamate neurotransmitter alterations in Alzheimer's disease. *NMR in Biomedicine 26*(4), 386–391. https://doi.org/10.1002/nbm.2875.

Hartimath, S. V., Draghiciu, O., van de Wall, S., Manuelli, V., Dierckx, R. A., Nijman, H. W., et al. (2017). Noninvasive monitoring of cancer therapy induced activated T cells using [(18)F]FB-IL-2 PET imaging. *Oncoimmunology 6*(1), e1248014. https://doi.org/10.1080/2162402X.2016.1248014.

Hautzel, H., Sander, O., Heinzel, A., Schneider, M., & Muller, H. W. (2008). Assessment of large-vessel involvement in giant cell arteritis with 18F-FDG PET: Introducing an ROC-analysis-based cutoff ratio. *Journal of Nuclear Medicine 49*(7), 1107–1113. https://doi.org/10.2967/jnumed.108.051920.

Hilderbrand, S. A., & Weissleder, R. (2010). Near-infrared fluorescence: Application to in vivo molecular imaging. *Current Opinion in Chemical Biology 14*(1), 71–79. https://doi.org/10.1016/j.cbpa.2009.09.029.

Hong, S., Leroueil, P. R., Majoros, I. J., Orr, B. G., Baker, J. R., Jr., & Banaszak Holl, M. M. (2007). The binding avidity of a nanoparticle-based multivalent targeted drug delivery platform. *Chemistry & Biology 14*(1), 107–115. https://doi.org/10.1016/j.chembiol.2006.11.015.

Htun, N. M., Chen, Y. C., Lim, B., Schiller, T., Maghzal, G. J., Huang, A. L., et al. (2017). Near-infrared autofluorescence induced by intraplaque hemorrhage and heme degradation as marker for high-risk atherosclerotic plaques. *Nature Communications 8*(1), 75. https://doi.org/10.1038/s41467-017-00138-x.

Huang, Q., & Zeng, Z. (2017). A review on real-time 3D ultrasound imaging technology. *BioMed Research International 2017*, 6027029. https://doi.org/10.1155/2017/6027029.

Hyafil, F., Cornily, J. C., Feig, J. E., Gordon, R., Vucic, E., Amirbekian, V., et al. (2007). Noninvasive detection of macrophages using a nanoparticulate contrast agent for computed tomography. *Nature Medicine 13*(5), 636–641. https://doi.org/10.1038/nm1571.

Ishino, S., Mukai, T., Kuge, Y., Kume, N., Ogawa, M., Takai, N., et al. (2008). Targeting of lectinlike oxidized low-density lipoprotein receptor 1 (LOX-1) with 99mTc-labeled anti-LOX-1 antibody: Potential agent for imaging of vulnerable plaque. *Journal of Nuclear Medicine 49*(10), 1677–1685. https://doi.org/10.2967/jnumed.107.049536.

Jacobs, P., Bissonnette, R., & Guenther, L. C. (2011). Socioeconomic burden of immune-mediated inflammatory diseases–focusing on work productivity and disability. *The Journal of Rheumatology. Supplement 88*, 55–61. https://doi.org/10.3899/jrheum.110901.

Jaffer, F. A., Calfon, M. A., Rosenthal, A., Mallas, G., Razansky, R. N., Mauskapf, A., et al. (2011). Two-dimensional intravascular near-infrared fluorescence molecular imaging of inflammation in atherosclerosis and stent-induced vascular injury. *Journal of the American College of Cardiology 57*(25), 2516–2526. https://doi.org/10.1016/j.jacc.2011.02.036.

Jaffer, F. A., Vinegoni, C., John, M. C., Aikawa, E., Gold, H. K., Finn, A. V., et al. (2008). Real-time catheter molecular sensing of inflammation in proteolytically active atherosclerosis. *Circulation 118*(18), 1802–1809. https://doi.org/10.1161/CIRCULATIONAHA.108.785881.

Jamar, F., Buscombe, J., Chiti, A., Christian, P. E., Delbeke, D., Donohoe, K. J., et al. (2013). EANM/SNMMI guideline for 18F-FDG use in inflammation and infection. *Journal of Nuclear Medicine 54*(4), 647–658. https://doi.org/10.2967/jnumed.112.112524.

James, M. L., & Gambhir, S. S. (2012). A molecular imaging primer: Modalities, imaging agents, and applications. *Physiological Reviews 92*(2), 897–965. https://doi.org/10.1152/physrev.00049.2010.

Jenkins, W. S., Vesey, A. T., Stirrat, C., Connell, M., Lucatelli, C., Neale, A., et al. (2017). Cardiac alphaVbeta3 integrin expression following acute myocardial infarction in humans. *Heart 103*(8), 607–615. https://doi.org/10.1136/heartjnl-2016-310115.

Jiang, Y., & Pu, K. (2017). Advanced photoacoustic imaging applications of near-infrared absorbing organic nanoparticles. *Small 13*(30). https://doi.org/10.1002/smll.201700710.

Jin, R., Lin, B., Li, D., & Ai, H. (2014). Superparamagnetic iron oxide nanoparticles for MR imaging and therapy: Design considerations and clinical applications. *Current Opinion in Pharmacology 18*, 18–27. https://doi.org/10.1016/j.coph.2014.08.002.

Jo, J., Xu, G., Cao, M., Marquardt, A., Francis, S., Gandikota, G., et al. (2017). A functional study of human inflammatory arthritis using photoacoustic imaging. *Scientific Reports 7*(1), 15026. https://doi.org/10.1038/s41598-017-15147-5.

Juffermans, L. J., Dijkmans, P. A., Musters, R. J., Visser, C. A., & Kamp, O. (2006). Transient permeabilization of cell membranes by ultrasound-exposed microbubbles is related to formation of hydrogen peroxide. *American Journal of Physiology. Heart and Circulatory Physiology 291*(4), H1595–H1601. https://doi.org/10.1152/ajpheart.01120.2005.

Kang, B., Afifi, M. M., Austin, L. A., & El-Sayed, M. A. (2013). Exploiting the nanoparticle plasmon effect: Observing drug delivery dynamics in single cells via Raman/fluorescence imaging spectroscopy. *ACS Nano 7*(8), 7420–7427. https://doi.org/10.1021/nn403351z.

van Kasteren, S. I., Campbell, S. J., Serres, S., Anthony, D. C., Sibson, N. R., & Davis, B. G. (2009). Glyconanoparticles allow pre-symptomatic in vivo imaging of brain disease. *Proceedings of the National Academy of Sciences of the United States of America 106*(1), 18–23. https://doi.org/10.1073/pnas.0806787106.

Kaufmann, B. A., Lewis, C., Xie, A., Mirza-Mohd, A., & Lindner, J. R. (2007). Detection of recent myocardial ischaemia by molecular imaging of P-selectin with targeted contrast

echocardiography. *European Heart Journal 28*(16), 2011–2017. https://doi.org/10.1093/eurheartj/ehm176.

Kaul, M. G., Weber, O., Heinen, U., Reitmeier, A., Mummert, T., Jung, C., et al. (2015). Combined preclinical magnetic particle imaging and magnetic resonance imaging: Initial results in mice. *Rofo 187*(5), 347–352. https://doi.org/10.1055/s-0034-1399344.

Kelly, K. A., Allport, J. R., Tsourkas, A., Shinde-Patil, V. R., Josephson, L., & Weissleder, R. (2005). Detection of vascular adhesion molecule-1 expression using a novel multimodal nanoparticle. *Circulation Research 96*(3), 327–336. https://doi.org/10.1161/01.RES.0000155722.17881.dd.

Khamis, R. Y., Woollard, K. J., Hyde, G. D., Boyle, J. J., Bicknell, C., Chang, S. H., et al. (2016). Near infrared fluorescence (NIRF) molecular imaging of oxidized LDL with an autoantibody in experimental atherosclerosis. *Scientific Reports 6*, 21785. https://doi.org/10.1038/srep21785.

Khanicheh, E., Mitterhuber, M., Xu, L., Haeuselmann, S. P., Kuster, G. M., & Kaufmann, B. A. (2013). Noninvasive ultrasound molecular imaging of the effect of statins on endothelial inflammatory phenotype in early atherosclerosis. *PLoS One 8*(3), e58761. https://doi.org/10.1371/journal.pone.0058761.

Kharlamov, A. N., Tyurnina, A. E., Veselova, V. S., Kovtun, O. P., Shur, V. Y., & Gabinsky, J. L. (2015). Silica-gold nanoparticles for atheroprotective management of plaques: Results of the NANOM-FIM trial. *Nanoscale 7*(17), 8003–8015. https://doi.org/10.1039/c5nr01050k.

Kilroy, J. P., Dhanaliwala, A. H., Klibanov, A. L., Bowles, D. K., Wamhoff, B. R., & Hossack, J. A. (2015). Reducing Neointima formation in a swine model with IVUS and Sirolimus microbubbles. *Annals of Biomedical Engineering 43*(11), 2642–2651. https://doi.org/10.1007/s10439-015-1315-6.

Kilroy, J. P., Klibanov, A. L., Wamhoff, B. R., Bowles, D. K., & Hossack, J. A. (2014). Localized in vivo model drug delivery with intravascular ultrasound and microbubbles. *Ultrasound in Medicine & Biology 40*(10), 2458–2467. https://doi.org/10.1016/j.ultrasmedbio.2014.04.007.

Kilroy, J. P., Patil, A. V., Rychak, J. J., & Hossack, J. A. (2014). An IVUS transducer for microbubble therapies. *IEEE Transactions on Ultrasonics, Ferroelectrics, and Frequency Control 61*(3), 441–449. https://doi.org/10.1109/TUFFC.2014.2929.

Kim, J. B., Park, K., Ryu, J., Lee, J. J., Lee, M. W., Cho, H. S., et al. (2016). Intravascular optical imaging of high-risk plaques in vivo by targeting macrophage mannose receptors. *Scientific Reports 6*, 22608. https://doi.org/10.1038/srep22608.

Kim, S., Lee, M. W., Kim, T. S., Song, J. W., Nam, H. S., Cho, H. S., et al. (2016). Intracoronary dual-modal optical coherence tomography-near-infrared fluorescence structural-molecular imaging with a clinical dose of indocyanine green for the assessment of high-risk plaques and stent-associated inflammation in a beating coronary artery. *European Heart Journal 37*(37), 2833–2844. https://doi.org/10.1093/eurheartj/ehv726.

Kircher, M. F., & Willmann, J. K. (2012). Molecular body imaging: MR imaging, CT, and US. part I. principles. *Radiology 263*(3), 633–643. https://doi.org/10.1148/radiol.12102394.

Klink, A., Lancelot, E., Ballet, S., Vucic, E., Fabre, J. E., Gonzalez, W., et al. (2010). Magnetic resonance molecular imaging of thrombosis in an arachidonic acid mouse model using an activated platelet targeted probe. *Arteriosclerosis, Thrombosis, and Vascular Biology 30*(3), 403–410. https://doi.org/10.1161/ATVBAHA.109.198556.

Knieling, F., Neufert, C., Hartmann, A., Claussen, J., Urich, A., Egger, C., et al. (2017). Multispectral optoacoustic tomography for assessment of Crohn's disease activity. *The New England Journal of Medicine 376*(13), 1292–1294. https://doi.org/10.1056/NEJMc1612455.

Konopka, C. J., Wozniak, M., Hedhli, J., Ploska, A., Schwartz-Duval, A., Siekierzycka, A., et al. (2018). Multimodal imaging of the receptor for advanced glycation end-products with molecularly targeted nanoparticles. *Theranostics 8*(18), 5012–5024. https://doi.org/10.7150/thno.24791.

Kosuge, H., Sherlock, S. P., Kitagawa, T., Dash, R., Robinson, J. T., Dai, H., et al. (2012). Near infrared imaging and photothermal ablation of vascular inflammation using single-walled carbon nanotubes. *Journal of the American Heart Association 1*(6), e002568. https://doi.org/10.1161/JAHA.112.002568.

Kucharzik, T., Kannengiesser, K., & Petersen, F. (2017). The use of ultrasound in inflammatory bowel disease. *Annals of Gastroenterology 30*(2), 135–144. https://doi.org/10.20524/aog.2016.0105.

Laing, S., Jamieson, L. E., Faulds, K., & Graham, D. (2017). Surface-enhanced Raman spectroscopy for in vivo biosensing. *Nature Reviews Chemistry 1*, 60. https://doi.org/10.1038/s41570-017-0060.

Lamare, F., Hinz, R., Gaemperli, O., Pugliese, F., Mason, J. C., Spinks, T., et al. (2011). Detection and quantification of large-vessel inflammation with 11C-(R)-PK11195 PET/CT. *Journal of Nuclear Medicine 52*(1), 33–39. https://doi.org/10.2967/jnumed.110.079038.

Lancelot, E., Amirbekian, V., Brigger, I., Raynaud, J. S., Ballet, S., David, C., et al. (2008). Evaluation of matrix metalloproteinases in atherosclerosis using a novel noninvasive imaging approach. *Arteriosclerosis, Thrombosis, and Vascular Biology 28*(3), 425–432. https://doi.org/10.1161/ATVBAHA.107.149666.

Lanza, G. M., Abendschein, D. R., Hall, C. S., Marsh, J. N., Scott, M. J., Scherrer, D. E., et al. (2000). Molecular imaging of stretch-induced tissue factor expression in carotid arteries with intravascular ultrasound. *Investigative Radiology 35*(4), 227–234.

Lewis, A. J. M., Miller, J. J., Lau, A. Z., Curtis, M. K., Rider, O. J., Choudhury, R. P., et al. (2018). Noninvasive immunometabolic cardiac inflammation imaging using hyperpolarized magnetic resonance. *Circulation Research 122*(8), 1084–1093. https://doi.org/10.1161/CIRCRESAHA.117.312535.

Li, D., Patel, A. R., Klibanov, A. L., Kramer, C. M., Ruiz, M., Kang, B. Y., et al. (2010). Molecular imaging of atherosclerotic plaques targeted to oxidized LDL receptor LOX-1 by SPECT/CT and magnetic resonance. *Circulation Cardiovascular Imaging 3*(4), 464–472. https://doi.org/10.1161/CIRCIMAGING.109.896654.

Li, W., & Chen, X. (2015). Gold nanoparticles for photoacoustic imaging. *Nanomedicine (London, England) 10*(2), 299–320. https://doi.org/10.2217/nnm.14.169.

Li, X., Heber, D., Leike, T., Beitzke, D., Lu, X., Zhang, X., et al. (2018). [68Ga]Pentixafor-PET/MRI for the detection of Chemokine receptor 4 expression in atherosclerotic plaques. *European Journal of Nuclear Medicine and Molecular Imaging 45*(4), 558–566. https://doi.org/10.1007/s00259-017-3831-0.

Ling, W., Regatte, R. R., Navon, G., & Jerschow, A. (2008). Assessment of glycosaminoglycan concentration in vivo by chemical exchange-dependent saturation transfer (gagCEST). *Proceedings of the National Academy of Sciences of the United States of America 105*(7), 2266–2270. https://doi.org/10.1073/pnas.0707666105.

Lohrke, J., Siebeneicher, H., Berger, M., Reinhardt, M., Berndt, M., Mueller, A., et al. (2017). (18)F-GP1, a novel PET tracer designed for high-sensitivity, low-background detection of thrombi. *Journal of Nuclear Medicine 58*(7), 1094–1099. https://doi.org/10.2967/jnumed.116.188896.

Luehmann, H. P., Pressly, E. D., Detering, L., Wang, C., Pierce, R., Woodard, P. K., et al. (2014). PET/CT imaging of chemokine receptor CCR5 in vascular injury model using targeted nanoparticle. *Journal of Nuclear Medicine 55*(4), 629–634. https://doi.org/10.2967/jnumed.113.132001.

Ma, R., Taruttis, A., Ntziachristos, V., & Razansky, D. (2009). Multispectral optoacoustic tomography (MSOT) scanner for whole-body small animal imaging. *Optics Express 17*(24), 21414–21426. https://doi.org/10.1364/OE.17.021414.

MacKenzie, J. D., Yen, Y. F., Mayer, D., Tropp, J. S., Hurd, R. E., & Spielman, D. M. (2011). Detection of inflammatory arthritis by using hyperpolarized 13C-pyruvate with MR imaging and spectroscopy. *Radiology 259*(2), 414–420. https://doi.org/10.1148/radiol.10101921.

MacRitchie, N., Grassia, G., Noonan, J., Garside, P., Graham, D., & Maffia, P. (2018). Molecular imaging of atherosclerosis: spotlight on Raman spectroscopy and surface-enhanced Raman scattering. *Heart 104*, 460–467.

Maeda, J., Zhang, M. R., Okauchi, T., Ji, B., Ono, M., Hattori, S., et al. (2011). In vivo positron emission tomographic imaging of glial responses to amyloid-beta and tau pathologies in mouse models of Alzheimer's disease and related disorders. *The Journal of Neuroscience 31*(12), 4720–4730. https://doi.org/10.1523/JNEUROSCI.3076-10.2011.

von Maltzahn, G., Park, J. H., Agrawal, A., Bandaru, N. K., Das, S. K., Sailor, M. J., et al. (2009). Computationally guided photothermal tumor therapy using long-circulating gold nanorod antennas. *Cancer Research 69*(9), 3892–3900. https://doi.org/10.1158/0008-5472.CAN-08-4242.

Malviya, G., Salemi, S., Lagana, B., Diamanti, A. P., D'Amelio, R., & Signore, A. (2013). Biological therapies for rheumatoid arthritis: Progress to date. *BioDrugs 27*(4), 329–345. https://doi.org/10.1007/s40259-013-0021-x.

Marnane, M., Merwick, A., Sheehan, O. C., Hannon, N., Foran, P., Grant, T., et al. (2012). Carotid plaque inflammation on 18F-fluorodeoxyglucose positron emission tomography predicts early stroke recurrence. *Annals of Neurology 71*(5), 709–718. https://doi.org/10.1002/ana.23553.

Mason, J. C., & Libby, P. (2015). Cardiovascular disease in patients with chronic inflammation: Mechanisms underlying premature cardiovascular events in rheumatologic conditions. *European Heart Journal 36*(8). https://doi.org/10.1093/eurheartj/ehu403482–489c.

Mathers, C. D., & Loncar, D. (2006). Projections of global mortality and burden of disease from 2002 to 2030. *PLoS Medicine 3*(11), e442. https://doi.org/10.1371/journal.pmed.0030442.

McAteer, M. A., Schneider, J. E., Ali, Z. A., Warrick, N., Bursill, C. A., & von zur Muhlen, C., et al. (2008). Magnetic resonance imaging of endothelial adhesion molecules in mouse atherosclerosis using dual-targeted microparticles of iron oxide. *Arteriosclerosis, Thrombosis, and Vascular Biology 28*(1), 77–83. https://doi.org/10.1161/ATVBAHA.107.145466.

McNay, G., Eustace, D., Smith, W. E., Faulds, K., & Graham, D. (2011). Surface-enhanced Raman scattering (SERS) and surface-enhanced resonance Raman scattering (SERRS): A review of applications. *Applied Spectroscopy 65*(8), 825–837. https://doi.org/10.1366/11-06365.

McQueenie, R., Stevenson, R., Benson, R., MacRitchie, N., McInnes, I., Maffia, P., et al. (2012). Detection of inflammation in vivo by surface-enhanced Raman scattering provides higher sensitivity than conventional fluorescence imaging. *Analytical Chemistry 84*(14), 5968–5975. https://doi.org/10.1021/ac3006445.

Meester, E. J., Krenning, B. J., de Blois, R. H., Norenberg, J. P., de Jong, M., Bernsen, M. R., et al. (2018). Imaging of atherosclerosis, targeting LFA-1 on inflammatory cells with (111)In-DANBIRT. *Journal of Nuclear Cardiology*. https://doi.org/10.1007/s12350-018-1244-5.

Michalska, M., Machtoub, L., Manthey, H. D., Bauer, E., Herold, V., Krohne, G., et al. (2012). Visualization of vascular inflammation in the atherosclerotic mouse by ultrasmall superparamagnetic iron oxide vascular cell adhesion molecule-1-specific nanoparticles. *Arteriosclerosis, Thrombosis, and Vascular Biology 32*(10), 2350–2357. https://doi.org/10.1161/ATVBAHA.112.255224.

Morawski, A. M., Winter, P. M., Yu, X., Fuhrhop, R. W., Scott, M. J., Hockett, F., et al. (2004). Quantitative "magnetic resonance immunohistochemistry" with ligand-targeted (19) F nanoparticles. *Magnetic Resonance in Medicine 52*(6), 1255–1262. https://doi.org/10.1002/mrm.20287.

Motz, J. T., Fitzmaurice, M., Miller, A., Gandhi, S. J., Haka, A. S., Galindo, L. H., et al. (2006). In vivo Raman spectral pathology of human atherosclerosis and vulnerable plaque. *Journal of Biomedical Optics 11*(2), 021003. https://doi.org/10.1117/1.2190967.

Motz, J. T., Gandhi, S. J., Scepanovic, O. R., Haka, A. S., Kramer, J. R., Dasari, R. R., et al. (2005). Real-time Raman system for in vivo disease diagnosis. *Journal of Biomedical Optics 10*(3), 031113. https://doi.org/10.1117/1.1920247.

Mulder, W. J., Jaffer, F. A., Fayad, Z. A., & Nahrendorf, M. (2014). Imaging and nanomedicine in inflammatory atherosclerosis. *Science Translational Medicine 6*(239), 239sr231. https://doi.org/10.1126/scitranslmed.3005101.

Muradali, D., & Goldberg, D. R. (2015). US of gastrointestinal tract disease. *RadioGraphics 35*(1), 50–68. https://doi.org/10.1148/rg.351140003.

Muro, S., Wiewrodt, R., Thomas, A., Koniaris, L., Albelda, S. M., Muzykantov, V. R., et al. (2003). A novel endocytic pathway induced by clustering endothelial ICAM-1 or PECAM-1. *Journal of Cell Science 116*(Pt 8), 1599–1609 Retrieved from http://www.ncbi.nlm.nih.gov/pubmed/12640043.

Myerson, J., He, L., Lanza, G., Tollefsen, D., & Wickline, S. (2011). Thrombin-inhibiting perfluorocarbon nanoparticles provide a novel strategy for the treatment and magnetic resonance imaging of acute thrombosis. *Journal of Thrombosis and Haemostasis 9*(7), 1292–1300. https://doi.org/10.1111/j.1538-7836.2011.04339.x.

Nahrendorf, M., Jaffer, F. A., Kelly, K. A., Sosnovik, D. E., Aikawa, E., Libby, P., et al. (2006). Noninvasive vascular cell adhesion molecule-1 imaging identifies inflammatory activation of cells in atherosclerosis. *Circulation 114*(14), 1504–1511. https://doi.org/10.1161/CIRCULATIONAHA.106.646380.

Nahrendorf, M., Keliher, E., Panizzi, P., Zhang, H., Hembrador, S., Figueiredo, J. L., et al. (2009). 18F-4V for PET-CT imaging of VCAM-1 expression in atherosclerosis. *JACC: Cardiovascular Imaging 2*(10), 1213–1222. https://doi.org/10.1016/j.jcmg.2009.04.016.

Nahrendorf, M., Zhang, H., Hembrador, S., Panizzi, P., Sosnovik, D. E., Aikawa, E., et al. (2008). Nanoparticle PET-CT imaging of macrophages in inflammatory atherosclerosis. *Circulation 117*(3), 379–387. https://doi.org/10.1161/CIRCULATIONAHA.107.741181.

Naik, H. B., Natarajan, B., Stansky, E., Ahlman, M. A., Teague, H., Salahuddin, T., et al. (2015). Severity of psoriasis associates with aortic vascular inflammation detected by FDG PET/CT and neutrophil activation in a prospective observational study. *Arteriosclerosis, Thrombosis, and Vascular Biology 35*(12), 2667–2676. https://doi.org/10.1161/ATVBAHA.115.306460.

Neuwelt, A., Sidhu, N., Hu, C. A., Mlady, G., Eberhardt, S. C., & Sillerud, L. O. (2015). Iron-based superparamagnetic nanoparticle contrast agents for MRI of infection and inflammation. *AJR. American Journal of Roentgenology 204*(3), W302–W313. https://doi.org/10.2214/AJR.14.12733.

Noh, T. S., Moon, S. H., Cho, Y. S., Hong, S. P., Lee, E. J., Choi, J. Y., et al. (2013). Relation of carotid artery 18F-FDG uptake to C-reactive protein and Framingham risk score in a large cohort of asymptomatic adults. *Journal of Nuclear Medicine 54*(12), 2070–2076. https://doi.org/10.2967/jnumed.113.119602.

Noonan, J., Asiala, S. M., Grassia, G., MacRitchie, N., Gracie, K., Carson, J., Moores, M., Girolami, M., Bradshaw, A. C., Guzik, T. J., Meehan, G. R., Scales, H. E., Brewer, J. M., McInnes, I. B., Sattar, N., Faulds, K., Garside, P., Graham, D., & Maffia, P. (2018). In vivo multiplex molecular imaging of vascular inflammation using surface-enhanced Raman spectroscopy. *Theranostics 8*, 6195–6209.

Ntziachristos, V., & Razansky, D. (2010). Molecular imaging by means of multispectral optoacoustic tomography (MSOT). *Chemical Reviews 110*(5), 2783–2794. https://doi.org/10.1021/cr9002566.

Ntziachristos, V., Tung, C. H., Bremer, C., & Weissleder, R. (2002). Fluorescence molecular tomography resolves protease activity in vivo. *Nature Medicine 8*(7), 757–760. https://doi.org/10.1038/nm729.

Ohshima, S., Petrov, A., Fujimoto, S., Zhou, J., Azure, M., Edwards, D. S., et al. (2009). Molecular imaging of matrix metalloproteinase expression in atherosclerotic plaques of mice deficient in apolipoprotein e or low-density-lipoprotein receptor. *Journal of Nuclear Medicine 50*(4), 612–617. https://doi.org/10.2967/jnumed.108.055889.

Oikonomou, E. K., Marwan, M., Desai, M. Y., Mancio, J., Alashi, A., Hutt Centeno, E., Thomas, S., Herdman, L., Kotanidis, C. P., Thomas, K. E., Griffin, B. P., Flamm, S. D., Antonopoulos, A. S., Shirodaria, C., Sabharwal, N., Deanfield, J., Neubauer, S., Hopewell, J. C., Channon, K. M., Achenbach, S., & Antoniades, C. (2018). Non-invasive detection of coronary inflammation using computed tomography and prediction of residual cardiovascular risk (the CRISP CT study): a post-hoc analysis of prospective outcome data. *Lancet 392*, 929–939.

Osborn, E. A., Kessinger, C. W., Tawakol, A., & Jaffer, F. A. (2017). Metabolic and molecular imaging of atherosclerosis and venous thromboembolism. *Journal of Nuclear Medicine 58*(6), 871–877. https://doi.org/10.2967/jnumed.116.182873.

Palekar, R. U., Jallouk, A. P., Lanza, G. M., Pan, H., & Wickline, S. A. (2015). Molecular imaging of atherosclerosis with nanoparticle-based fluorinated MRI contrast agents. *Nanomedicine (London, England) 10*(11), 1817–1832. https://doi.org/10.2217/nnm.15.26.

Palmer, A. W., Guldberg, R. E., & Levenston, M. E. (2006). Analysis of cartilage matrix fixed charge density and three-dimensional morphology via contrast-enhanced microcomputed tomography. *Proceedings of the National Academy of Sciences of the United States of America 103*(51), 19255–19260. https://doi.org/10.1073/pnas.0606406103.

Pan, H., Myerson, J. W., Hu, L., Marsh, J. N., Hou, K., Scott, M. J., et al. (2013). Programmable nanoparticle functionalization for in vivo targeting. *The FASEB Journal 27*(1), 255–264. https://doi.org/10.1096/fj.12-218081.

Panagiotopoulos, N., Duschka, R. L., Ahlborg, M., Bringout, G., Debbeler, C., Graeser, M., et al. (2015). Magnetic particle imaging: current developments and future directions. *International Journal of Nanomedicine 10*, 3097–3114. https://doi.org/10.2147/IJN.S70488.

Patel, D. C., Gunasekaran, S. S., Goettl, C., Sweiss, N. J., & Lu, Y. (2017). FDG PET-CT findings of extra-thoracic sarcoid are associated with cardiac sarcoid: A rationale for using FGD PET-CT for cardiac sarcoid evaluation. *Journal of Nuclear Cardiology*. https://doi.org/10.1007/s12350-017-0962-4.

Pelletier-Galarneau, M., & Ruddy, T. D. (2019). Molecular imaging of coronary inflammation. *Trends in Cardiovascular Medicine 29*(4), 191–197. https://doi.org/10.1016/j.tcm.2018.08.004.

Petibon, Y., Guehl, N. J., Reese, T. G., Ebrahimi, B., Normandin, M. D., Shoup, T. M., et al. (2017). Impact of motion and partial volume effects correction on PET myocardial perfusion imaging using simultaneous PET-MR. *Physics in Medicine and Biology 62*(2), 326–343. https://doi.org/10.1088/1361-6560/aa5087.

Phillips, E., Penate-Medina, O., Zanzonico, P. B., Carvajal, R. D., Mohan, P., Ye, Y., et al. (2014). Clinical translation of an ultrasmall inorganic optical-PET imaging nanoparticle probe. *Science Translational Medicine 6*(260), 260ra149. https://doi.org/10.1126/scitranslmed.3009524.

Pissuwan, D., & Hattori, Y. (2016). Detection of adhesion molecules on inflamed macrophages at early-stage using SERS probe gold nanorods. *Nano-Micro Letters 9*(1), 8. https://doi.org/10.1007/s40820-016-0111-7.

Prodanovich, S., Kirsner, R. S., Kravetz, J. D., Ma, F., Martinez, L., & Federman, D. G. (2009). Association of psoriasis with coronary artery, cerebrovascular, and peripheral vascular diseases and mortality. *Archives of Dermatology 145*(6), 700–703. https://doi.org/10.1001/archdermatol.2009.94.

Qian, X., Peng, X. -H., Ansari, D. O., Yin-Goen, Q., Chen, G. Z., Shin, D. M., et al. (2008). In vivo tumor targeting and spectroscopic detection with surface-enhanced Raman nanoparticle tags. *Nature Biotechnology 26*(1), 83–90. http://www.nature.com/nbt/journal/v26/n1/suppinfo/nbt1377_S1.html.

Qin, J., Peng, Z., Li, B., Ye, K., Zhang, Y., Yuan, F., et al. (2015). Gold nanorods as a theranostic platform for in vitro and in vivo imaging and photothermal therapy of inflammatory macrophages. *Nanoscale 7*(33), 13991–14001. https://doi.org/10.1039/c5nr02521d.

Rajendran, K., Lobker, C., Schon, B. S., Bateman, C. J., Younis, R. A., de Ruiter, N. J., et al. (2017). Quantitative imaging of excised osteoarthritic cartilage using spectral CT. *European Radiology 27*(1), 384–392. https://doi.org/10.1007/s00330-016-4374-7.

Rami, L., Gomez-Anson, B., Bosch, B., Sanchez-Valle, R., Monte, G. C., Villar, A., et al. (2007). Cortical brain metabolism as measured by proton spectroscopy is related to memory performance in patients with amnestic mild cognitive impairment and Alzheimer's disease. *Dementia and Geriatric Cognitive Disorders 24*(4), 274–279. https://doi.org/10.1159/000107487.

Razansky, D., Harlaar, N. J., Hillebrands, J. L., Taruttis, A., Herzog, E., Zeebregts, C. J., et al. (2012). Multispectral optoacoustic tomography of matrix metalloproteinase activity in vulnerable human carotid plaques. *Molecular Imaging and Biology 14*(3), 277–285. https://doi.org/10.1007/s11307-011-0502-6.

Ricard, I., Payet, M. D., & Dupuis, G. (1998). VCAM-1 is internalized by a clathrin-related pathway in human endothelial cells but its α4β1 integrin counter-receptor remains associated with the plasma membrane in human T lymphocytes. *European Journal of Immunology 28*(5), 1708–1718. https://doi.org/10.1002/(SICI)1521-4141(199805)28:05<1708::AID-IMMU1708>3.0.CO;2-Y.

Rose, S., Sheth, N. H., Baker, J. F., Ogdie, A., Raper, A., Saboury, B., et al. (2013). A comparison of vascular inflammation in psoriasis, rheumatoid arthritis, and healthy subjects by FDG-PET/CT: A pilot study. *American Journal of Cardiovascular Disease 3*(4), 273–278 Retrieved from http://www.ncbi.nlm.nih.gov/pubmed/24224139.

Rouleau, L., Berti, R., Ng, V. W., Matteau-Pelletier, C., Lam, T., Saboural, P., et al. (2013). VCAM-1-targeting gold nanoshell probe for photoacoustic imaging of atherosclerotic plaque in mice. *Contrast Media & Molecular Imaging 8*(1), 27–39. https://doi.org/10.1002/cmmi.1491.

Rudd, J. H., Warburton, E. A., Fryer, T. D., Jones, H. A., Clark, J. C., Antoun, N., et al. (2002). Imaging atherosclerotic plaque inflammation with [18F]-fluorodeoxyglucose positron emission tomography. *Circulation 105*(23), 2708–2711 Retrieved from http://www.ncbi.nlm.nih.gov/pubmed/12057982.

Ruehm, S. G., Corot, C., Vogt, P., Kolb, S., & Debatin, J. F. (2001). Magnetic resonance imaging of atherosclerotic plaque with ultrasmall superparamagnetic particles of iron oxide in hyperlipidemic rabbits. *Circulation 103*(3), 415–422 Retrieved from http://www.ncbi.nlm.nih.gov/pubmed/11157694.

Ruiz-Cabello, J., Barnett, B. P., Bottomley, P. A., & Bulte, J. W. (2011). Fluorine (19F) MRS and MRI in biomedicine. *NMR in Biomedicine 24*(2), 114–129. https://doi.org/10.1002/nbm.1570.

Sadat, U., Usman, A., Howarth, S. P., Tang, T. Y., Alam, F., Graves, M. J., et al. (2014). Carotid artery stiffness in patients with symptomatic carotid artery disease with contralateral asymptomatic carotid artery disease and in patients with bilateral asymptomatic carotid artery disease: A cine phase-contrast carotid MR study. *Journal of Stroke and Cerebrovascular Diseases 23*(4), 743–748. https://doi.org/10.1016/j.jstrokecerebrovasdis.2013.06.037.

Sandfort, V., Lima, J. A., & Bluemke, D. A. (2015). Noninvasive imaging of atherosclerotic plaque progression: Status of coronary computed tomography angiography. *Circulation. Cardiovascular Imaging 8*(7), e003316. https://doi.org/10.1161/CIRCIMAGING.115.003316.

Saritas, E. U., Goodwill, P. W., Croft, L. R., Konkle, J. J., Lu, K., Zheng, B., et al. (2013). Magnetic particle imaging (MPI) for NMR and MRI researchers. *Journal of Magnetic Resonance 229*, 116–126. https://doi.org/10.1016/j.jmr.2012.11.029.

Scales, H. E., Ierna, M., Smith, K. M., Ross, K., Meiklejohn, G. R., Patterson-Kane, J. C., et al. (2016). Assessment of murine collagen-induced arthritis by longitudinal non-invasive duplexed molecular optical imaging. *Rheumatology (Oxford) 55*(3), 564–572. https://doi.org/10.1093/rheumatology/kev361.

Scepanovic, O. R., Fitzmaurice, M., Miller, A., Kong, C. R., Volynskaya, Z., Dasari, R. R., et al. (2011). Multimodal spectroscopy detects features of vulnerable atherosclerotic plaque. *Journal of Biomedical Optics 16*(1), 011009. https://doi.org/10.1117/1.3525287.

Schinkel, A. F., Kaspar, M., & Staub, D. (2016). Contrast-enhanced ultrasound: Clinical applications in patients with atherosclerosis. *The International Journal of Cardiovascular Imaging 32*(1), 35–48. https://doi.org/10.1007/s10554-015-0713-z.

Schmieder, A. H., Caruthers, S. D., Keupp, J., Wickline, S. A., & Lanza, G. M. (2015). Recent advances in 19Fluorine magnetic resonance imaging with perfluorocarbon emulsions. *Engineering (Beijing) 1*(4), 475–489. https://doi.org/10.15302/J-ENG-2015103.

Schmitt, B., Zbyn, S., Stelzeneder, D., Jellus, V., Paul, D., Lauer, L., et al. (2011). Cartilage quality assessment by using glycosaminoglycan chemical exchange saturation

transfer and (23)Na MR imaging at 7 T. *Radiology 260*(1), 257–264. https://doi.org/10.1148/radiol.11101841.

Schmitz, S. A., Coupland, S. E., Gust, R., Winterhalter, S., Wagner, S., Kresse, M., et al. (2000). Superparamagnetic iron oxide-enhanced MRI of atherosclerotic plaques in Watanabe hereditable hyperlipidemic rabbits. *Investigative Radiology 35*(8), 460–471 Retrieved from http://www.ncbi.nlm.nih.gov/pubmed/10946973.

Schneider, M., Anantharam, B., Arditi, M., Bokor, D., Broillet, A., Bussat, P., et al. (2011). BR38, a new ultrasound blood pool agent. *Investigative Radiology 46*(8), 486–494. https://doi.org/10.1097/RLI.0b013e318217b821.

Serkova, N. J., Renner, B., Larsen, B. A., Stoldt, C. R., Hasebroock, K. M., Bradshaw-Pierce, E. L., et al. (2010). Renal inflammation: Targeted iron oxide nanoparticles for molecular MR imaging in mice. *Radiology 255*(2), 517–526. https://doi.org/10.1148/radiol.09091134.

Serrano, D., Bhowmick, T., Chadha, R., Garnacho, C., & Muro, S. (2012). Intercellular adhesion molecule 1 engagement modulates sphingomyelinase and ceramide, supporting uptake of drug carriers by the vascular endothelium. *Arteriosclerosis, Thrombosis, and Vascular Biology 32*(5), 1178–1185. https://doi.org/10.1161/ATVBAHA.111.244186.

Shangguan, H., Casperson, L. W., Shearin, A., & Prahl, S. A. (1996). Investigation of cavitation bubble dynamics using particle image velocimetry: implications for photoacoustic drug delivery. *Paper presented at the Photonics West '96*.

Shao, X., Zhang, H., Rajian, J. R., Chamberland, D. L., Sherman, P. S., Quesada, C. A., et al. (2011). 125I-labeled gold nanorods for targeted imaging of inflammation. *ACS Nano 5*(11), 8967–8973. https://doi.org/10.1021/nn203138t.

Sheng, W. S., Xu, H. L., Zheng, L., Zhuang, Y. D., Jiao, L. Z., Zhou, J. F., et al. (2018). Intrarenal delivery of bFGF-loaded liposome under guiding of ultrasound-targeted microbubble destruction prevent diabetic nephropathy through inhibition of inflammation. *Artificial Cells, Nanomedicine, and Biotechnology 46*(sup2), 373–385. https://doi.org/10.1080/21691401.2018.1457538.

Shim, C. Y., Liu, Y. N., Atkinson, T., Xie, A., Foster, T., Davidson, B. P., et al. (2015). Molecular imaging of platelet-endothelial interactions and endothelial von Willebrand factor in early and mid-stage atherosclerosis. *Circulation. Cardiovascular Imaging 8*(7), e002765. https://doi.org/10.1161/CIRCIMAGING.114.002765.

Silvola, J. M., Virtanen, H., Siitonen, R., Hellberg, S., Liljenback, H., Metsala, O., et al. (2016). Leukocyte trafficking-associated vascular adhesion protein 1 is expressed and functionally active in atherosclerotic plaques. *Scientific Reports 6*, 35089. https://doi.org/10.1038/srep35089.

Sinharay, S., & Pagel, M. D. (2016). Advances in magnetic resonance imaging contrast agents for biomarker detection. *Annual Review of Analytical Chemistry (Palo Alto, California) 9*(1), 95–115. https://doi.org/10.1146/annurev-anchem-071015-041514.

Smith, B. R., & Gambhir, S. S. (2017). Nanomaterials for in vivo imaging. *Chemical Reviews 117*(3), 901–986. https://doi.org/10.1021/acs.chemrev.6b00073.

Smolen, J. S., Aletaha, D., & McInnes, I. B. (2016). Rheumatoid arthritis. *Lancet 388*(10055), 2023–2038. https://doi.org/10.1016/S0140-6736(16)30173-8.

Song, J., Zhou, J., & Duan, H. (2012). Self-assembled plasmonic vesicles of SERS-encoded amphiphilic gold nanoparticles for cancer cell targeting and traceable intracellular drug delivery. *Journal of the American Chemical Society 134*(32), 13458–13469. https://doi.org/10.1021/ja305154a.

Southworth, R., Kaneda, M., Chen, J., Zhang, L., Zhang, H., Yang, X., et al. (2009). Renal vascular inflammation induced by Western diet in ApoE-null mice quantified by (19)F NMR of VCAM-1 targeted nanobeacons. *Nanomedicine 5*(3), 359–367. https://doi.org/10.1016/j.nano.2008.12.002.

Steinl, D. C., Xu, L., Khanicheh, E., Ellertsdottir, E., Ochoa-Espinosa, A., Mitterhuber, M., et al. (2016). Noninvasive contrast-enhanced ultrasound molecular imaging detects myocardial inflammatory response in autoimmune Myocarditis. *Circulation. Cardiovascular Imaging 9*(8). https://doi.org/10.1161/CIRCIMAGING.116.004720.

Stendahl, J. C., & Sinusas, A. J. (2015). Nanoparticles for cardiovascular imaging and therapeutic delivery, part 1: Compositions and features. *Journal of Nuclear Medicine 56*(10), 1469–1475. https://doi.org/10.2967/jnumed.115.160994.

Stern, J. M., Kibanov Solomonov, V. V., Sazykina, E., Schwartz, J. A., Gad, S. C., & Goodrich, G. P. (2016). Initial evaluation of the safety of nanoshell-directed photothermal therapy in the treatment of prostate disease. *International Journal of Toxicology 35*(1), 38–46. https://doi.org/10.1177/1091581815600170.

Stevenson, R., Hueber, A. J., Hutton, A., McInnes, I. B., & Graham, D. (2011). Nanoparticles and inflammation. *ScientificWorldJournal 11*, 1300–1312. https://doi.org/10.1100/tsw.2011.106.

Stone, G. W., Maehara, A., Lansky, A. J., de Bruyne, B., Cristea, E., Mintz, G. S., et al. (2011). A prospective natural-history study of coronary atherosclerosis. *The New England Journal of Medicine 364*(3), 226–235. https://doi.org/10.1056/NEJMoa1002358.

Su, H., Gorodny, N., Gomez, L. F., Gangadharmath, U. B., Mu, F., Chen, G., et al. (2014). Atherosclerotic plaque uptake of a novel integrin tracer (1)(8)F-Flotegatide in a mouse model of atherosclerosis. *Journal of Nuclear Cardiology 21*(3), 553–562. https://doi.org/10.1007/s12350-014-9879-3.

Suter, M. J., Nadkarni, S. K., Weisz, G., Tanaka, A., Jaffer, F. A., Bouma, B. E., et al. (2011). Intravascular optical imaging technology for investigating the coronary artery. *JACC: Cardiovascular Imaging 4*(9), 1022–1039. https://doi.org/10.1016/j.jcmg.2011.03.020.

Tabas, I., & Glass, C. K. (2013). Anti-inflammatory therapy in chronic disease: Challenges and opportunities. *Science 339*(6116), 166–172. https://doi.org/10.1126/science.1230720.

Tarkin, J. M., Joshi, F. R., Evans, N. R., Chowdhury, M. M., Figg, N. L., Shah, A. V., et al. (2017). Detection of atherosclerotic inflammation by (68)Ga-DOTATATE PET compared to [(18)F]FDG PET imaging. *Journal of the American College of Cardiology 69*(14), 1774–1791. https://doi.org/10.1016/j.jacc.2017.01.060.

Terreno, E., & Aime, S. (2015). MRI contrast agents for pharmacological research. *Frontiers in Pharmacology 6*, 290. https://doi.org/10.3389/fphar.2015.00290.

Terreno, E., Castelli, D. D., Milone, L., Rollet, S., Stancanello, J., Violante, E., et al. (2008). First ex-vivo MRI co-localization of two LIPOCEST agents. *Contrast Media & Molecular Imaging 3*(1), 38–43. https://doi.org/10.1002/cmmi.225.

Thakor, A. S., Jokerst, J. V., Ghanouni, P., Campbell, J. L., Mittra, E., & Gambhir, S. S. (2016). Clinically approved nanoparticle imaging agents. *Journal of Nuclear Medicine 57*(12), 1833–1837. https://doi.org/10.2967/jnumed.116.181362.

Thakor, A. S., Luong, R., Paulmurugan, R., Lin, F. I., Kempen, P., Zavaleta, C., et al. (2011). The fate and toxicity of Raman-active silica-gold nanoparticles in mice. *Science Translational Medicine 3*(79), 79ra33. https://doi.org/10.1126/scitranslmed.3001963.

Tipping, W. J., Lee, M., Serrels, A., Brunton, V. G., & Hulme, A. N. (2016). Stimulated Raman scattering microscopy: An emerging tool for drug discovery. *Chemical Society Reviews 45*(8), 2075–2089. https://doi.org/10.1039/c5cs00693g.

Tocci, G., Goletti, D., Marino, V., Matucci, A., Milano, G. M., Cantini, F., et al. (2016). Cardiovascular outcomes and tumour necrosis factor antagonists in chronic inflammatory rheumatic disease: A focus on rheumatoid arthritis. *Expert Opinion on Drug Safety 15*(sup1), 55–61. https://doi.org/10.1080/14740338.2016.1218469.

Tran, L., Huitema, A. D., van Rijswijk, M. H., Dinant, H. J., Baars, J. W., Beijnen, J. H., et al. (2011). CD20 antigen imaging with (1)(2)(4)I-rituximab PET/CT in patients with rheumatoid arthritis. *Human Antibodies 20*(1–2), 29–35. https://doi.org/10.3233/HAB20110239.

Tumati, S., Martens, S., & Aleman, A. (2013). Magnetic resonance spectroscopy in mild cognitive impairment: Systematic review and meta-analysis. *Neuroscience and Biobehavioral Reviews 37*(10 Pt 2), 2571–2586. https://doi.org/10.1016/j.neubiorev.2013.08.004.

Ughi, G. J., Wang, H., Gerbaud, E., Gardecki, J. A., Fard, A. M., Hamidi, E., et al. (2016). Clinical characterization of coronary atherosclerosis with dual-modality OCT and near-infrared autofluorescence imaging. *JACC: Cardiovascular Imaging 9*(11), 1304–1314. https://doi.org/10.1016/j.jcmg.2015.11.020.

Vaalma, S., Rahmer, J., Panagiotopoulos, N., Duschka, R. L., Borgert, J., Barkhausen, J., et al. (2017). Magnetic particle imaging (MPI): Experimental quantification of vascular stenosis using stationary stenosis phantoms. *PLoS One 12*(1), e0168902. https://doi.org/10.1371/journal.pone.0168902.

Valluru, K. S., Wilson, K. E., & Willmann, J. K. (2016). Photoacoustic imaging in oncology: Translational preclinical and early clinical experience. *Radiology 280*(2), 332–349. https://doi.org/10.1148/radiol.16151414.

Varasteh, Z., Hyafil, F., Anizan, N., Diallo, D., Aid-Launais, R., Mohanta, S., et al. (2017). Targeting mannose receptor expression on macrophages in atherosclerotic plaques of apolipoprotein E-knockout mice using (111)In-tilmanocept. *EJNMMI Research 7*(1), 40. https://doi.org/10.1186/s13550-017-0287-y.

Verjans, J. W., Osborn, E. A., Ughi, G. J., Calfon Press, M. A., Hamidi, E., Antoniadis, A. P., et al. (2016). Targeted near-infrared fluorescence imaging of atherosclerosis: Clinical and intracoronary evaluation of indocyanine green. *JACC: Cardiovascular Imaging 9*(9), 1087–1095. https://doi.org/10.1016/j.jcmg.2016.01.034.

Verma, A., Kumar, I., Verma, N., Aggarwal, P., & Ojha, R. (2016). Magnetic resonance spectroscopy - revisiting the biochemical and molecular milieu of brain tumors. *BBA Clinical 5*, 170–178. https://doi.org/10.1016/j.bbacli.2016.04.002.

Vinegoni, C., Botnaru, I., Aikawa, E., Calfon, M. A., Iwamoto, Y., Folco, E. J., et al. (2011). Indocyanine green enables near-infrared fluorescence imaging of lipid-rich, inflamed atherosclerotic plaques. *Science Translational Medicine 3*(84), 84ra45. https://doi.org/10.1126/scitranslmed.3001577.

Virmani, R., Kolodgie, F. D., Burke, A. P., Finn, A. V., Gold, H. K., Tulenko, T. N., et al. (2005). Atherosclerotic plaque progression and vulnerability to rupture: Angiogenesis as a source of intraplaque hemorrhage. *Arteriosclerosis, Thrombosis, and Vascular Biology 25*(10), 2054–2061. https://doi.org/10.1161/01.ATV.0000178991.71605.18.

Viswanathan, S., Kovacs, Z., Green, K. N., Ratnakar, S. J., & Sherry, A. D. (2010). Alternatives to gadolinium-based metal chelates for magnetic resonance imaging. *Chemical Reviews 110*(5), 2960–3018. https://doi.org/10.1021/cr900284a.

Wang, B., Yantsen, E., Larson, T., Karpiouk, A. B., Sethuraman, S., Su, J. L., et al. (2009). Plasmonic intravascular photoacoustic imaging for detection of macrophages in atherosclerotic plaques. *Nano Letters 9*(6), 2212–2217. https://doi.org/10.1021/nl801852e.

Wang, H., Felt, S. A., Machtaler, S., Guracar, I., Luong, R., Bettinger, T., et al. (2015). Quantitative assessment of inflammation in a porcine acute terminal ileitis model: US with a molecularly targeted contrast agent. *Radiology 276*(3), 809–817. https://doi.org/10.1148/radiol.2015142478.

Wang, H., Machtaler, S., Bettinger, T., Lutz, A. M., Luong, R., Bussat, P., et al. (2013). Molecular imaging of inflammation in inflammatory bowel disease with a clinically translatable dual-selectin-targeted US contrast agent: Comparison with FDG PET/CT in a mouse model. *Radiology 267*(3), 818–829. https://doi.org/10.1148/radiol.13122509.

Wang, L., Tang, X., Xiang, X., Tang, Y., & Qiu, L. (2019). Experimental study of TNF-alpha receptor gene transfection by ultrasound-targeted microbubble destruction to treat collagen-induced arthritis in rats in vivo. *Experimental and Therapeutic Medicine 17*(3), 1601–1610. https://doi.org/10.3892/etm.2019.7158.

Wang, S., Unnikrishnan, S., Herbst, E. B., Klibanov, A. L., Mauldin, F. W., Jr., & Hossack, J. A. (2017). Ultrasound molecular imaging of inflammation in mouse abdominal aorta. *Investigative Radiology 52*(9), 499–506. https://doi.org/10.1097/RLI.0000000000000373.

Wang, X., Chamberland, D. L., & Jamadar, D. A. (2007). Noninvasive photoacoustic tomography of human peripheral joints toward diagnosis of inflammatory arthritis. *Optics Letters 32*(20), 3002–3004. https://doi.org/10.1364/OL.32.003002.

Wang, X., Gkanatsas, Y., Palasubramaniam, J., Hohmann, J. D., Chen, Y. C., Lim, B., et al. (2016). Thrombus-targeted theranostic microbubbles: A new technology towards concurrent rapid ultrasound diagnosis and bleeding-free fibrinolytic treatment of thrombosis. *Theranostics 6*(5), 726–738. https://doi.org/10.7150/thno.14514.

Wang, X., Hagemeyer, C. E., Hohmann, J. D., Leitner, E., Armstrong, P. C., Jia, F., et al. (2012). Novel single-chain antibody-targeted microbubbles for molecular ultrasound imaging of thrombosis: Validation of a unique noninvasive method for rapid and sensitive

detection of thrombi and monitoring of success or failure of thrombolysis in mice. *Circulation 125*(25), 3117–3126. https://doi.org/10.1161/CIRCULATIONAHA.111.030312.

Wang, X., & Peter, K. (2017). Molecular imaging of Atherothrombotic diseases: Seeing is believing. *Arteriosclerosis, Thrombosis, and Vascular Biology 37*(6), 1029–1040. https://doi.org/10.1161/ATVBAHA.116.306483.

Wei, L., Chen, Z., Shi, L., Long, R., Anzalone, A. V., Zhang, L., et al. (2017). Super-multiplex vibrational imaging. *Nature 544*(7651), 465–470. https://doi.org/10.1038/nature22051.

Weiberg, D., Thackeray, J. T., Daum, G., Sohns, J. M., Kropf, S., Wester, H. J., et al. (2018). Clinical molecular imaging of Chemokine receptor CXCR4 expression in atherosclerotic plaque using (68)Ga-Pentixafor PET: Correlation with cardiovascular risk factors and calcified plaque burden. *Journal of Nuclear Medicine 59*(2), 266–272. https://doi.org/10.2967/jnumed.117.196485.

Weizenecker, J., Gleich, B., Rahmer, J., Dahnke, H., & Borgert, J. (2009). Three-dimensional real-time in vivo magnetic particle imaging. *Physics in Medicine and Biology 54*(5), L1–L10. https://doi.org/10.1088/0031-9155/54/5/L01.

White, P. L., Hibbitts, S. J., Perry, M. D., Green, J., Stirling, E., Woodford, L., et al. (2014). Evaluation of a commercially developed semiautomated PCR-surface-enhanced raman scattering assay for diagnosis of invasive fungal disease. *Journal of Clinical Microbiology 52*(10), 3536–3543. https://doi.org/10.1128/JCM.01135-14.

Wildgruber, M., Swirski, F. K., & Zernecke, A. (2013). Molecular imaging of inflammation in atherosclerosis. *Theranostics 3*(11), 865–884. https://doi.org/10.7150/thno.5771.

Willmann, J. K., Bonomo, L., Carla Testa, A., Rinaldi, P., Rindi, G., Valluru, K. S., et al. (2017). Ultrasound molecular imaging with BR55 in patients with breast and ovarian lesions: First-in-human results. *Journal of Clinical Oncology 35*(19), 2133–2140. https://doi.org/10.1200/JCO.2016.70.8594.

Willmann, J. K., Cheng, Z., Davis, C., Lutz, A. M., Schipper, M. L., Nielsen, C. H., et al. (2008). Targeted microbubbles for imaging tumor angiogenesis: Assessment of whole-body biodistribution with dynamic micro-PET in mice. *Radiology 249*(1), 212–219. https://doi.org/10.1148/radiol.2491072050.

Wilson, K., Homan, K., & Emelianov, S. (2012). Biomedical photoacoustics beyond thermal expansion using triggered nanodroplet vaporization for contrast-enhanced imaging. *Nature Communications 3*, 618. https://doi.org/10.1038/ncomms1627.

Withana, N. P., Saito, T., Ma, X., Garland, M., Liu, C., Kosuge, H., et al. (2016). Dual-modality activity-based probes as molecular imaging agents for vascular inflammation. *Journal of Nuclear Medicine 57*(10), 1583–1590. https://doi.org/10.2967/jnumed.115.171553.

Wolfbeis, O. S. (2015). An overview of nanoparticles commonly used in fluorescent bioimaging. *Chemical Society Reviews 44*(14), 4743–4768. https://doi.org/10.1039/c4cs00392f.

Woodside, D. G., Tanifum, E. A., Ghaghada, K. B., Biediger, R. J., Caivano, A. R., Starosolski, Z. A., et al. (2018). Magnetic resonance imaging of atherosclerotic plaque at clinically relevant field strengths (1T) by targeting the Integrin alpha4beta1. *Scientific Reports 8*(1), 3733. https://doi.org/10.1038/s41598-018-21893-x.

Wu, C., Li, F., Niu, G., & Chen, X. (2013). PET imaging of inflammation biomarkers. *Theranostics 3*(7), 448–466. https://doi.org/10.7150/thno.6592.

Wu, C., Zhang, Y., Li, Z., Li, C., & Wang, Q. (2016). A novel photoacoustic nanoprobe of ICG@PEG-Ag2S for atherosclerosis targeting and imaging in vivo. *Nanoscale 8*(25), 12531–12539. https://doi.org/10.1039/c6nr00060f.

Wu, Z., Curaj, A., Fokong, S., Liehn, E. A., Weber, C., Lammers, T., et al. (2013). Rhodamine-loaded intercellular adhesion molecule-1-targeted microbubbles for dual-modality imaging under controlled shear stresses. *Circulation. Cardiovascular Imaging 6*(6), 974–981. https://doi.org/10.1161/CIRCIMAGING.113.000805.

Xie, F., Lof, J., Matsunaga, T., Zutshi, R., & Porter, T. R. (2009). Diagnostic ultrasound combined with glycoprotein IIb/IIIa-targeted microbubbles improves microvascular recovery after acute coronary thrombotic occlusions. *Circulation 119*(10), 1378–1385. https://doi.org/10.1161/CIRCULATIONAHA.108.825067.

Xie, L., Lin, A. S., Levenston, M. E., & Guldberg, R. E. (2009). Quantitative assessment of articular cartilage morphology via EPIC-microCT. *Osteoarthritis and Cartilage 17*(3), 313–320. https://doi.org/10.1016/j.joca.2008.07.015.

Zainon, R., Ronaldson, J. P., Janmale, T., Scott, N. J., Buckenham, T. M., Butler, A. P., et al. (2012). Spectral CT of carotid atherosclerotic plaque: Comparison with histology. *European Radiology 22*(12), 2581–2588. https://doi.org/10.1007/s00330-012-2538-7.

de la Zerda, A., Bodapati, S., Teed, R., May, S. Y., Tabakman, S. M., Liu, Z., et al. (2012). Family of enhanced photoacoustic imaging agents for high-sensitivity and multiplexing studies in living mice. *ACS Nano 6*(6), 4694–4701. https://doi.org/10.1021/nn204352r.

de la Zerda, A., Liu, Z., Bodapati, S., Teed, R., Vaithilingam, S., Khuri-Yakub, B. T., et al. (2010). Ultrahigh sensitivity carbon nanotube agents for photoacoustic molecular imaging in living mice. *Nano Letters 10*(6), 2168–2172. https://doi.org/10.1021/nl100890d.

Zhang, H. F., Maslov, K., Stoica, G., & Wang, L. V. (2006). Functional photoacoustic microscopy for high-resolution and noninvasive in vivo imaging. *Nature Biotechnology 24*(7), 848–851. https://doi.org/10.1038/nbt1220.

Zhao, Y., Wei, C., Chen, X., Liu, J., Yu, Q., Liu, Y., et al. (2019). Drug delivery system based on near-infrared light-responsive molybdenum disulfide Nanosheets controls the high-efficiency release of Dexamethasone to inhibit inflammation and treat osteoarthritis. *ACS Applied Materials & Interfaces*. https://doi.org/10.1021/acsami.8b20372.

Zhong, J., Yang, S., Wen, L., & Xing, D. (2016). Imaging-guided photoacoustic drug release and synergistic chemo-photoacoustic therapy with paclitaxel-containing nanoparticles. *Journal of Controlled Release 226*, 77–87. https://doi.org/10.1016/j.jconrel.2016.02.010.

Zhong, M., Girolami, M., Faulds, K., & Graham, D. (2011). Bayesian methods to detect dye-labelled DNA oligonucleotides in multiplexed Raman spectra. *Journal of the Royal Statistical Society: Series C: Applied Statistics 60*(2), 187–206. https://doi.org/10.1111/j.1467-9876.2010.00744.x.

Zhu, X., Schuff, N., Kornak, J., Soher, B., Yaffe, K., Kramer, J. H., et al. (2006). Effects of Alzheimer disease on fronto-parietal brain N-acetyl aspartate and myo-inositol using magnetic resonance spectroscopic imaging. *Alzheimer Disease and Associated Disorders 20*(2), 77–85. https://doi.org/10.1097/01.wad.0000213809.12553.fc.

Zhuang, H., & Codreanu, I. (2015). Growing applications of FDG PET-CT imaging in non-oncologic conditions. *Journal of Biomedical Research 29*(3), 189–202. https://doi.org/10.7555/JBR.29.20140081.